industriell elektroteknik och automation
LUNDS TEKNISKA HÖGSKOLA

Torque Control of a Novel Switched Reluctance Machine

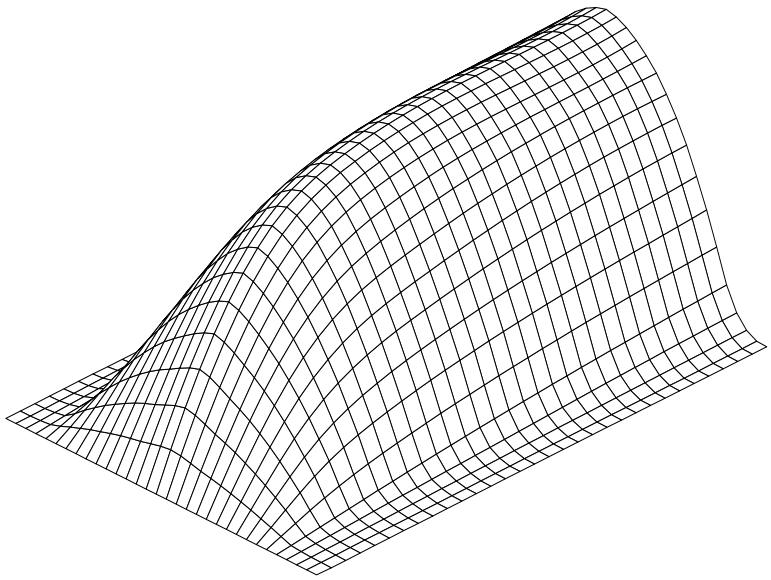

Lars Sjöberg

DEPARTMENT OF INDUSTRIAL ELECTRICAL ENGINEERING AND AUTOMATION
LUND INSTITUTE OF TECHNOLOGY

Torque Control of a Novel Switched Reluctance Machine

Lars Sjöberg

Department of
Industrial Electrical Engineering and Automation (IEA)
Lund Institute of Technology (LTH)
P.O. Box 118
S - 221 00 LUND
SWEDEN

ISBN 91-88934-03-9
CODEN:LUTEDX/(TEIE-1013)/1-115(1996)

Printed in Sweden by Reprocentralen, Lund University
Lund 1996

Abstract

This work is focused on torque control and performance analysis of two switched reluctance machines having six stator poles and four rotor poles. The first machine is a conventional design, built with a laminated iron core, whereas the second is a novel construction where the magnetic flux conductor consists of a soft magnetic composite material. A table based torque control scheme is developed which allows the user to specify the permissible torque ripple. The current reference values for all phases are written into a large memory, which is addressed by the torque reference, rotor angular position and rotor angular speed, all in digital form. The phase currents are controlled with hysteresis controllers, one for each phase. The updating frequency of the controller is in excess of 100 kHz, which makes it attractive for high speed applications. Models for the iron and copper losses as well as for the torque production capability of the switched reluctance machines are developed. Both the theoretical analysis and experimental verification are performed on two switched reluctance machines rated 9.5 Nm at 4600 rpm. It is shown that the iron losses in both machines are almost the same, and that 70 - 75 % of the iron losses are confined to the stator. The iron losses greatly exceed the copper losses at the nominal operating point. Finally, it is concluded that increasing magnetic frequency is favourable if the iron core is made with the soft magnetic composite material tested.

Contents

Acknowledgements

This work has been carried out at the Department of Industrial Electrical Engineering and Automation, Lund Institute of Technology. I wish to express my sincere gratitude to my supervisor professor Mats Alaküla for his support during this project. He has shown a great ability to create a friendly and stimulating atmosphere at the department, and he has found a lot of time for discussing and turning problems into interesting challenges.

I would also like to thank professor Gustaf Olsson, the staff and my fellow graduate students for their assistance and for making my work pleasant.

The work has been supported by NUTEK (Swedish National Board for Industrial and Technical Development) within the program "Electric and Electric Hybrid Vehicles", contract No. P456-3.

Finally, I would like to thank Weronice and my parents who have supported me and taken an interest in my work for a long time.

Lund, May 1996

Lars Sjöberg

1

Introduction

The switched reluctance machine is an odd member of the family of electrical machines. It belongs to the very few machines that depend on reluctance torque for rotation. Despite being the oldest form of electrical machine, its use has been limited throughout this century. The phenomenological principle dates back to the days of Ampère, who discovered, in the 1820s, the equivalence of a solenoid with an iron core to a permanent magnet. Moreover, Ampère found that this electrically controlled magnet produced forces upon nearby iron elements and that the forces were dependent on the magnitude of the current in the solenoid. At that time it was also realised that the forces in the system acted in such a way that the reluctance of the magnetic flux path was minimised, although the term ”reluctance” was not used.

The earliest recorded construction of a switched reluctance machine is around 1840. It was a machine that drove a battery powered vehicle on the Edinburgh - Glasgow railway. The vehicle weight was 6 tonnes and the reported maximum speed was 6 km/h.

During the last two or three decades the switched reluctance machine has been in focus for a lot of research. The tools for analysing and designing switched reluctance machine drive systems (comparable with other conventional electrical drive systems) has improved. Finite element programs for solving the non-linear electromagnetic field problems are today a standard tool for any machine designer. Having optimised the machine geometry, simulation toolboxes for handling the machine dynamics and developing control strategies are also readily available.

Apart from the tools, components in the electrical drive system have developed as well, such as high power rated IGBT modules and low cost digital signal processors.

It is hard to develop explicit analytical expressions for the electro-magnetic/mechanical system, to be used for control of the switched reluctance machine. As all electrical machines, it requires extensive numerical calculations for both design, control and simulations.

Few papers are published that compare the performance of different electrical machine types. The reason is probably that it is difficult to agree on what should be the basis for comparison. The only fair ground for comparison is to list a large number of performance data and choose the machine that best matches the demands given by the application. In an electrical drive system, the electrical energy converter should also be included in the comparison, since for instance a switched reluctance machine is useless without power electronics.

The switched reluctance machine has a number of nice features that ought to be mentioned. It has been shown (Harris et al, 1988, Miller et al, 1989 and Krishnan et al, 1991) that the switched reluctance machine has a comparable or even higher torque density than the induction machine, but fails to exceed the permanent magnet synchronous machine in that respect. In other words, if a switched reluctance motor with a given volume is to be designed, the efficiency is inherently higher than an induction motor of the same size. The theoretical maximum torque density for a switched reluctance machine is investigated in (Radun, 1994). A limit of approximately 25000 Nm / m^3 is stated. A switched reluctance machine with this maximum torque density is reported in (Radun, 1992). A switched reluctance machine is capable of high speed operation and (MacMinn, 1989) describes a switched reluctance aircraft engine starter/generator capable of a maximum speed of 48000 rpm. The power range in which the switched reluctance machine is capable to operate is wide. The range (Lawrenson, 1992) is from 10 W (at 10000 rpm) to 5 MW (at 50 rpm).

The rotor of the switched reluctance machine contains no magnets or windings, which means that the rotor losses can be extremely low. The rotor of a switched reluctance machine is sometimes referred to as a "cold" rotor. The majority of the losses in the machine are confined to the stator, where cooling is easier. Another advantage is that the torque is independent on the operating temperature of the machine.

It has also been shown (Miller, 1985) that there exists a close interaction between the design of the switched reluctance machine geometry and the rating of the electrical energy converter. If iron saturation effects are taken into account, the rating of the electrical energy converter for the switched reluctance machine matches that of an induction motor producing the same shaft power.

In spite of the enthusiasm surrounding electrical drive systems with switched reluctance machines during the last two decades, the machine has never quite reached the big markets. In contrast to the induction motor, the switched reluctance machine can not be used without an electrical energy converter feeding it with the appropriate currents. It is entirely an electronic motor, used only in applications where a variable speed or torque is required. Each controller has to be individually calculated for each individual switched reluctance machine type. Moreover, a highly optimised switched reluctance machine tends to have a higher noise level (Wallace et al, 1990) than a corresponding induction machine.

For high dynamic performance, the control of the switched reluctance machine requires accurate knowledge of the rotor angular position. There exists a number of different rotor angular position observer designs (Ray et al, 1993), and recent results (Ehsani et al, 1994) indicate that the entire speed and torque range can be covered. In this thesis, the problem of rotor angular position detection is not dealt with. Instead, the rotor angular position is detected by a resolver on the shaft end, and a resolver-to-digital circuit is presenting the rotor angular position as a 10 bit digital word.

Background

A new iron powder composite material with unique electromagnetic properties has been developed in co-operation between the Department of Production and Materials Engineering and the Department of Industrial Electrical Engineering and Automation, Lund Institute of Technology, and Höganäs AB. A switched reluctance machine with six stator poles and four rotor poles was built with the iron composite material as a magnetic flux conductor in 1995. The machine was rated 9.5 Nm at 1500 rpm. The machine was tested with a commercially available controller utilising open loop voltage control and compared with an identical machine built with a stack of laminated iron. Test results reported in (Alaküla et al, 1995) indicated that the iron losses in the iron composite based machine were only slightly higher than the conventionally built machine.

Scope of the Work

The scope of this work is to examine the performance of a switched reluctance machine built in the newly developed composite material, and to compare it with an identical switched reluctance machine built with a conventional laminated iron core. For this purpose, the machines were wound for a speed of 4600 rpm in order to investigate the high frequency qualities of the iron composite material.

Calculations of the expected torque as well as calculations of the losses in the switched reluctance machines are performed. The calculations of the losses are confined to the nominal operating point.

To test the drive system, a table based torque controller for switched reluctance machines has been developed. A method for controlling the torque is presented, both for the conventional machine and the one built with an iron powder composite core.

The entire electrical drive system has been built and tested, and theoretical results and simulations have been verified experimentally.

Overview of the Thesis

In Chapter 2 the different parts constituting the electrical drive system are explained, with the design and rating of both the motor and the electrical energy converter. In Chapter 3, the concept of reluctance torque is reviewed, both generally and applied to the switched reluctance machine used in the thesis. A model for the losses in the machine is also described. In the next chapter, torque control of the switched reluctance machine is discussed. An algorithm for smooth torque control as well as for torque ripple limit control is explained. Before reaching the conclusions, theoretical results and simulations are compared with experimental measurements in Chapter 5.

2

The Drive System

In this chapter an overview of the control system for the electrical drive systems is given. The origin of the switched reluctance machine used is explained. The iron lamination based drive system and the iron powder core based drive system is defined by the description of the size and power rating. The principal mode of operation for the electrical energy converter is also stated.

Cascaded Controllers

An electrical drive system is any system that converts electrical energy into mechanical energy or vice versa. The mechanical motion can be rotational or translationary or a combination of both. For a rotary motion such as in a rotating electrical machine, high performance rotor angular speed control and/or rotor angular position control requires good torque control. It may be important that the torque quality is high, which means

- no stationary errors,
- fast dynamic response,
- low harmonic content,
- temperature independence.

Usually, the control structure in electrical drive systems is cascade control and this scheme is seen in Fig. 2.1. The controllers are arranged with the fastest loop in the system, the torque loop, as the innermost loop, while the outer loops are the speed and position loops. However, in some applications, the torque loop may be the outmost, since torque is the only controlled variable and thus no speed and position loop is required.

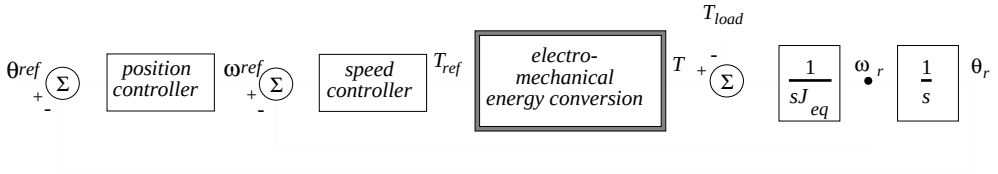

Fig. 2.1 *Torque, speed and position controllers coupled in cascade.*

The difference between various electrical drive systems lies in the electromechanical energy conversion process. Common to all electrical drives is that in order to control the torque, current has to be controlled. A good torque control design depends on accurate determination of the relationship between current and torque. The electrical energy conversion process in Fig. 2.1 is splitted into the parts seen in Fig. 2.2.

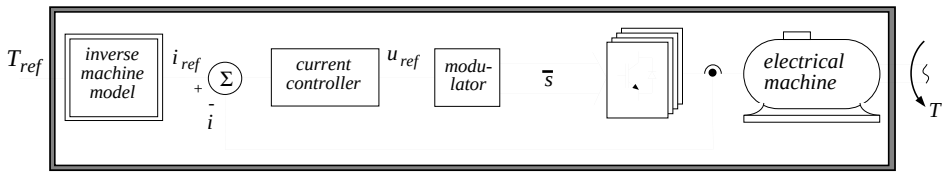

Fig. 2.2 *Electrical drive system specific parts in the electro-mechanical energy conversion process.*

The different parts in Fig. 2.2 are machine and application dependent. The current controller is derived with the knowledge of the machine dynamics. The application determines whether the machine has to operate in 1,2 or 4 quadrants and this of course affects the choise of electrical energy converter bridge configuration. The bridge configuration used also influences the parameters in the current controller as well as the choise of modulator. The task of the modulator is to determine the switching state (on/off) for all the transistors in the power electronics in order to produce the demanded voltage. Sometimes it is not possible to distinguish between the current controller and the modulator; they are the same unit. This is the case for the controller in this thesis, and the reason for that is discussed in Chapter 4.

The relationship between torque and current can be very simple, as for the seperately excited DC machine where the relationship is simply a scaling factor. For the switched reluctance machine it is quite the opposite. The relationship is highly non-linear and other parameters such as the rotor

angular position and rotor angular speed are needed to accurately calculate the current reference values.

Drive System Selection

The electrical drive system application studied in this context consists of a switched reluctance machine with six stator poles and four rotor poles (see Appendix C for details) and an electrical energy converter with two transistors per phase. The design of the switched reluctance machine descends from a local company. The machine is used as a motor in a pump application. The thermal rating of the machine is 9.5 Nm at 1500 rpm (1.5 kW), and it is self cooled with a fan mounted onto the shaft. If the performance requirements are low, it is possible to combine the speed loop with the inner loops of Figs. 2.1 and 2.2. Then, no current control is used and the speed is directly controlled with the duty cycle and turn-on/turn-off angles of the phase voltages. The torque quality is low, as well as the dynamic performance.

For evaluation purposes, a high performance torque control system is developed within the scope of this work. This control system is capable of supplying optimal phase current combinations for an arbitrary torque reference regardless of the rotor angular speed and position. This is accomplished within the full operating range of the machine.

Iron Cores

The two machines tested have different iron cores. Since switched reluctance machine analysis rather than design is the key issue in this thesis, the conventional laminated version is chosen as a reference machine. This machine is rewound for a DC link voltage of 300 Volt and a speed of 4600 rpm, keeping the same torque, which means that the new power rating of the switched reluctance machine is 4.6 kW. Details of the machine parameters and a list of the measures are given in Appendix C. A copy of the iron lamination based machine is built with a compressed iron powder core. Both the stator and the rotor are first produced in a cylindrical shape and then machine tooled to their final shape. Windings are attached to the stator and the package is fitted into the same housing as the iron lamination based machine. More data on the iron lamination core and the iron powder core are given in Appendix B. A more theoretical approach on the iron powder core material is found in (Cedell, 1995).

Electrical Energy Converter

A large number of electrical energy converter topologies (Vucosavic et al, 1991, De Doncker et al, 1991 and Park et al 1992) have been suggested for switched reluctance machines. The "classic" converter with two transistors per phase, seen in Fig. 2.3, is used throughout this thesis.

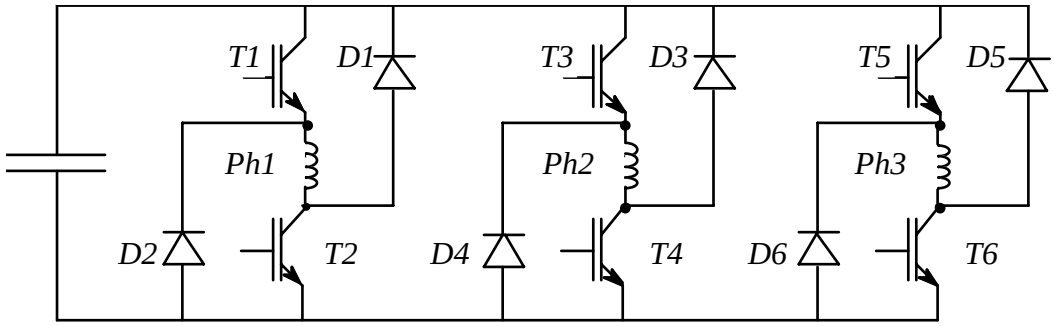

Fig. 2.3 *"Classic" converter topology for a three phase switched reluctance machine.*

However, a topology as the one in Fig. 2.3 was not readily available at the time of the start of the project. Two three phase self commutated converters were used instead. One phase coil of the switched reluctance machine is coupled between two phase legs as indicated in Fig. 2.4.

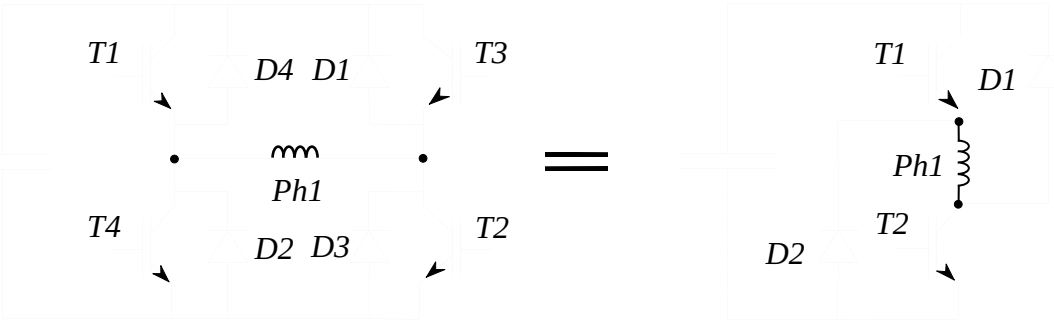

Fig. 2.4 *One phase leg for the switched reluctance machine electrical energy converter formed out of two phase legs in a three phase self commutated converter.*

If transistors *T3* and *T4* are always switched off, the freewheeling diodes *D3* and *D4* are redundant, and the circuit topology is identical to the one to the right in Fig. 2.4. The laboratory is equipped with a large number of three phase self commutated converters with specially built gate driver/user interface, so instead of building a new kind of electrical energy converter, two three phase self commutated converters were combined. This is merely for saving time in the laboratory.

One three phase self commutated converter consists of three IGBT modules (MG100Q2YS40) from TOSHIBA. The current rating is 100 A and the voltage rating is 1200 V. The power circuit, the IGBT driver card as well as the monitor and diagnosis card were designed by a local company. The converters were stripped of their control electronics and instead a user interface card was added. This allows the user to design the control algorithms. The states of the transistors are controlled by applying either +7.5 ... +15 V (upper transistor on, lower transistor off), -15 ... -7.5 V (upper transistor off, lower transistor on) or -7.5 ... +7.5 V (both transistors off).

Transistor Mode of Operation

If the switched reluctance machine is running at speeds below base speed, the back emf is not enough to limit the current. Chopping of the current is therefore necessary. Without going into details of machine dynamics, the power electronics mode of operation is described. In Fig. 2.5 the two different states of the electrical energy converter utilising "hard chopping", is seen. In Fig. 2.5 (a) both transistors are switched on and the full DC link voltage is applied to the coil. To limit the current, both transistors are switched off and the coil sees the full negative DC link voltage and the decreasing current is freewheeling through the diodes. This is seen in Fig. 2.5 (b). During this period, most of the energy is fed back to the DC link capacitor. The reason "hard chopping" is used throughout this thesis is that this provides the best possibility to shape the current waveform. Shaping the current waveform is crucial in accomplishing smooth torque operation. This is explained in Chapter 4.

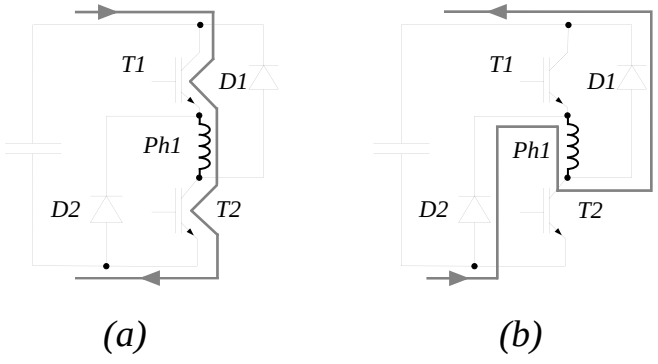

Fig. 2.5 *Electrical energy converter transistor operation. In (a) both transistors are turned on and in (b) they are turned off.*

3

Machine Dynamics

To properly design a torque controller for a switched reluctance machine it is crucial to understand the origin and magnitude of reluctance torque in magnetic systems. A complete description of the origin of the reluctance torque is found in (Slemon, 1966). In this chapter, torque in non-linear singly excited magnetic systems (such as a switched reluctance machine) is first described in general terms. The special case of torque in linear magnetic systems is derived from the more general expressions for torque. The laws governing reluctance torque are then applied to a switched reluctance machine with six stator poles and four rotor poles. To fully understand an electrical machine, the losses as well as the torque production capability must be known. A review of a simplified scheme for calculating iron losses in a switched reluctance machine is given together with a calculation of the copper losses.

Torque in a Nonlinear Singly Excited Magnetic System

The underlying physics in the torque production process is a very intricate and difficult subject. Electromechanical energy conversion in a rotational singly excited system, such as a switched reluctance machine will therefore be based on the energy conservation approach. The advantage of this method lies in the relatively simple expressions for the torque. The simplicity is achieved at the expense of the understanding of the physical phenomena causing the rotor to rotate. It is thus possible to determine the magnitude of the torque acting on the rotor, but reveals nothing about the force density distribution.

Consider the magnetic system in Fig. 3.1. It consists of a stationary iron core wound with a number of turns connected to an external electrical system. An iron rotor which is free to rotate around a horisontal shaft is placed in the airgap. The goal is to find the torque acting on the rotor as a function of the properties of the magnetic material and the source characteristics.

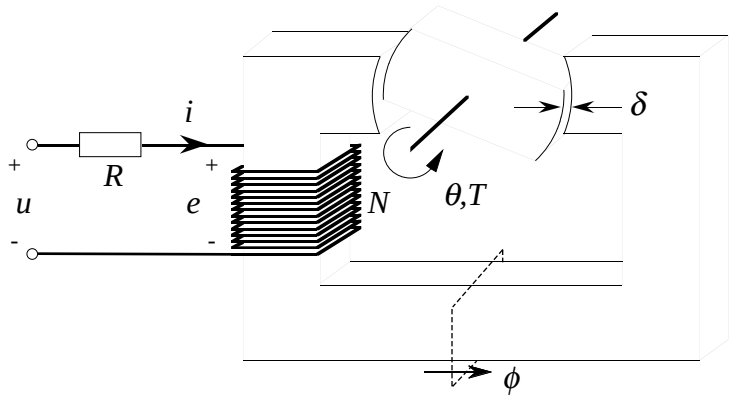

Fig. 3.1 *Electromagnetic system with a rotor free to rotate around the shaft indicated in the figure.*

For any rotor angular position, the law of conservation of energy requires that

$$\begin{matrix}\textit{energy}\\ \textit{input}\end{matrix} = \begin{matrix}\textit{energy}\\ \textit{lost}\end{matrix} + \begin{matrix}\textit{increase in}\\ \textit{stored energy}\end{matrix} + \begin{matrix}\textit{energy}\\ \textit{output}\end{matrix} \tag{3.1}$$

Supposing that we allow an incremental angular rotation, $d\theta_r$, the increments of the energy input, energy loss, storage energy and mechanical output energy are related by

$$dW_{elec.} = dW_{loss} + dW_{stored} + dW_{mech.} \tag{3.2}$$

The energy losses in the system consist of resistive copper losses, iron core losses and friction losses. If the resistance in the winding is lumped to one parameter and assigned to the electrical side while the friction in the same way is assigned to the mechanical side, and the iron losses are assumed to be zero, the result is a lossless magnetic energy storage system, that is

$$dW_{loss} = 0 \tag{3.3}$$

The relationship between the magnetic field strength, *H*, and the magnetic flux density, *B*, is a two valued function known as the hysteresis curve.

Changes of the magnetic state of the circuit depend on the history at which the circuit arrived to its current magnetic state. A dehysterised curve is formed from the hysteresis curve by taking the mean value of the hysteresis loop, and the hysteresis losses are ignored. The magnitude of the eddy currents induced in the iron depends on the time interval between two different magnetic states. If the time interval between two magnetic states is very short, high eddy currents are induced and the losses depend on the resistivity and the geometry of the iron. In electrical machines thin laminations of high grade electrical steel are used. Considering the relatively low frequency used in most electrical machines, assigning zero iron losses when deriving an expression for the torque is not a serious restriction.

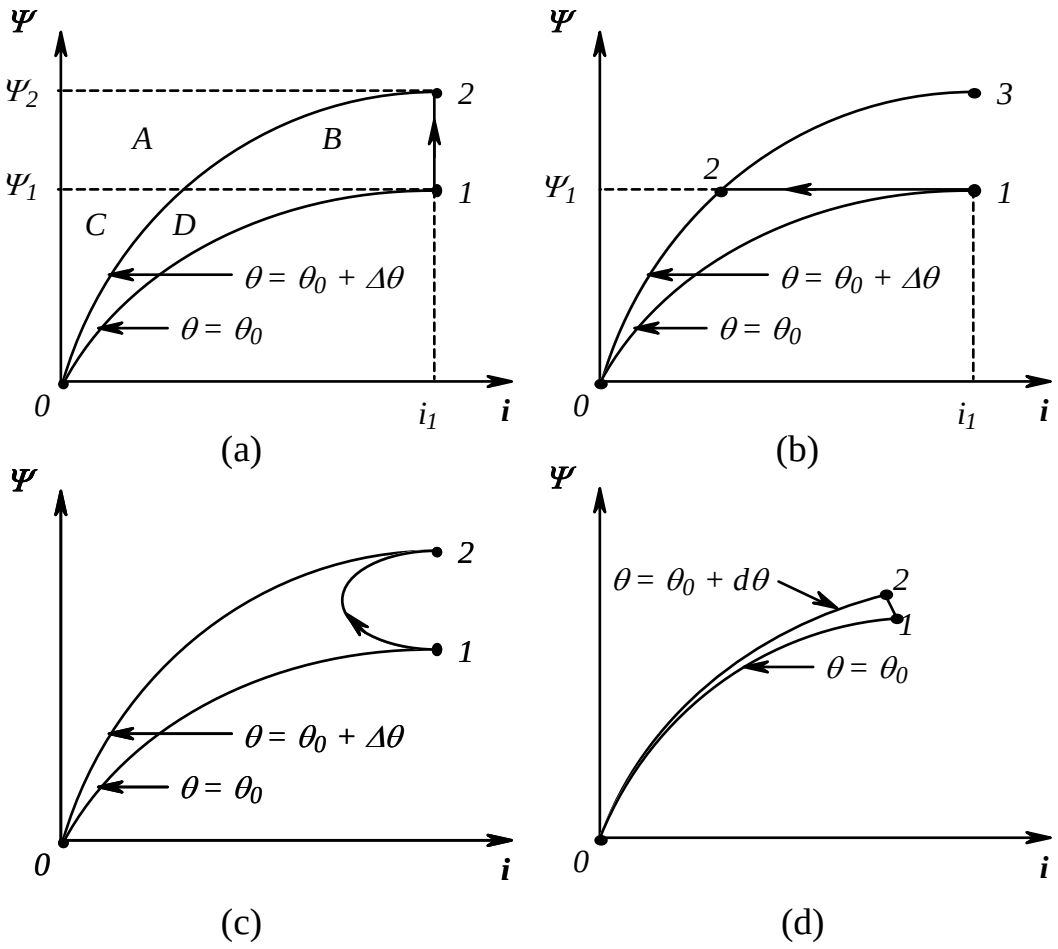

Fig. 3.2 *(a) displacement with constant current, (b) displacement with constant flux linkage, (c) general locus during displacement, (d) infinitesimal displacement.*

In Fig. 3.2 (a), the relationship between the flux linkage and current for the rotor angular position $\theta=\theta_0$ is shown. First, the current is increased to the value i_1 with $\theta=\theta_0$. Secondly, the rotor is rotated very slowly an increment $\Delta\theta$. During this slow rotation the induced voltage in the coil is negligable and therefore the current remains almost constant. The Ψ-i locus is moving from point 1 to point 2. During this rotation the energy balance of equation (3.1) must be satisfied. The electrical energy input during this displacement is

$$\Delta W_{elec.} = \int_{\Psi_1}^{\Psi_2} id\Psi = area(A+B) \tag{3.4}$$

The increase in stored energy is the stored energy at point 2 minus the stored energy at point 1. The stored energy at point 1 is equal to the electrical energy input to increase the current from zero to i_1 at constant rotor angular position θ_0, which means that

$$W_{stored,1} = \int_{0}^{\Psi_1} id\Psi = area(C+D) \tag{3.5}$$

In the same way, the stored energy at point 2 is equal to the electrical energy input to increase the current from zero to i_1 at the angular position $\theta_0+\Delta\theta$, and

$$W_{stored,2} = \int_{0}^{\Psi_2} id\Psi = area(A+C) \tag{3.6}$$

The increase in stored energy is

$$\Delta W_{stored} = W_{stored,2} - W_{stored,1} = area(A-D) \tag{3.7}$$

The assumption of a lossless rotation leads to the conclusion that

$$\Delta W_{mech.} = \Delta W_{elec.} - \Delta W_{stored} = area(B+D) \tag{3.8}$$

This area represents an inrease in the coenergy

$$\Delta W_{mech.} = \Delta W_{coenergy} \tag{3.9}$$

which is defined as

$$\Delta W_{coenergy} = \Psi di \tag{3.10}$$

It is also useful to consider the case when the rotation from point 1 to 2 takes place very rapidly. The flux linkage does not change much but the rate of change of flux linkage is high, causing a considerably high induced voltage. This voltage reduces the current, as seen in Fig. 3.2 (b). During the rotation the flux linkage is almost constant which means that no energy is supplied fom the source and the energy needed for the rotation is taken from the stored magnetic energy in the airgap, so

$$\Delta W_{mech.} = -\Delta W_{stored} = -\left(\int_{0 \to 2}^{\Psi_1} id\Psi - \int_{0 \to 1}^{\Psi_1} id\Psi \right) \tag{3.11}$$

which is the area (*D*). This area represents a decrease in the stored energy. After the rotor has reached point 2 the current can rise towards the stationary value i_1 at point 3. During this period all of the input energy is stored in the magnetic field.

In Fig 3.2 (c) a general Ψ-i locus is represented. The shape of the locus depends both on the external mechanical system and the source. The mechanical output energy is represented by the area inside the flux linkage - current trajectory.

The torque at a specific rotor angle is found if the mechanical output energy during an incremental rotation is divided by the angular increment letting the angular increment become infinitesimally small. If the flux linkage is considered to be constant during an infinitesimal rotation the torque is found from

$$T = - \left. \frac{\delta W_{stored}}{\delta \theta_r} \right|_{\Psi = const} \tag{3.12}$$

However, the torque can also be found from the change of coenergy if the current is considered constant

$$T = \left.\frac{\delta W_{coenergy}}{\delta \theta_r}\right|_{i=const} \tag{3.13}$$

Both these ways of expressing the torque are equal. Equation (3.12) is more convenient when the current is expressed as a function of flux linkage for the magnetic system and equation (3.13) leads to easier calculations when the flux linkage of the system is expressed as a function of the current, especially if we want an answer where the torque is a function of current.

Torque in a Linear Singly Excited Magnetic System

From Faraday's law an induced voltage, *e*, arises from a change in the flux linkage

$$e = \frac{d\Psi}{dt} \tag{3.14}$$

which is defined as the actual flux in the core ϕ multiplied by the number of turns *N* linking the actual flux,

$$\Psi = N\phi \tag{3.15}$$

In a linear magnetic system, the flux linkage is proportional to the current in the windings and the constant of proportionality is the inductance *L*,

$$\Psi = Li \tag{3.16}$$

At any stationary rotor angular position, θ_r, the amount of stored energy is equal to

$$W_{stored} = \int_0^{\Psi} id\Psi = \int_0^{\Psi} \frac{\Psi}{L} d\Psi = \frac{1}{2}\frac{\Psi^2}{L} = \frac{1}{2} i\Psi \tag{3.17}$$

Equation (3.17) holds for any rotor angular position and

$$dW_{mech.} = dW_{elec.} - dW_{stored} \tag{3.18}$$

The differential electrical energy input is

$$dW_{elec.} = eidt = id\Psi \tag{3.19}$$

and the differential stored energy is derived from equation (3.17)

$$dW_{stored} = \frac{1}{2} i d\Psi + \frac{1}{2} \Psi di \tag{3.20}$$

The torque acting on the rotor is given by

$$T = \frac{dW_{mech.}}{d\theta_r} = \frac{1}{2} i \frac{d\Psi}{d\theta_r} - \frac{1}{2} \Psi \frac{di}{d\theta_r} \tag{3.21}$$

Equation (3.16) is substituted into equation (3.21) to eliminate the flux linkage term and the torque can be rewritten in terms of current and inductance

$$T = \frac{1}{2} i(i \frac{dL}{d\theta_r} + L \frac{di}{d\theta_r}) - \frac{1}{2} Li \frac{di}{d\theta_r} = \frac{1}{2} i^2 \frac{dL}{d\theta_r} \tag{3.22}$$

For a linear magnetic singly excited system, such as the one in Fig. 3.1, the torque acting on the rotor is proportional to the current squared and the rate of change of the inductance.

The torque can also be expressed in terms of the magnetic reluctance R, which is defined by the relationship between the magnetomotive force F, and the magnetic flux ϕ,

$$F = R\phi \tag{3.23}$$

The magnetomotive force is equal to the number of turns N multiplied with the current i which gives an expression for the current

$$i = R \frac{\Psi}{N^2} \tag{3.24}$$

Substituting this expression for the current into equation (3.21) and evaluating gives

$$T = -\frac{1}{2} \phi^2 \frac{dR}{d\theta_r} \tag{3.25}$$

The negative sign indicates that the torque is always acting in such a direction as to reduce the reluctance of the magnetic system.

Torque in a Switched Reluctance Machine

This section provides information on the average torque production capability for a switched reluctance machine consisting of six stator poles and four rotor poles. Various methods for computing the instantaneous torque from non-linear magnetisation data can be found in (Stephenson et al, 1979).

For a non-linear magnetic system such as the switched reluctance machine the most important characteristic is the flux linkage as a function of the current supplied to the coil. This function is calculated or measured at equidistant rotor angular positions between the unaligned and aligned position. The aligned and unaligned rotor angular position as well as the position at beginning of overlap are shown in Fig. 3.3.

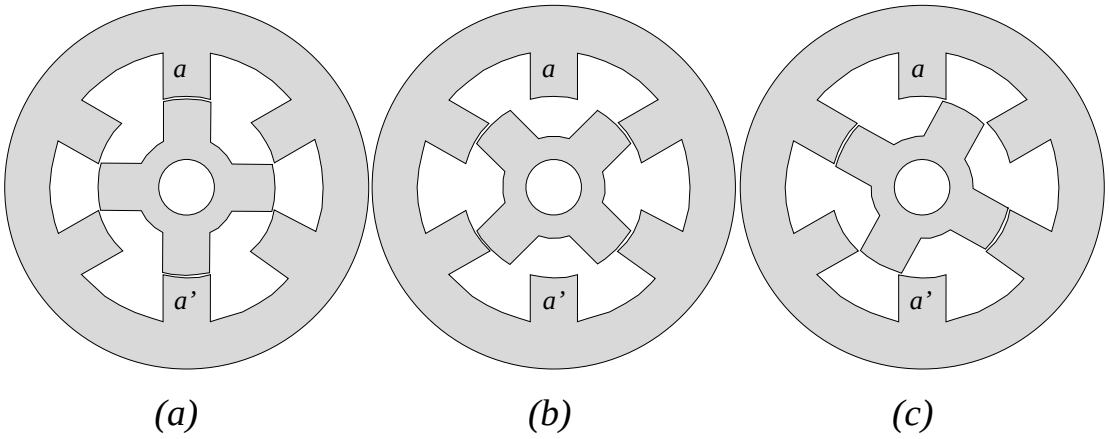

Fig. 3.3 *A cutaway view of a switched reluctance machine magnetic circuit showing in (a) the aligned rotor position, in (b) the unaligned rotor position and in (c) the position at the beginning of overlap for phase a.*

Fig. 3.4 shows the flux linkage as a function of the current at three different rotor angular positions. The lower curve represents the unaligned position, the upper curve the aligned position and the curve in between these two represents a rotor angular position where the commutation takes place.

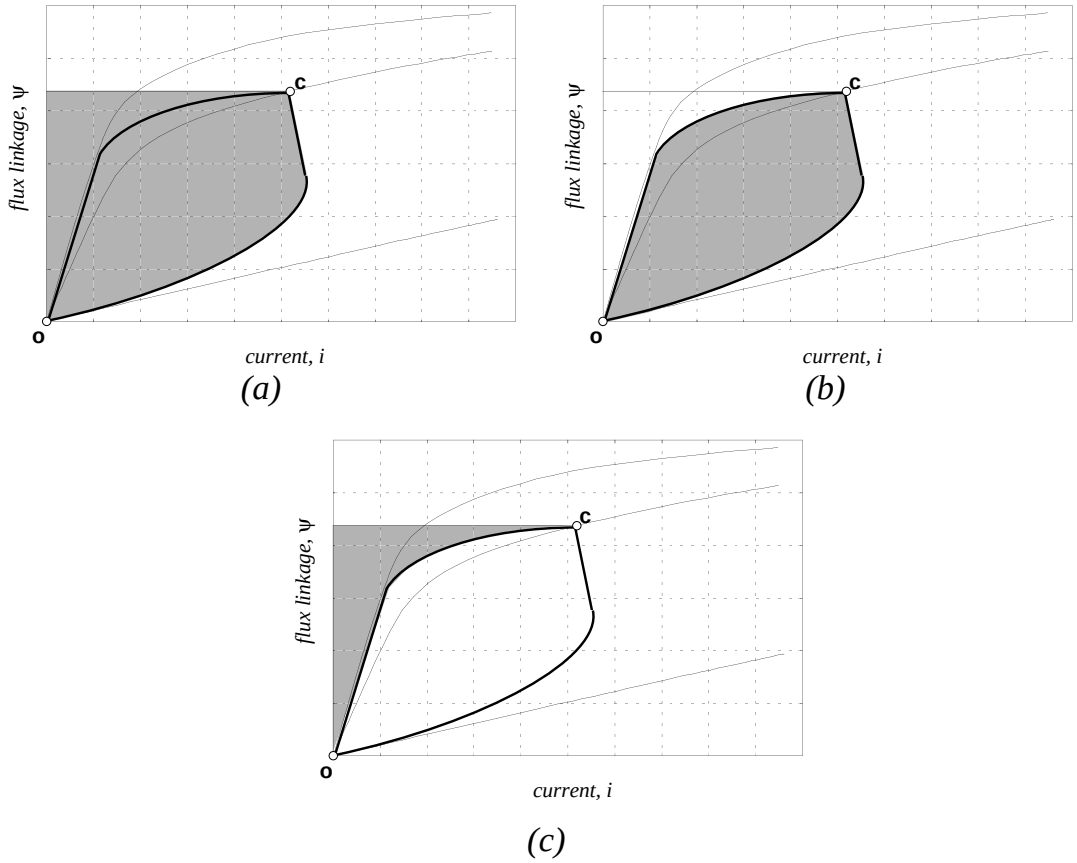

Fig. 3.4 *Flux linkage current trajectories showing in (a) the total supplied electrical energy during one energy conversion. The energy converted into mechanical work is seen in (b) and the energy which is returned to the supply is seen in (c).*

Fig. 3.4 (a) - (c) also provides an intuitive understanding of an energy conversion process during one stroke. Assume that the operation point of interest is rated speed and torque. Before start of overlap both transistors are switched on (denoted by **o** in Fig. 3.4 (a) - (c)), and the full DC link voltage is applied to the coil. The current is rising fast. At the same time the inductance is increasing contributing to an increasing back emf. The back emf rises until it reaches the same amplitude as the DC link voltage and the current derivative becomes zero. The back emf might even be slightly higher than the DC link voltage, forcing the current to decrease. At some rotor angular position, (denoted by **c** in Fig. 3.4 (a) - (c)), both transistors are turned off and the current decreases to zero under the influence of the full negative DC link voltage. During this energy conversion process, the total amount of supplied electrical energy is seen as the shaded area in Fig. 3.4 (a). The total amount of energy converted into mechanical work is the shaded area in Fig. 3.4 (b) and the energy that is fed back to the supply is the shaded area in Fig. 3.4 (c).

For a switched reluctance machine with three phases, m=3, and four rotor poles, N_r=4, the number of strokes, or energy conversions, per revolution is

$$m \cdot N_r = 12 \tag{3.26}$$

The energy converted to mechanical work in one revolution is 12 times the area of one energy conversion loop or

$$W_{mech.} = m \cdot N_r \cdot \oint \psi di \tag{3.27}$$

The mechanical energy during one revolution can be written as

$$W_{mech.} = \int_0^{2\pi} T_{avg.} d\theta = 2\pi T_{avg.} \tag{3.28}$$

so the exprssion for the average torque is found from combining equation (3.27) and (3.28) as

$$T_{avg.} = \frac{mN_r}{2\pi} \oint \psi di = \frac{12}{2\pi} \oint \psi di \tag{3.29}$$

Iron Losses

The iron losses constitute an important fraction of the losses in electrical machines. The objective of this section is to calculate the iron losses in the switched reluctance machine in stationary operation at rated conditions (rated load and speed). The time variation of the magnetic flux density in one pair of diametrically opposite stator poles is extracted from simulations and from this the magnetic flux density in all other parts of the machine is synthesised. The calculation of iron losses in a switched reluctance machine is complicated since the variation of the magnetic flux density is non-sinusoidal, in some parts of the machine the magnetic flux density varies centered around a large bias and finally because the poles in the machine can be heavily saturated. Moreover, the exciting current contains a high frequency ripple due to the transitor switching. The models for the iron losses can either be empirical or based on the solution of Maxwell's equations. Only a limited amount of papers have addressed the problem of calculating the iron losses in switched reluctance machines. An approach based on finite element calculations for a switched reluctance machine with four stator poles and two rotor poles is given in (Boivie, 1995). If the flux

density variation in every part of the machine is known, the time variation of the magnetic flux density can be Fourier transformed. The iron losses associated with the individual frequency components can be found from loss data given by the iron lamination manufacturers. This approach is taken in (Materu et al, 1988). An attempt, based on empirical equations, to include the iron losses due to the high frequency current ripple is given in (Hayashi et al, 1994).

Hysteresis Losses

Calculations of the iron losses are based on the theory of separation of losses, which means that the losses are divided into hysteresis losses and dynamical (eddy current) losses,

$$P_{Fe} = P_{Fe,h} + P_{Fe,e} \tag{3.30}$$

The hysteresis losses are calculated using the area of the quasi-static hysteresis loop multiplied with the frequency. In Fig 3.5 a quasi-static magnetisation curve is shown.

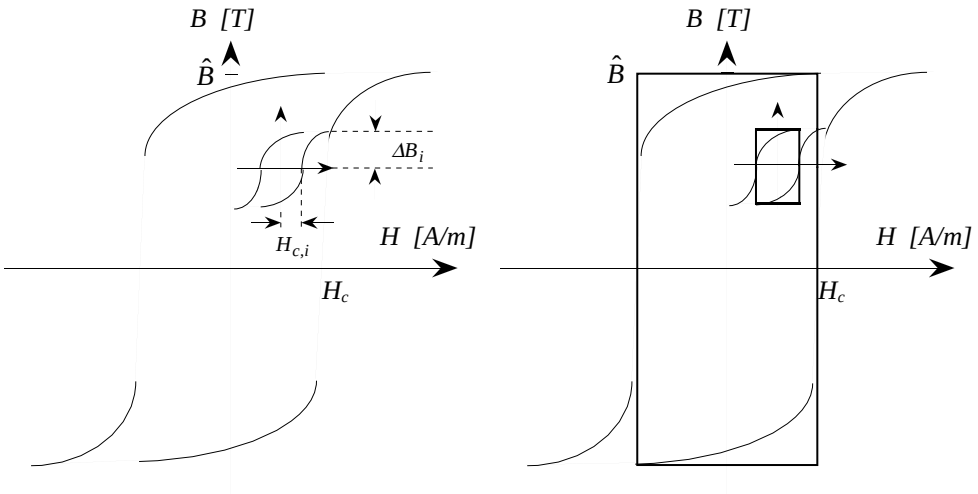

Fig. 3.5 *Magnetic flux density as a function of magnetic field strength, showing the major loop and one minor loop. The solid rectangular shaped box to the right indicates the area used for iron hysteresis loss calculations.*

Note that the hysteresis loop width is greatly exaggerated. The area within the hysteresis loop is approximated with a rectangular box and the area is given by the maximum flux density $\hat{B}$ multiplied by the coercive force H_c times four,

$$P_{Fe,h} = 4\hat{B}H_c f \tag{3.31}$$

where f is the frequency. The loop that is followed depends on the maximum flux density. Observations of hysteresis curves for iron laminations reveal that the coercive force increases fast with increasing flux densities at low values of the peak flux density. As the peak flux density is increasing even further, the coercive force is not rising that fast. The assumption made here is that the coercive force is related to the maximum flux density as

$$H_c = H_{c,\max}(1 - e^{-\hat{B}/0.4}) \tag{3.32}$$

Combining equation (3.31) and (3.32) gives the expression for the hysteresis losses in W/m^3. Dividing with the density ρ of the material yields the losses in W/kg.

$$P_{Fe,h} = \frac{4H_{c,\max}}{\rho}(1 - e^{-\hat{B}/0.4}) f\hat{B} \tag{3.33}$$

In some parts of switched reluctance machines the flux density varies with a large bias. A large bias tends to increase the hysteresis losses because the area encircled for a given peak-to-peak flux density is bigger if the variation takes place centered around a bias than around zero. The following empirical rule is found in (Köfler, 1990) to be valid for various qualities of iron laminations,

$$P_{Fe,h(biased)} = P_{Fe,h(unbiased)}(1 + k_{dc}B_{dc}^3) \tag{3.34}$$

where the constant k_{dc} is a material constant depending on the quality of the iron.

Eddy Current Losses

The objective of this section is to calculate the iron eddy current losses in the switched reluctance machine in stationary operation at rated conditions (rated load and speed). A simple model for the eddy current losses is used. If a perfectly homogenous magnetisation is assumed it can be shown (Boivie, 1995) that for an iron lamination of thickness d and conductivity σ and for frequencies where the skin effect is negligable the eddy current losses term can be written as

$$P_{Fe,e} = \frac{\pi^2 \sigma d^2}{6\rho} f^2 \hat{B}^2 \tag{3.35}$$

The eddy current loss term can be rewritten (Miller, 1993) by noticing that for a sinusoidally varying magnetic flux density B the average of $(dB/dt)^2$ is

$$\left(\frac{dB}{dt}\right)^2\Bigg|_{average} = 2\pi^2 f^2 \hat{B}^2 \tag{3.36}$$

Combining equation (3.35) and (3.36) gives

$$P_{Fe,e} = \frac{\sigma d^2}{12\rho}\left(\frac{dB}{dt}\right)^2_{average} \tag{3.37}$$

Knowing the time function of the magnetic flux density in every part of the machine, it is possible to calculate the total losses in the machine as the sum of the losses in each part multiplied by the weight of the individual parts.

Flux Density Waveforms

In order to succesfully determine the iron losses in the machine, the flux density variation in every part of the machine must be known. Therefore, the machine is divided into 20 different parts as seen in Fig. 3.6 and each part is assigned a positive reference direction. Clockwise rotor rotation is assumed. This approach represents a compromise between simplicity and accuracy. The derivation of the flux density waveforms is given in (Lawrenson et al, 1980). If the flux density variation in the stator poles are known, it is possible to construct the flux density variation in all other parts by appropriate summation (with respect to phase and sign) of the stator pole flux density variations.

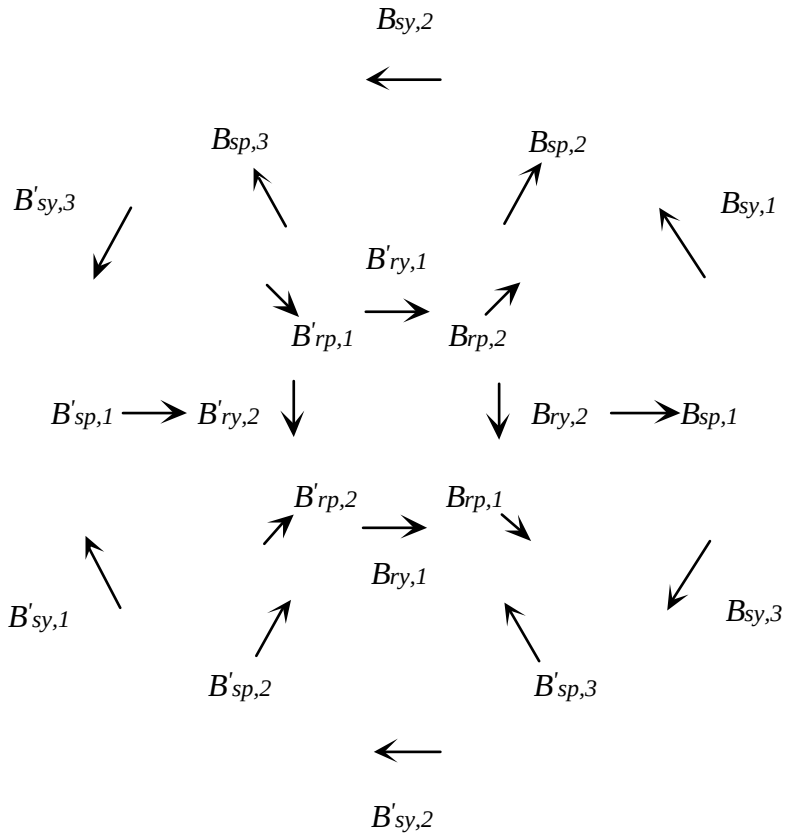

Fig. 3.6 *Definition of the magnetic flux density in the machine.*

At rated speed and load the machine is running in "single puls" operation. Rated speed, also known as base speed, is the maximum speed at which the machine can deliver rated torque. At this operating point both transistors are turned on at a specific rotor angular position in the start of the energy conversion process and turned off at another specific position in the end of the energy conversion process. During the *on* time the full DC link voltage is applied to the coil and during the *off* time the coil sees the full negative DC link voltage. It is then possible to conclude (if the resistive voltage drop is neglected) that the flux linkage rises and falls linearly with rotor position. From simulations of the machine the flux linkage in phase 1 as a function of the rotor position is extracted, which reveals that this assumption is correct. If the flux linkage for phase 1 is divided by the number of turns and the stator pole cross sectional area, the result is the average flux density variation in the stator pole. The local flux density in the stator pole can differ from this average value since during overlap between a stator pole and a rotor pole local saturation of the pole tips takes place. This is a restriction that has to be born in mind when the losses are quantified.

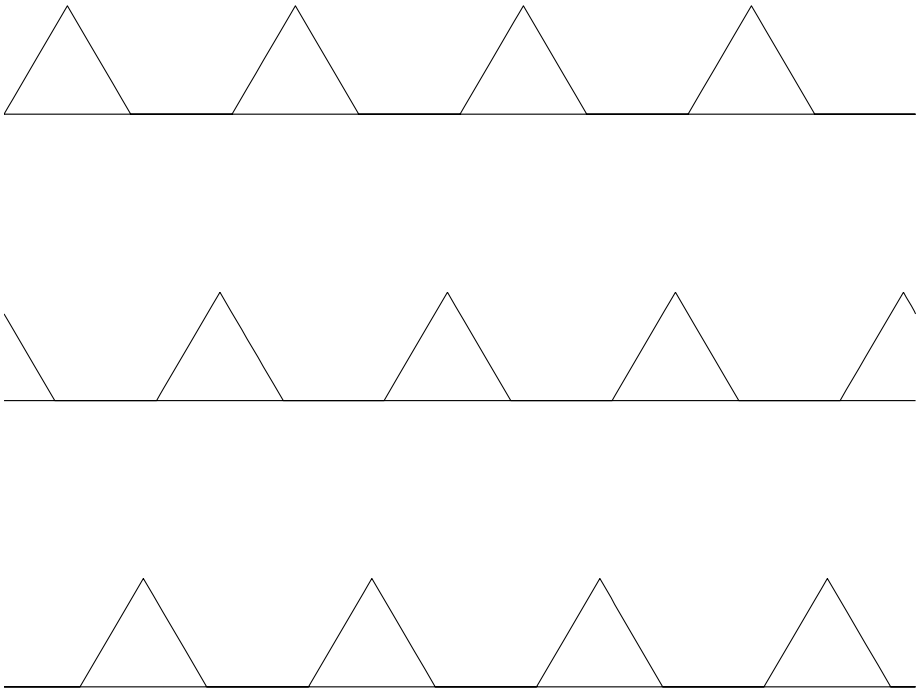

Fig. 3.7 *Stator pole flux density $B_{sp,1}$ (top), $B_{sp,2}$ (middle) and $B_{sp,3}$ (bottom).*

In Fig. 3.7 the principle stator pole flux density variation in all the stator poles are given. The curves for $B_{sp,2}$ and $B_{sp,3}$ are constructed by shifting the curve for $B_{sp,1}$ 60 degrees and 120 degrees, respectively.

Assume that the winding polarities of the phases coincide with the reference direction of the stator poles in Fig. 3.6, in other words that the phases produce flux in the positive reference direction of the stator poles. If the stator yoke width is assumed to be equal to half the stator pole width, the flux density in the stator yoke $B_{sy,3}$ is given by

$$B_{sy,3} = B_{sp,1} + B_{sp,2} + B_{sp,3} \tag{3.38}$$

and

$$B'_{sy,3} = B_{sy,3} \tag{3.39}$$

The stator yoke flux density $B_{sy,2}$ is given by

$$B_{sy,2} = B_{sp,1} + B_{sp,2} - B_{sp,3} \tag{3.40}$$

and

$$B'_{sy,2} = B_{sy,2} \tag{3.41}$$

Finally, the stator yoke flux density $B_{sy,1}$ is given by

$$B_{sy,1} = B_{sp,1} - B_{sp,2} - B_{sp,3} \tag{3.42}$$

and consequently,

$$B'_{sy,1} = B_{sy,1} \tag{3.43}$$

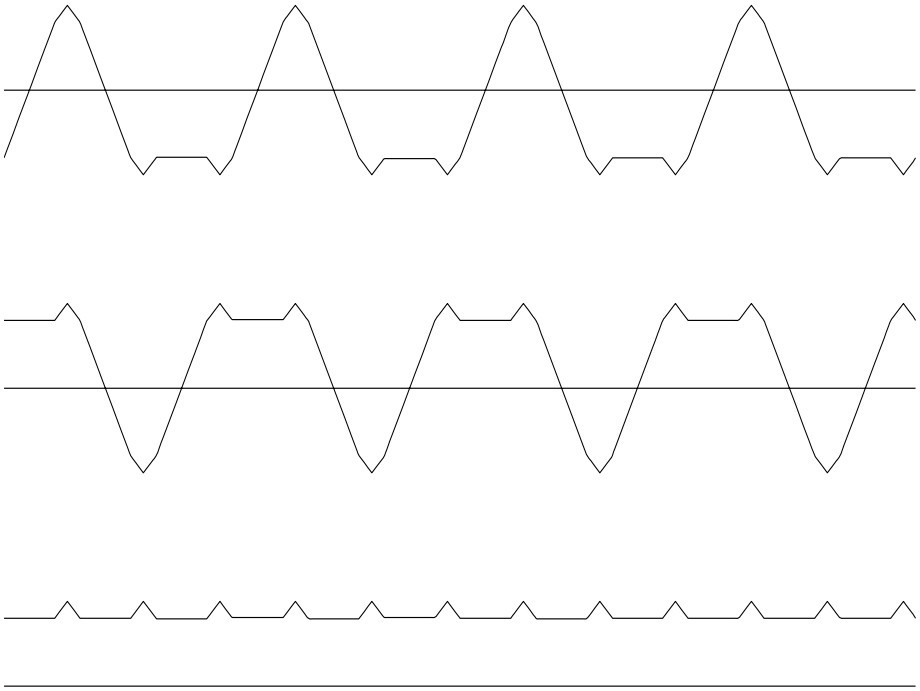

Fig. 3.8 *Stator yoke flux density variation in $B_{sy,1}$ (top), $B_{sy,2}$ (middle) and $B_{sy,3}$ (bottom).*

In Fig. 3.8, the stator yoke flux density variation for $B_{sy,1}$, $B_{sy,2}$ and $B_{sy,3}$ are shown.

The flux density in the rotor poles can be extracted from the stator pole flux density waveforms by noticing that the flux density in the rotor pole carries the same flux as the excited stator pole. Note that after half a revolution the flux reverses. The rotor pole flux density $B_{rp,1}$ and $B_{rp,2}$ are seen in Fig. 3.9. For the rotor pole flux density it is noticed that

$$B'_{rp,1} = B_{rp,1} \tag{3.44}$$

and

$$B'_{rp,2} = B_{rp,2} \tag{3.45}$$

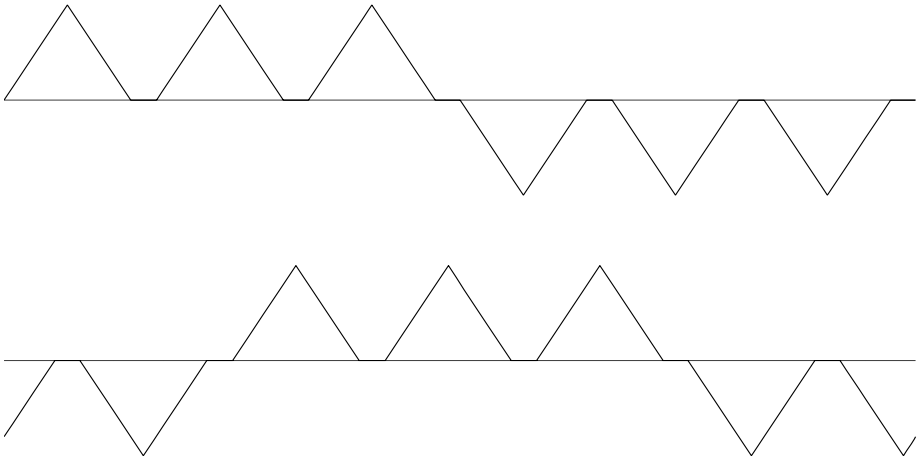

Fig. 3.9 *Rotor pole flux density $B_{rp,1}$ (top) and $B_{rp,2}$ (bottom).*

The rotor yoke flux density is constructed by direct addition of the rotor pole flux density variation, under the assumption that the rotor yoke width is equal to half the rotor pole width,

$$B_{ry,1} = B_{rp,1} + B_{rp,2} \tag{3.46}$$

and $B_{ry,2}$ is constructed by shifting $B_{ry,1}$ 90 degrees.

Note that

$$B'_{ry,1} = B_{ry,1} \tag{3.47}$$

and

$$B'_{ry,2} = B_{ry,2} \tag{3.48}$$

The rotor yoke flux density variation is seen in Fig. 3.10.

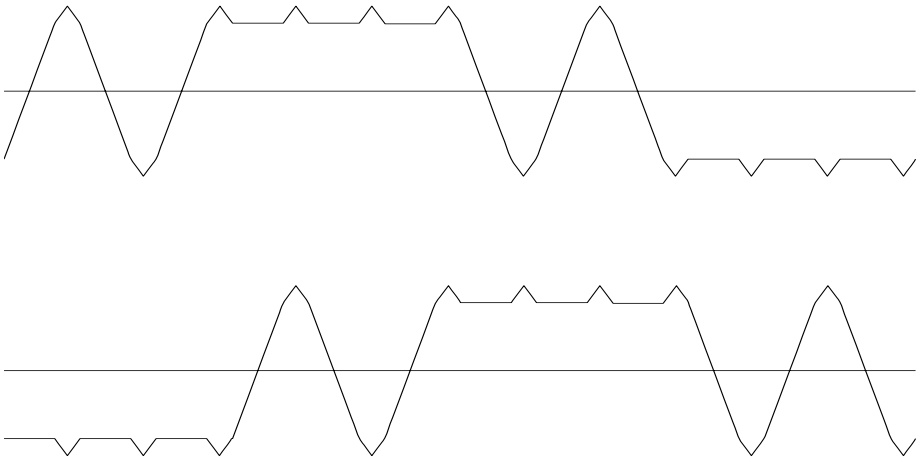

Fig. 3.10 *Rotor yoke flux density $B_{ry,1}$ (top) and $B_{ry,2}$ (bottom).*

Copper Losses

The copper losses are calculated as

$$P_{Cu} = 3 \cdot R \cdot i_{rms}^2 \tag{3.49}$$

where R is the phase resistance. Neglecting the skin effect in the winding, and using the definitions in Fig. 3.11, the resistance is given by

$$R = \rho_{cu} \frac{l_w}{A_w} = \rho_{cu} \frac{N2(\sigma l_{stk} + l_{oh})}{\pi\left(\frac{D_w}{2}\right)^2} \tag{3.50}$$

where ρ_{cu} is the copper resistivity. The length of the winding is parametrised in terms of machine geometry.

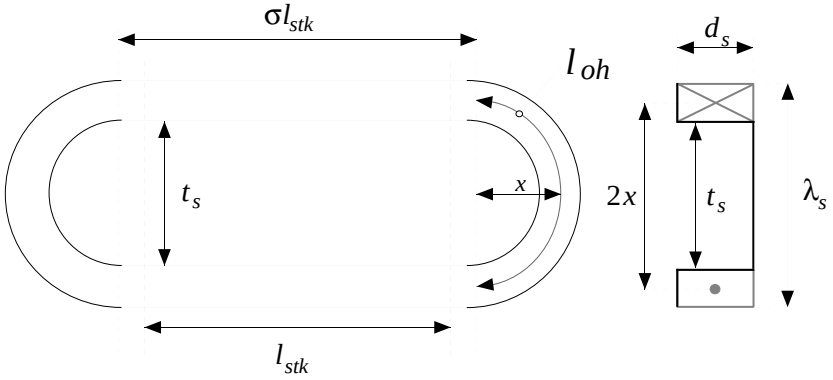

Fig. 3.11 *Definitions of parameters for calculation of the length of the winding.*

If the stator curvature is neglected, the stator slot pitch λ_s is given by

$$\lambda_s = 2\pi\left(\frac{D_r}{2} + \frac{d_s}{2}\right)\frac{1}{N_s} \tag{3.51}$$

and

$$x = \frac{t_s}{4} + \frac{\lambda_s}{4} \tag{3.52}$$

However, if the stator curvature is included it is found that the distance *x* is smaller than the one calculated with equation (3.52). In fact it can be shown (after some trigonometri) that the actual value of the distance *x* is 0.72 times the value calculated in equation (3.52).

Combining equation (3.51) and (3.52) and including the curvature yields an expression for the overhang length, l_{oh}, as

$$l_{oh} = \pi x \cdot 0.72 = \frac{\pi}{4}(t_s + \frac{\pi}{6}(D_r + d_s)) \cdot 0.72 \tag{3.53}$$

Inserting equation (3.53) into (3.50) gives an expression for the winding resistance in terms of known geometrical quantities and winding diameter.

$$R = \rho_{cu}\frac{2 \cdot N(\sigma l_{stk} + \frac{\pi}{4}(t_s + \frac{\pi}{6}(D_r + d_s)) \cdot 0.72)}{\pi\left(\frac{D_w}{2}\right)^2} \tag{3.54}$$

The copper resistivity changes with temperature according to

$$\rho_{cu}(T) = \rho_{cu,T_0}(1 + \alpha(T - T_0)) \tag{3.55}$$

T_0 is usually room temperature and the temperature coefficient α for copper is 0.00392 /K at room temperature. To accurately determine the phase resistance it is essential that the winding temperature is measured. Both the iron powder machine and the iron lamination machine are equipped with thermoelements in all three phases.

4

Torque Control

A switched reluctance machine consisting of six stator poles and four rotor poles is capable of producing smooth torque. A procedure for calculating current reference values resulting in smooth torque operation is given in (Shramm et al, 1992) for a four phase machine with eight stator poles and six rotor poles. The idea was to let the torque produced by one phase fall linearly at the same time as the torque production for the next phase rises linearly in those rotor angular intervals when more than one phase is capable of producing torque. This strategy is referred to as the constant rate of change of torque strategy. (Moreira, 1992) proposed a scheme where the torque was calculated on line based on measurements of the applied voltage and current. The calculated torque was compared with the reference torque and the error influenced the switching state of the transistors. However, the strategy to handle the rotor position interval when more than one phase is capable of producing torque was not described. (Rochford et al, 1993) describe an off line commissioning procedure where the magnetic characteristics, the flux linkage and torque as a function of rotor angular position and current, is calculated based on a series of voltage steps at different rotor angular positions. Having done that, the strategy used for smooth torque control is based on the constant rate of change of torque mentioned above. (Reay et al, 1993) describes the possibility to train neural networks on line in order to learn the current profiles needed to produce smooth torque. During the training process, torque measurement is required.

In this chapter another strategy is considered. In those intervals when more than one phase is capable of producing torque, all the possible

combinations of currents resulting in the desired torque is calculated. The combination that gives the lowest copper losses is chosen.

Smooth torque operation is however not the most efficient way of operating a switched reluctance machine with six stator poles and four rotor poles. The reason is that a lot of current has to be injected into the windings at rotor angular positions where the torque per ampere ratio is low. Nevertheless, a control strategy resulting in smooth torque operation is presented here since it is a good starting point when determining a more suitable control strategy. Having produced smooth torque it is possible to allow a specified deviation from this in a controlled manner. Allowing a certain amount of torque ripple leads to more efficient operation. Based on the smooth torque control system, a torque reference with a specified ripple is created. The shape of the ripple is sculptured to take advantage of the machine when the torque production capability is high. The idea is to take advantage of the torque per ampere ratio to scale the constant torque reference value in order to introduce a controllable torque ripple. This strategy is believed to be new and not found elsewhere in the literature. Therefore, a control strategy where the magnitude of the torque ripple can be user specified is also presented. Thus, the user can choose between smooth torque operation or high efficiency operation and all compromises in between, depending on the application. Both these methods of control are refered to as *indirect torque control*, and they are implemented in hardware specially built for evaluation purposes. This control strategy allows four quadrant operation and can be extended to switched reluctance machines having other number of phases and poles.

Hardware Design of the Controller

The idea behind the controller is to let the torque reference and the measured rotor angular position and velocity address a large memory, in which the precalculated phase current reference values are written. The phase current references are compared with the measured phase currents and the error signals are feeding three hysteresis controllers (one for each phase). Depending on the sign and magnitude of the error signals both the transistors in the corresponding phaseleg are either turned *on* or *off*.

Two controller cards have been built and they will be referred to as the *current reference generator* card and the *current regulator* card. The purpose of the current reference generator card is to look up phase current reference values based on the rotor position, rotor speed and torque

reference. The current regulator card includes hysteresis controllers for the three phase currents and produces logical signals to the IGBT drive circuits in the electrical energy converter.

The Current Reference Generator

This card includes the look-up table, A/D and D/A converters, PAL circuits programmed for adding, control logics and some additional operational amplifiers for adjusting signal levels. A block diagram of the card is shown in Fig. 4.1. A detailed description of the circuit solution, component lists and control logics program is given in (Brogren et al, 1995).

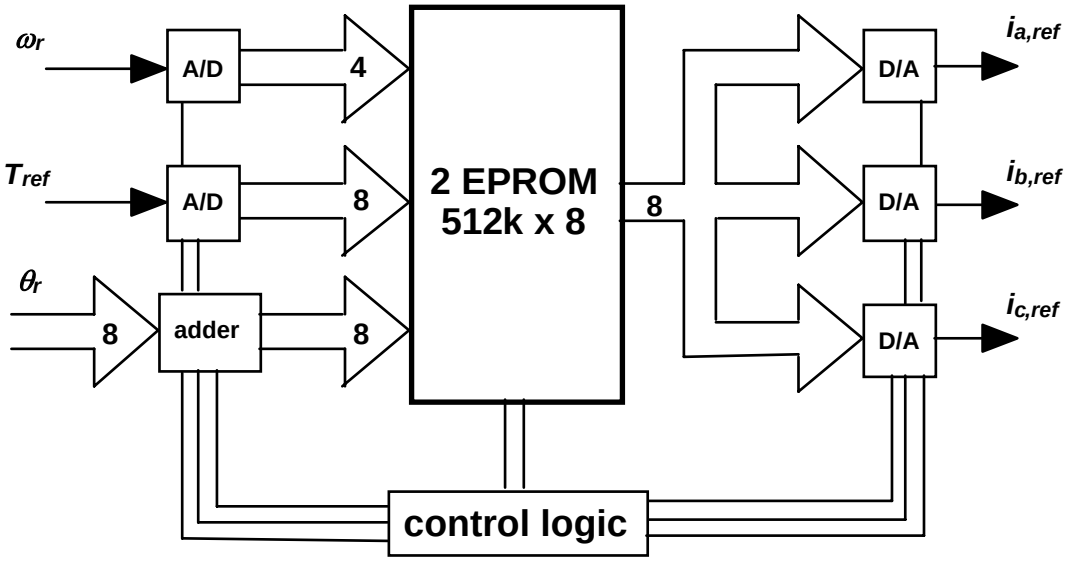

Fig. 4.1 *Block diagram of the current reference generator card showing the input and output signals and the number of bits that are used for representation.*

For a switched reluctance machine with four rotor poles it is only necessary to store current references for one 90 degree interval. The rotor angular speed and the torque reference are sampled using the two A/D converters at the input. The digital representation of these signals together with the rotor angular position address one of the two large EPROMs. The current reference value at that address is propagated to the D/A converter associated with phase *a*. In order to find the address associated with phase *b*, 120 degrees is added to the rotor angular position and modulo 90 is performed on the result. The current reference value at that address is propageted to the D/A converter associated with phase *b*. Finally, 240 degrees is added to the rotor position and modulo 90 is performed on the

result. The current reference value at that address is propagated to the D/A converter associated with phase *c*. This cycle is then repeated, and the three current reference values are fed to the current regulator card.

Eight bits are used for representing the rotor position which is given directly in digital form. With eight bits representing a 90 degree interval the rotor angular position resolution is

$$\Delta\theta_r = \frac{90}{2^8} = 0.35 \text{ degrees} \tag{4.1}$$

Eight bits are used for representing the torque reference in the interval [-35 Nm, +35 Nm]. The most significant bit is dedicated for the sign and the other seven bits represent the magnitude which results in a torque reference resolution of

$$\Delta T_{ref} = \frac{35}{2^7} = 0.27 \text{ Nm} \tag{4.2}$$

The current reference values have to be speed compensated due to the finite inductance near the aligned and unaligned position. The number of speed intervals is a compromise between resolution and memory size. Four bits are used for representing speed. The most significant bit represents the sign and the other three represent magnitude. Since the maximum speed is 4600 rpm the resolution is

$$\Delta n = \frac{4600}{2^3} = 575 \text{ rpm} \tag{4.3}$$

Eight bits are used for representing the current reference values. Maximum current reference is set to 60 A which gives a resolution of

$$\Delta i_{ref} = \frac{60}{2^8} = 0.23 \text{ A} \tag{4.4}$$

An EPROM with 20 bits input and 8 bits output is needed to fulfill the requirements above. Two EPROM with 19 bits input and 8 bits output is chosen and the sign bit of the speed is used to select which EPROM to read from. For an application where only one direction of rotation is required, one EPROM can be excluded.

The total time interval between two successive sets of output current reference values is approximately 6 μs. This short time delay enables the controller to be used for high speed applications.

The Current Regulator

This card consists of operational amplifiers used for signal level adjustment, adding, hysteresis regulator and buffer circuits for the logical signals to the IGBT gate drivers. A complete description of the current regulator card as well as component lists, circuit solutions and design is given in (Bojrup et al, 1995). The magnitude of the current ripple is controlled by varying the hysteresis width Δi in the regulator as seen in Fig. 4.2. The positive and negative time derivatives of the current are not constant during one stroke. They change as the phase inductance change, which means that the current time derivative is a function of the current magnitude and the rotor position.

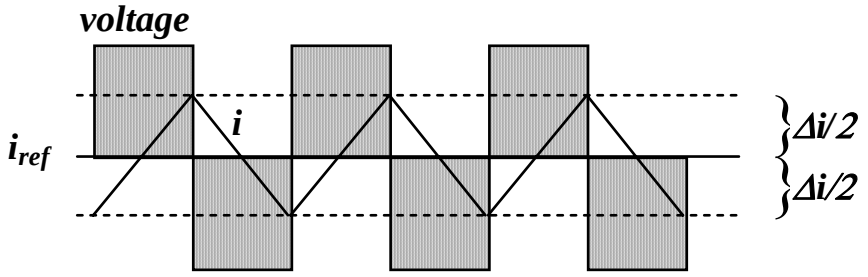

Fig. 4.2 *Principle of the hysteresis current regulator. If the current is lower than the lowest current level the corresponding phase is turned on, and if the current exceeds the upper current level the corresponding phase is turned off.*

The time delay from the input current reference values via the logical output signals to the IGBT drive circuits is approximately 2 μs.

Indirect Torque Control

Indirect torque control implies accurate measurements (or calculations) of the electrical and electromechanical characteristics of the switched reluctance machine, as well as measurements of all the phase currents. Furthermore, it requires knowlege about the rotor position and velocity. A variety of methods has been proposed for calculation of the rotor position and velocity based on measurements of the current and voltage, but since sensorless position detection is out of the scope of this thesis, the rotor position is measured using a resolver.

The flux linkage and the torque, both as a function of current and rotor angular position, must be known in advance. The term indirect refers to the fact that if the mapping of the torque as a function of current and rotor angular position is accurate, then the torque is indirectly controlled by controlling the currents in the phase windings. Producing smooth torque is a matter of shaping the waveform of the phase current references to account for the non-linear relationship between the current and torque at various rotor angular positions.

Smooth Torque Control

In Fig. 4.3 a cross sectional view of the magnetic circuit of the switched reluctance machine seen from the shaft end is shown. Positive direction of rotation is defined as clockwise rotation. The phases are labeled *a-c*. The rotor position in Fig. 4.3 is defined as 0 degrees and is incresing in the positive direction of rotation.

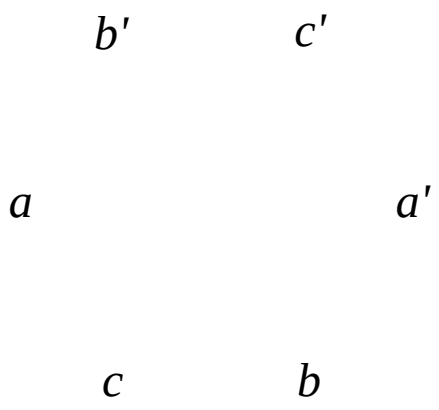

Fig. 4.3 *Cross sectional view of the switched reluctance machine as seen from the shaft end showing the definition of the phases a-c. Positive direction of rotation is defined as clockwise rotation.*

The stator and rotor pole arcs are approximately 30 degrees. This means that if one 90 degree interval is subdivided into 15 degree intervals it is possible to determine the phases that are capable of producing torque in each subinterval. As can be seen from Fig. 4.4 in every second rotor position interval two phases can contribute to the overall torque production.

If smooth torque is to be acquired, the distribution of the torque production between the phases in these intervals has to be solved. The most extreme solution is to let only one phase produce all the required torque in the interval. This will however not be very efficient. A more promising strategy for distributing the torque is to calculate all possible combinations of currents in the two phases that can produce the required torque, and choose the distribution that gives the lowest copper losses.

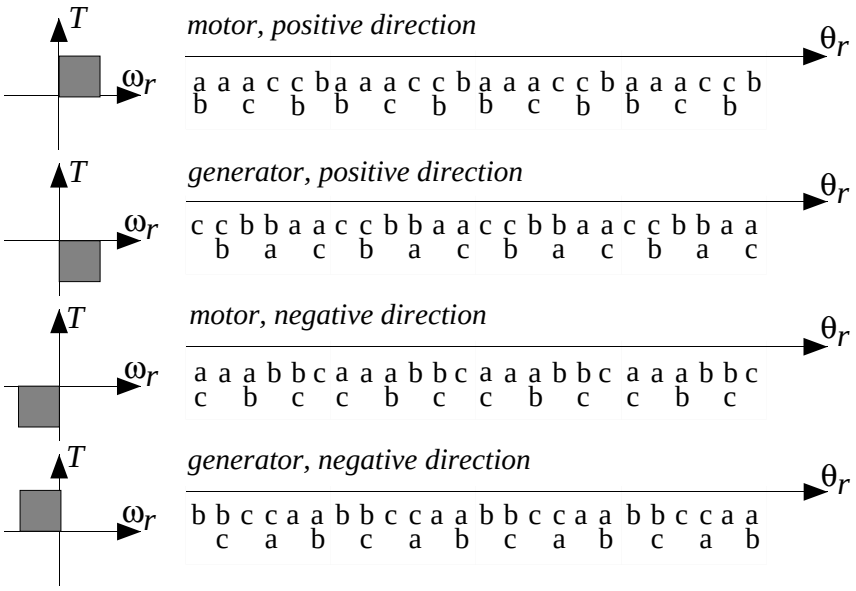

Fig. 4.4 *A table showing the phase sequence for all the four quadrants of operation. In each 15 degree interval the phases that are capable of producing torque are listed.*

A prerequisite for calculating the torque distribution between the phases is that the torque as a function of current and rotor position is known. This is not a serious restriction since this performance is always calculated in a new switched reluctance machine design. After the construction, measurements on the motor are performed, which is a standard procedure for any new machine design.

In the following chapters, smooth torque control and torque ripple limit control strategies are derived for the iron powder switched reluctance machine. Exactly the same procedure is followed when calculating tables for the iron lamination machine. The only difference lies in the input data to the procedure. The iron lamination machine has another relation between the torque and the rotor angular position and current. This difference is evident when Figs. 4.5 and 4.25 are compared.

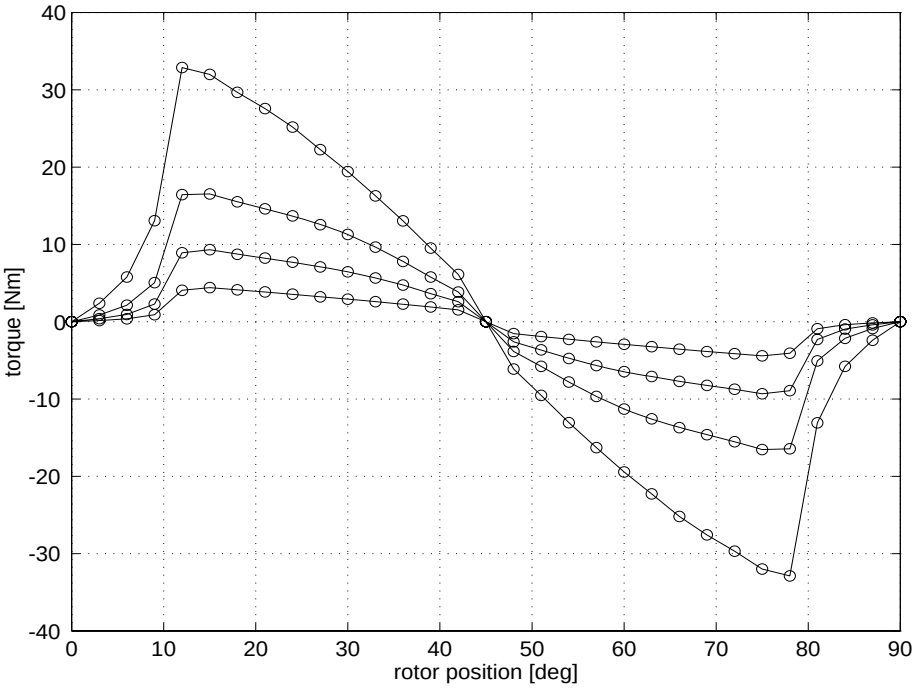

Fig. 4.5 *Torque as a function of rotor position for four different current levels (60, 36, 24, and 15 A). The operating points in the figure are calculated using a finite element program.*

Fig. 4.5 shows the calculated torque as a function of current and rotor angular position. The calculations are carried out at rotor position increments of three degrees using a finite element program, and the current levels for which the torque is calculated are (0, 3, 9, 15, 24, 36, 60) ampere. The torque for the four highest current levels are shown in Fig. 4.5.

The goal is to implement a look-up table with rotor position and torque reference as inputs and current reference values as outputs. Since eight bits will be used for both rotor position and torque reference representation, a 256 by 256 matrix from this raw calculated data is formed. This *torque matrix* is seen in Fig. 4.6 and is interpolated using the raw data.

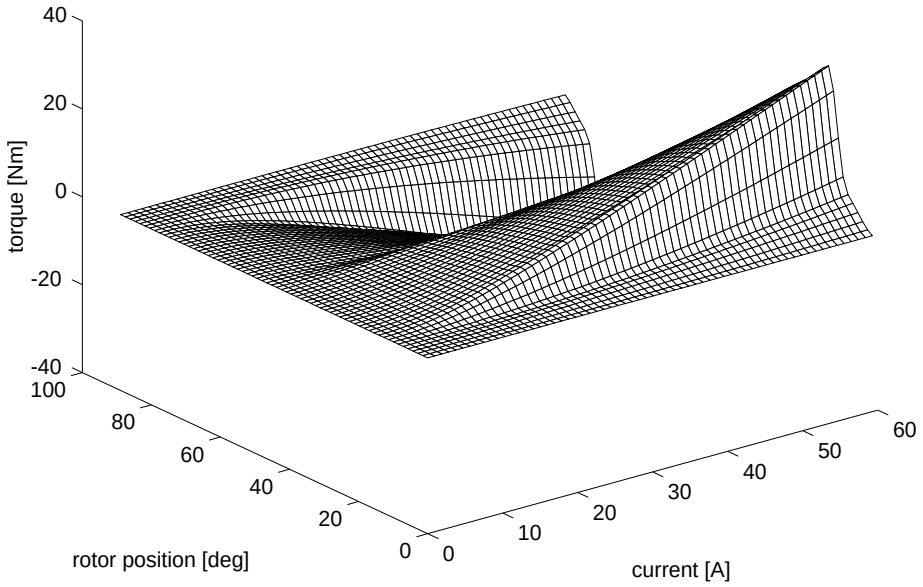

Fig. 4.6 *A 256 by 256 matrix is interpolated from the crude calculated data. This matrix shows the torque for all the possible combinations of rotor positions and currents.*

Knowing the torque as a function of rotor position and current, it is possible to rearrange this matrix to another matrix showing the current as a function of rotor position and torque. It is now possible to determine the current needed to produce a given torque in one single phase, and this matrix is given in Fig. 4.7. The current level approaches infinity for torque values other than zero near the aligned and unaligned position. That is why the matrix is restricted to 60 A.

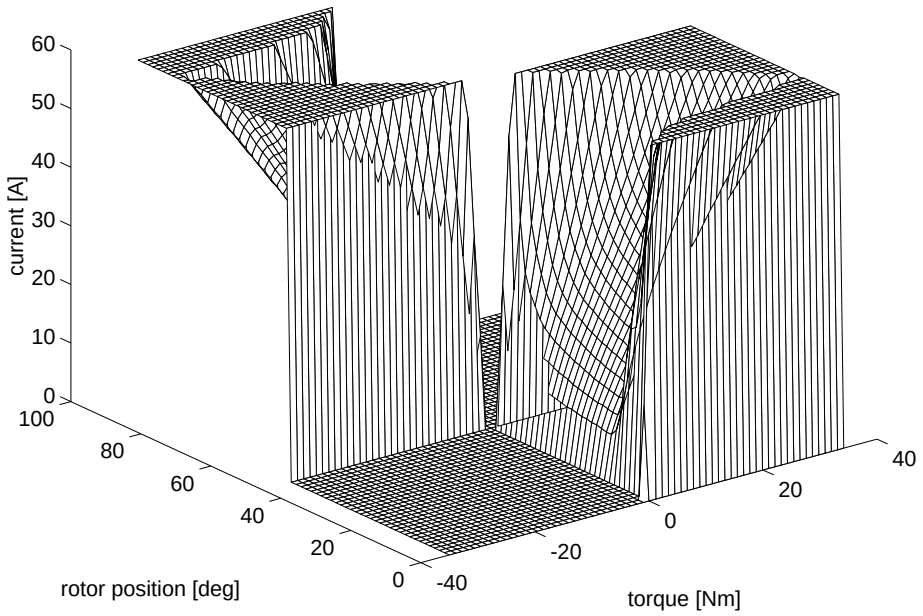

Fig. 4.7 *Currents needed to produce smooth torque with one phase only in the motoring interval [0,45] degrees and in the generating interval [45,90] degrees.*

Consider the rotor position interval [0,15] degrees. According to the definitions in Fig. 4.4, phase *b* is capable of producing torque and phase *a* is entering its torque production interval. To create a new current reference matrix that takes into account the torque distribution between the phases, for every rotor position between 0 and 15 degrees all the possible combinations that gives the desired torque are considered. The combination that gives the lowest copper losses is chosen and the corresponding current reference for phase *a* is written into the memory at the address given by the torque reference and the rotor position. The current reference for phase *b* is written into the memory at the address given by the torque reference and the rotor position plus 30 degrees. This enables all the appropriate phase current reference values to be read from the same look-up table. The matrix consisting of the current reference values where the distribution of torque between the phases is taken into account is referred to as the *current reference matrix*.

Figs. 4.8 and 4.9 show an example of the current reference matrix where the torque reference is 6.8 Nm and - 6.8 Nm, respectively. In these figures it is possible to see that it is only for a few degrees that two phases are contributing to the overall torque. The dash dotted lines in Figs. 4.8 and 4.9 represent the current needed to produce smooth torque with one phase

alone. The entire current reference matrix is shown in Fig. 4.10. If these current references are followed a smooth torque is produced and this is achieved with a minimum of copper losses. The inductance at the unaligned position sets a limit to the maximum time derivative of the current. Therefore, it is only possible to follow the references up to a certain speed.

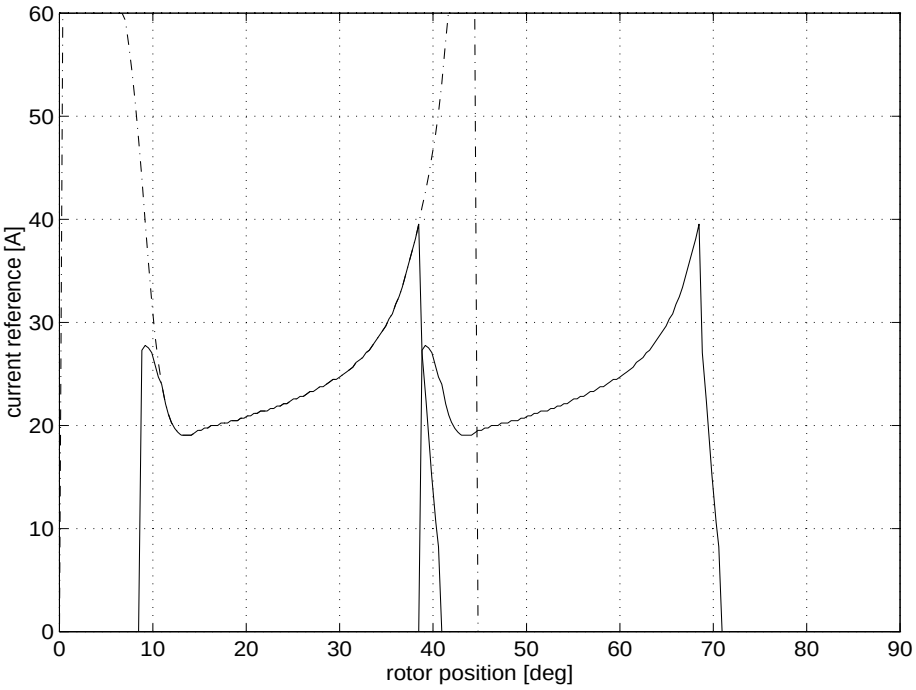

Fig. 4.8 *Current reference values for phases a and c for a torque reference of 6.8 Nm. The dash dotted line is the uncompensated current reference value for phase a alone.*

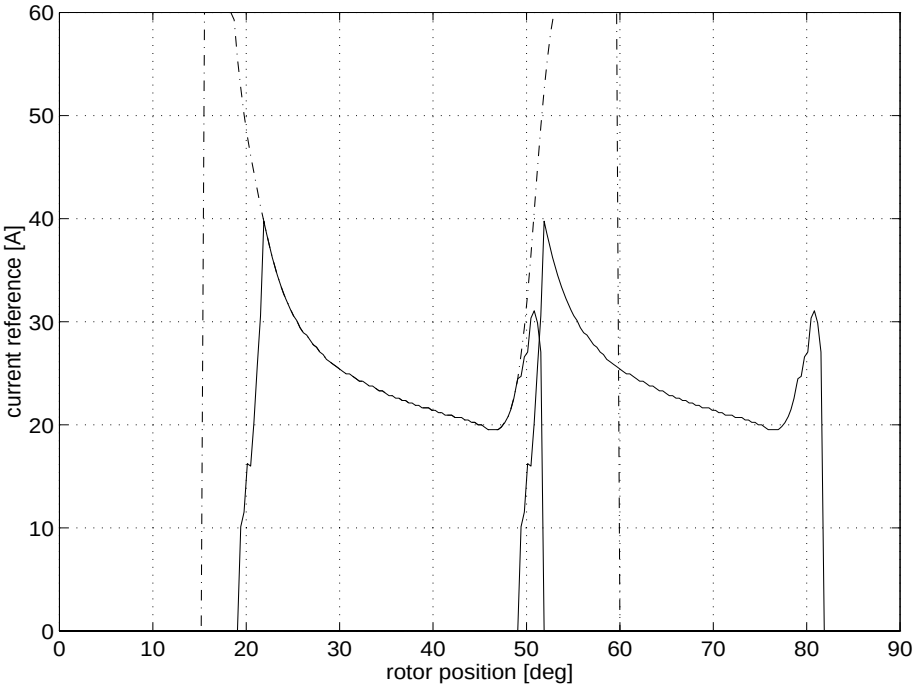

Fig. 4.9 *Current reference values for phase b and a for a torque reference of - 6.8 Nm. The dash dotted line represents the uncompensated current reference for phase b alone.*

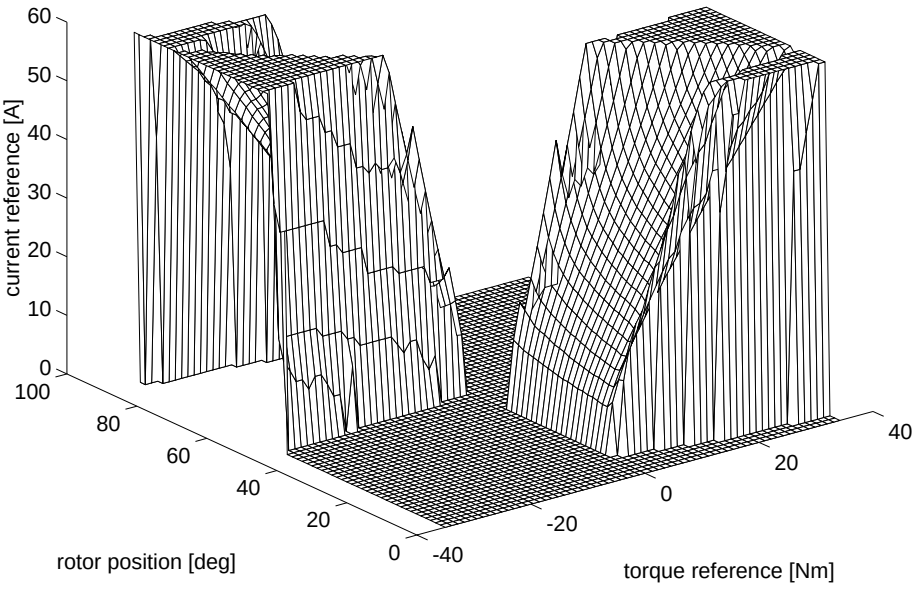

Fig. 4.10 *The entire current reference matrix. This matrix can be used in the look-up table for very low speed.*

Speed Compensation

The switched reluctance machine has to be magnetised from the stator phase coil every stroke. When the current is to be injected into the winding, the time derivative of the current is limited by the inductance. In order to follow a predefined current reference waveform, the turn-on angle for the transistors has to be advanced in the beginning of every energy conversion process. One way to do this is to look in the current reference matrix for the first current peak and integrate backwards to find the turn on angle. This can be seen in Fig. 4.11, which is an example where the torque reference is 6.8 Nm and the speed is 4600 rpm. The backward integration is based on equation (4.5), the voltage equation. The voltage during this rotor position interval is considered to be 300 Volt and the angular speed is assumed to be constant,

$$u = Ri + \frac{d\psi}{dt} = Ri + \omega_r \frac{d\psi}{d\theta_r} \approx Ri + \omega_r \frac{\Delta\psi}{\Delta\theta_r} \tag{4.5}$$

The starting current for the backward integration is known. The flux linkage as a function of current and rotor position is a non-linear function that is measured or calculated à priori. The flux linkage ψ_k is thus uniquely determined by the current i_k and the rotor position. The flux linkage decrement is calculated and subtracted from the flux linkage as in equation (4.6),

$$\psi_{k-1} = \psi_k - \Delta\psi_k, \text{ where } \Delta\psi_k = \frac{\Delta\theta_r}{\omega_r}(u_k - Ri_k) \tag{4.6}$$

The new value of the flux linkage ψ_{k-1} together with the new rotor position $\theta_{r_{k-1}}$ determines the new current i_{k-1} as seen in equation (4.7),

$$i_{k-1} = f(\psi_{k-1}, \theta_{r_{k-1}}), \text{ where } \theta_{r_{k-1}} = \theta_{r_k} - \Delta\theta_r \tag{4.7}$$

These calculations are repeated until zero current is reached, for all torque reference values in the interval [-35,35] Nm. Examples of the backward integration are found in Figs. 4.11 and 4.12, both for positive and negative torque reference values.

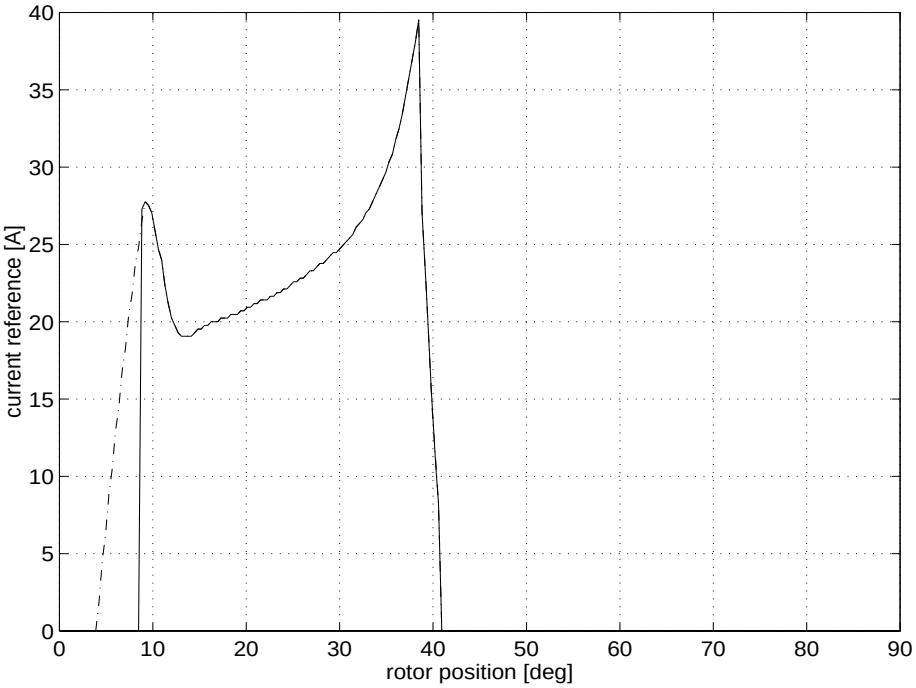

Fig. 4.11 *The dash dotted line represents the backward integration starting at the current peak. This is the fastest possible rise time of the current.*

The backward integration process is carried out for all the torque reference values and results in a *speed compensated current reference matrix*. For positive torque reference values the current is driven up at the unaligned position, where the inductance is low and not changing very much with rotor position. The current rises fast and almost linearly, as seen in Fig. 4.11. Around the aligned position, the non-linear inductance is high and changing fast with rotor position. Therefore, if the torque reference is negative the backward integration results in a current rise with a changing time derivative, as seen in Fig. 4.12. The entire speed compensated current reference matrix is seen in Fig. 4.13. This current reference matrix is used for the highest speed interval. Advancing the turn on angle in the beginning of each energy conversion contributes to the torque. Since this takes place near the aligned and unaligned position the contribution to the overall torque is small and therefore neglected.

Rotor angular speed is represented with four bits. Therefore, 16 current reference matrixes are calculated, one for each speed interval, and stored in the two EPROMs.

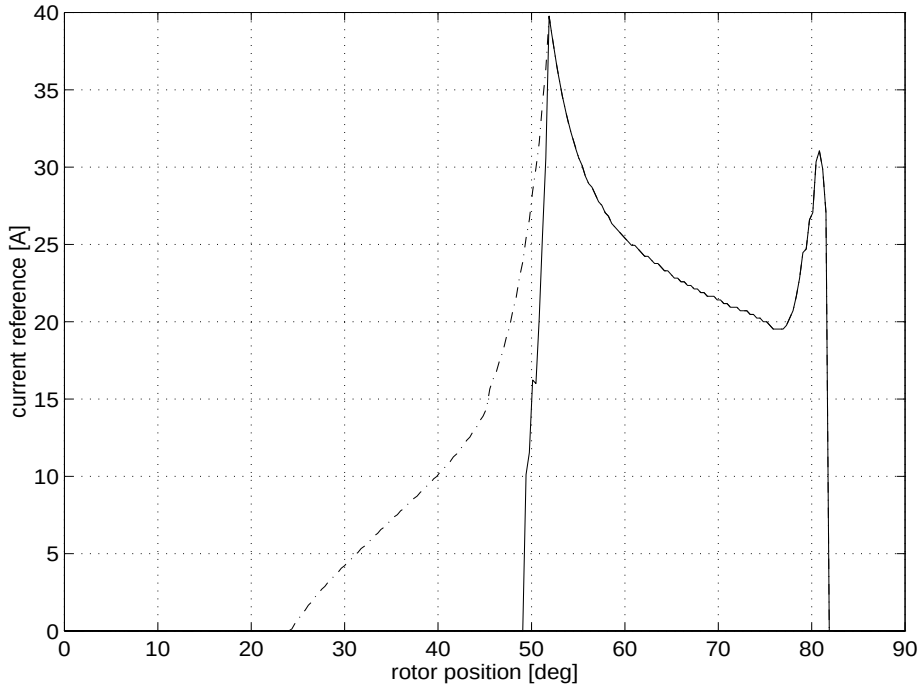

Fig. 4.12 *The dash dotted line represents the current as a result of the backward integration when the torque reference value is negative.*

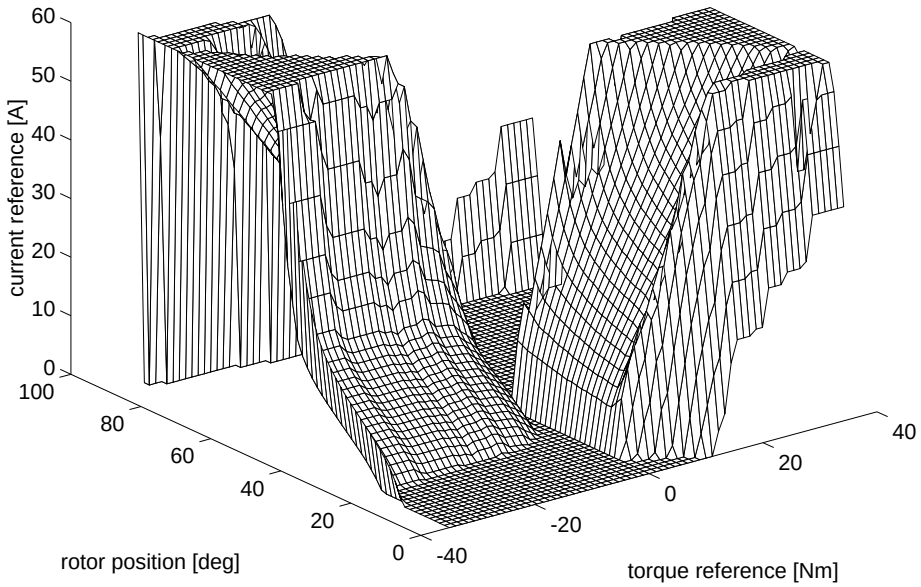

Fig. 4.13 *The entire speed compensated current reference matrix for a speed of 4600 rpm.*

Torque Ripple Limit Control

If torque ripple is accepted, it is possible to calculate current references that are higher in rotor position intervals where the torque per current ratio is high and lower when the torque per current ratio is low. A higher efficiency is therefore expected, at the expense of torque quality. Looking at Fig. 4.5 the torque as a function of current and rotor position, it is seen that the highest torque producing capability for a given current occurs around the beginning of overlap between the stator and rotor pole.

The problem of finding a new set of current reference values can be approached in different ways. One approach is to calculate a new set of current reference values (according to some rules) and then afterwards check that the torque ripple is within the given limits and that the average torque is not affected. Another approach is to generate a torque reference with a given torque ripple and correct average value, and then afterwards calculate the corresponding current reference values. The second approach is described below.

A torque reference with a given ripple and average has to be generated under some constraints. The current reference values corresponding to the new torque reference waveform must be high in the rotor position interval where the torque per current ratio is high and vice versa. Furthermore, all three phases have to be considered at the same time since there exist intervals where two phases can contribute to the overall torque. The idea is to use the maximum torque per current waveform as a scaling function for the torque ripple. A scale factor is then used for scaling the magnitude of the torque ripple.

First, consider the torque per current ratio for one phase only. This matrix is shown in Fig. 4.14. For all the positive torque reference values, the torque is divided by the current needed to produce that torque. The torque per current ratio is then plotted as a function of torque reference and rotor position.

Consider the torque per current ratio of the other phases, and for each position select the phase which has the highest ratio in the interval between 0 and 45 degrees. This matrix is shown in Fig. 4.15. At rotor angular positions close to aligned and unaligned, the torque producing capability of the first phase is low, and one of the other two phases contribute to the torque per current matrix.

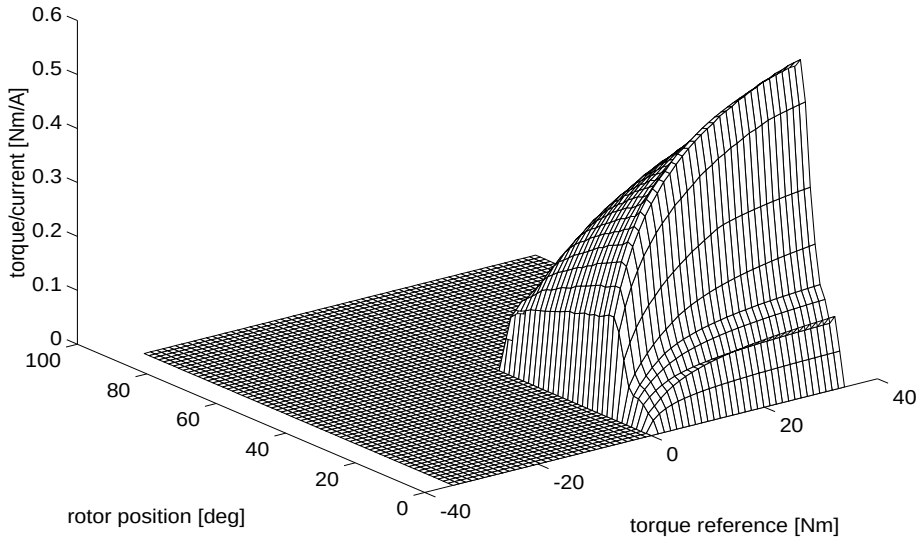

Fig. 4.14 *A matrix showing the torque per ampere ratio for one phase only. Note that only the motoring current references are displayed.*

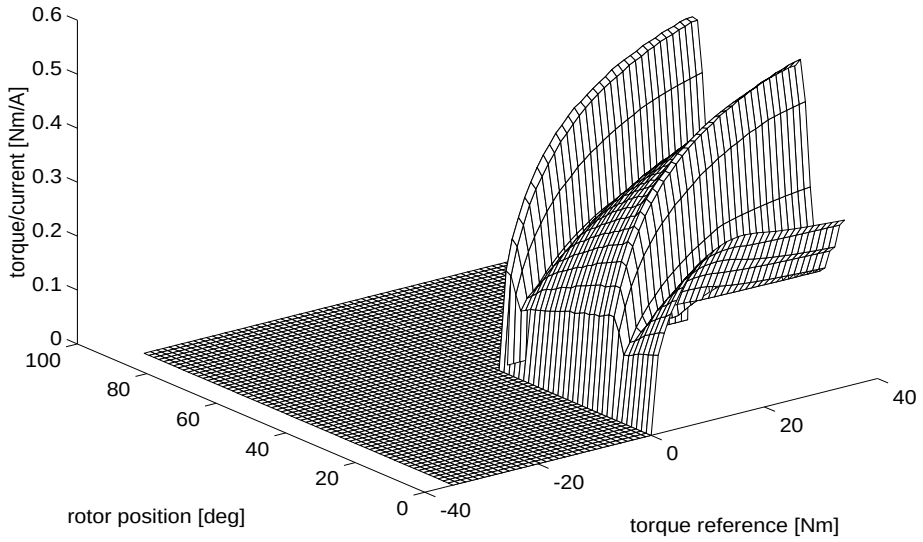

Fig. 4.15 *A matrix showing the torque per ampere ratio when the torque producing capability of all the phases are considered. Note that only the motoring current references are displayed.*

In order to use this matrix as a scaling function for the torque ripple it must be normalised. The average value of each individual torque reference waveform is calculated. Every torque per current value associated with a given torque reference is then divided with this average value. The result is a waveform for each torque reference with unity average value. The entire normalised scaling matrix is shown for motoring torque in Fig. 4.16.

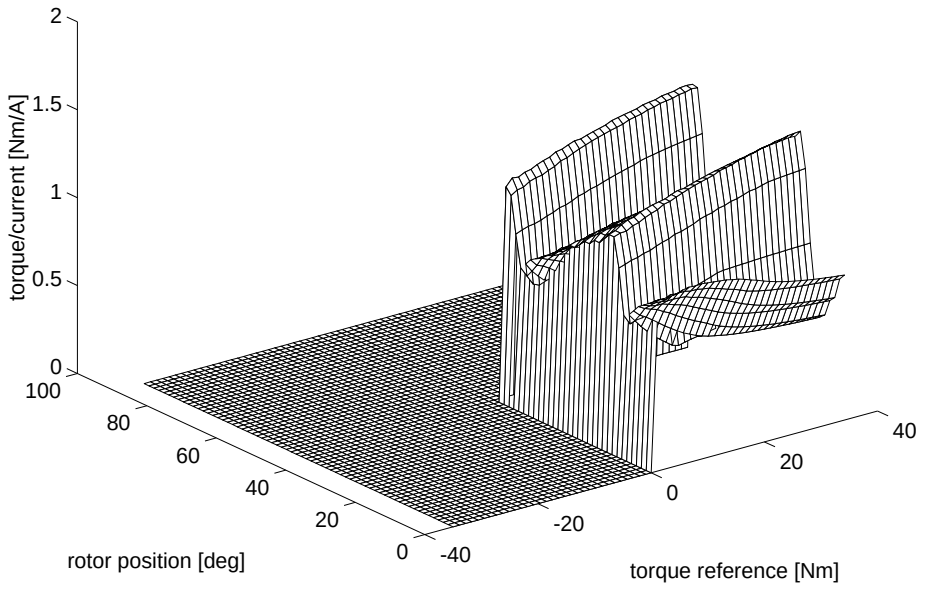

Fig. 4.16 *A matrix showing the normalised torque per ampere ratio when the torque producing capability of all the phases are considered. Note that only the motoring current references are displayed.*

These curves are used as a scaling waveform for the torque ripple and they are superimposed on the constant torque reference. The calculation of the current references associated with this torque reference follows the same pattern as if the torque reference was constant. This means that a single scaling parameter, k_{ripple}, is introduced in the current reference calculating program and the magnitude of this parameter determines the allowed torque ripple as indicated in equation (4.8)

$$T_{ref,ripple}(T_{ref},\theta_r) = T_{ref} \cdot \left[1 + k_{ripple} \cdot T_{ripple}(T_{ref},\theta_r)\right] \qquad (4.8)$$

where $T_{ripple}(T_{ref},\theta_r)$ is the ripple waveform seen in Fig. 4.16 and T_{ref} is the constant torque. If k_{ripple} is set to zero, constant torque references are produced. An example of the normalisation is given in Fig.4.17 for a torque reference of 6.8 Nm and k_{ripple} equals one.

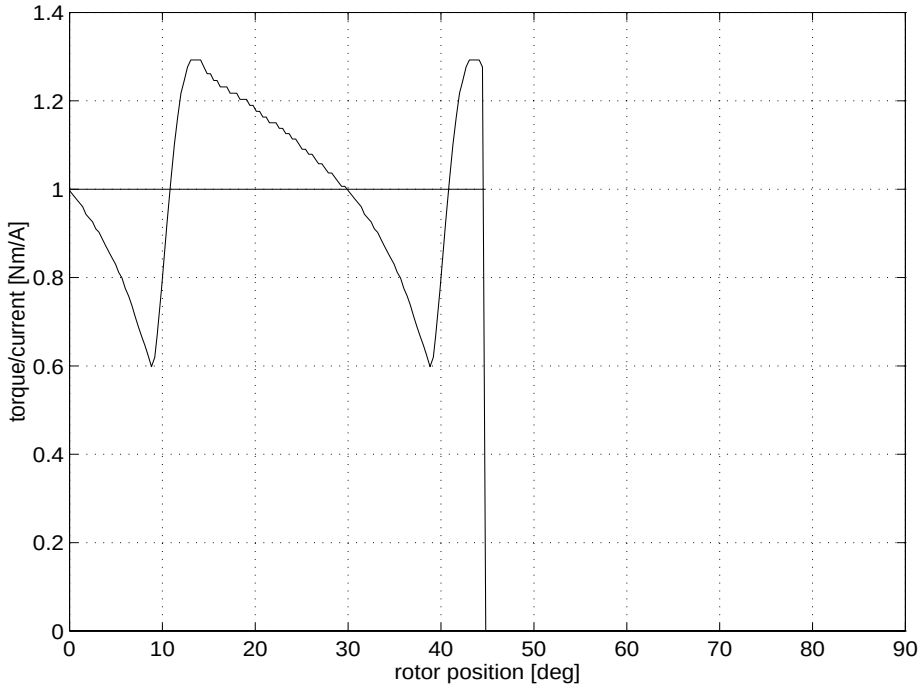

Fig. 4.17 *Normalised torque ripple scaling waveform for a torque reference of 6.8 Nm.*

Increasing the allowed torque ripple by increasing the scaling parameter in the current reference calculating program leads in motoring mode to less pronounced current peaks in the beginning and the end of each current pulse. This is expected since in these intervals the torque per current ratio is very low and approaching zero at the aligned and unaligned position. Allowing a torque ripple leads to a decrease in the current in positions where the torque per current ratio is low. To maintain the average torque, the current references are slightly higher in the middle of the interval. The average torque is unaffected, but the large current peaks needed to produce smooth torque have disappered. A comparison between the current waveforms in Fig. 4.18 shows the change of the current reference values in smooth torque operation and torque ripple limit control for a torque reference of 6.8 Nm. The torque ripple is scaled to approximately 0.7 p.u as seen in Fig. 4.17. Allowing torque ripple reduces the high current peaks and leads to a smaller rms value of the current. This has an impact of the rating of the electrical energy converter as well as on machine efficiency.

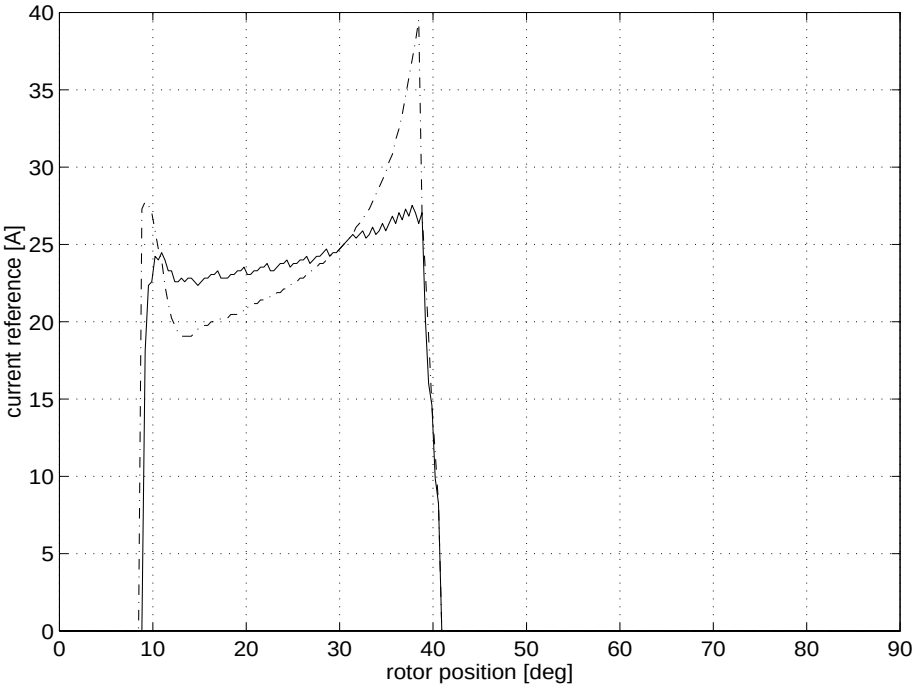

Fig. 4.18 *A comparison between current waveforms at smooth torque control and torque ripple limit control for a torque reference of 6.8 Nm.*

The current reference values for the torque ripple limit control with a torque reference of 6.8 Nm and a torque ripple of 0.7 p.u is seen in Fig. 4.19. A torque reference of - 6.8 Nm produces the current references seen in Fig. 4.20. Note that they are the mirror image (around 45 degrees) of the values for positive torque. The dash dotted lines in Figs. 4.19 and 4.20 represent the current needed to produce smooth torque with one phase alone.

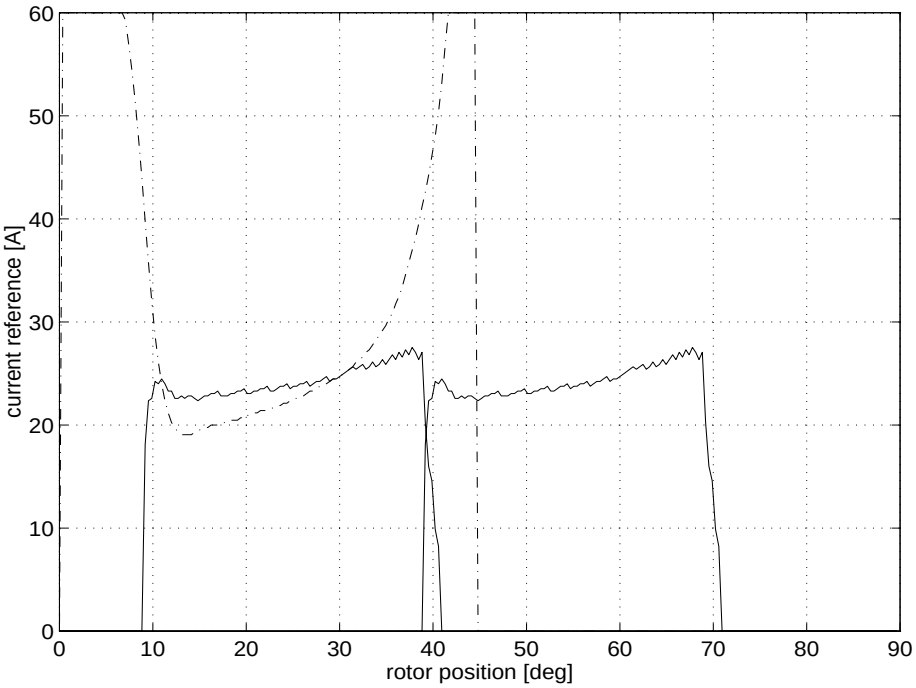

Fig 4.19 *Current reference values for two successive phases in motoring mode - a torque reference of 6.8 Nm.*

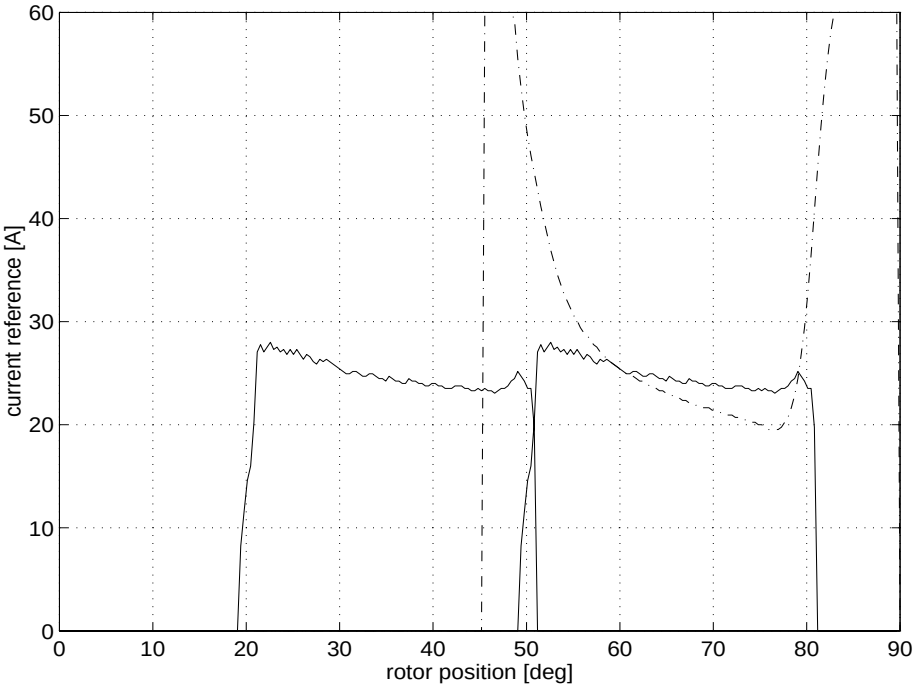

Fig 4.20 *Current reference values for two successive phases in generating mode - a torque reference of - 6.8 Nm.*

As in the case of smooth torque operation, the current reference matrix must be speed compensated for higher speed intervals. This procedure is independent of the torque control strategy used. In Figs. 4.21 and 4.22 an example is shown of speed compensated current references values for a torque reference value of 6.8 Nm and - 6.8 Nm . The matrix is compensated for 4600 rpm, which means that these current references are to be used in the highest speed interval.

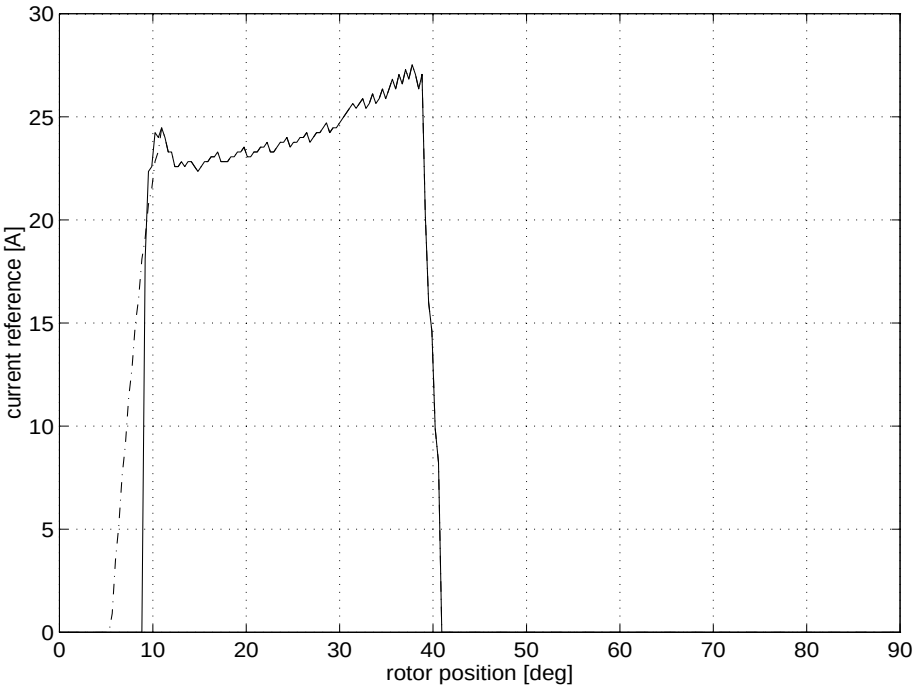

Fig. 4.21 *Speed compensated current reference values in motoring mode for a torque reference of 6.8 Nm.*

In torque ripple limit control the high peaks in the current reference in the beginning and the end of the torque producing interval are reduced. As a result of this the voltage can be applied a few degrees later in order to reach the first peak in the uncompensated current reference values. This means that the copper losses associated with speed compensation are reduced.

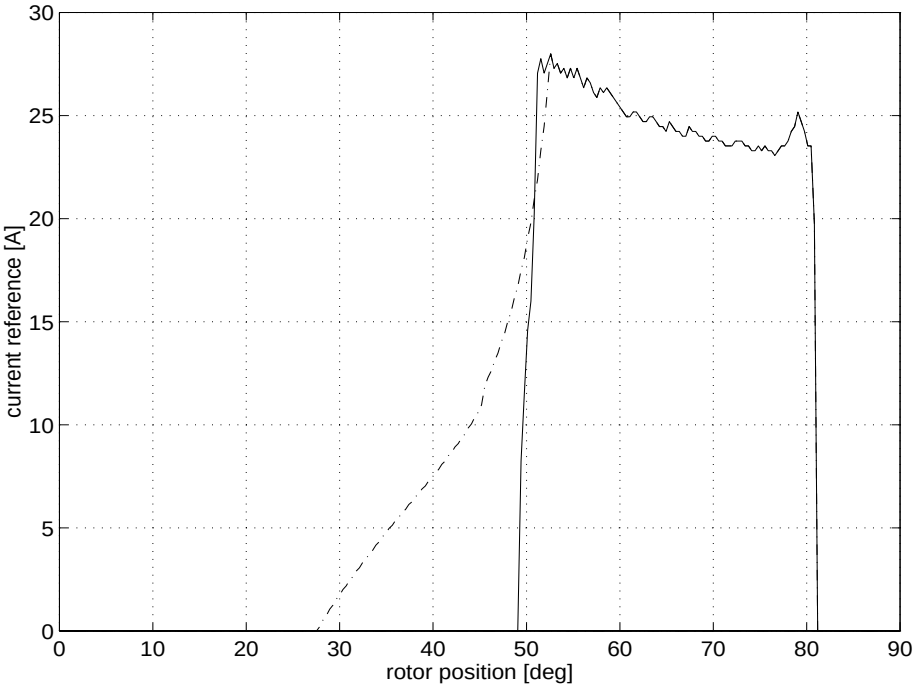

Fig. 4.22 *Speed compensated current reference valus in generating mode for a torque reference of - 6.8 Nm.*

Fig. 4.23 shows the uncompensated current reference matrix and Fig. 4.24 shows the current reference matrix compensated for a speed of 4600 rpm.

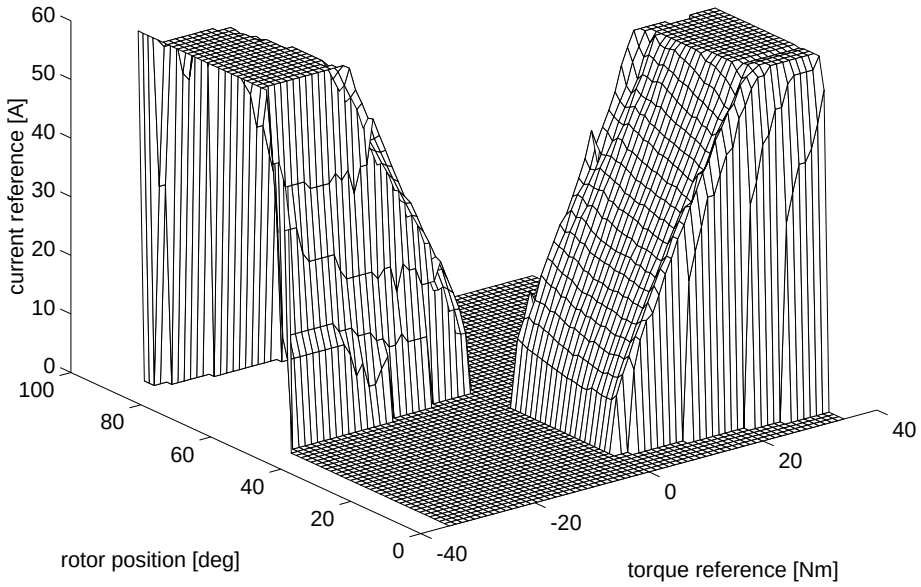

Fig. 4.23 *Uncompensated current reference matrix for torque ripple limit control.*

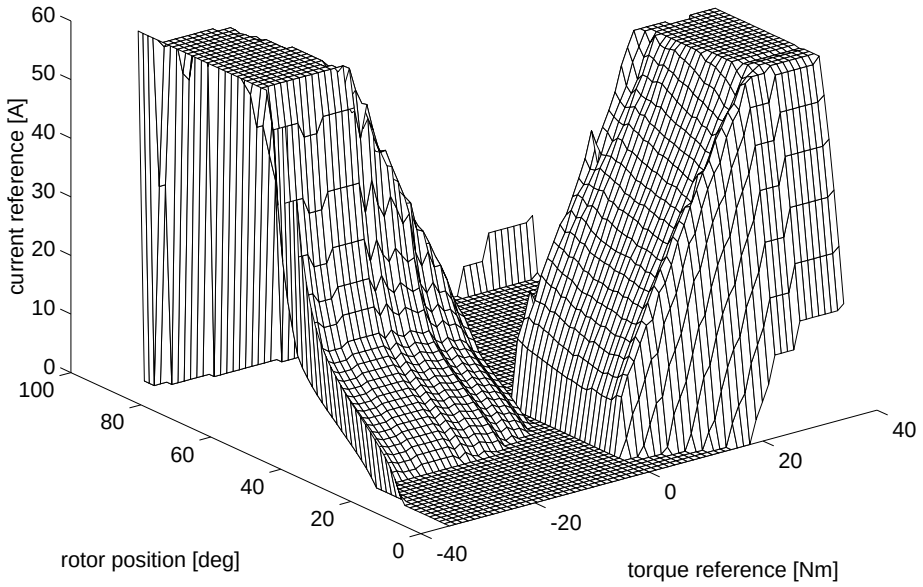

Fig. 4.24 *Speed compensated current reference matrix compensated for a speed of 4600 rpm.*

Since four bits are used to represent the rotor angular velocity, 16 matrixes like the one in Fig. 4.24 must be generated - one for each speed interval. Note that for high torque references the turn-on angle must be advanced before the unaligned position of the phase in question. This interferes negatively with the torque production. This is however not a problem since the nominal torque of the machine is 9.5 Nm and the torque references for which this phenomenon occur are well beyond the rated torque (as well as the thermal limits) of the machine.

Since eight different speed intervals are considered in the forward direction (as well as eight in the backward direction), it is possible to assign a permissible torque ripple to each one of the intervals individually. One strategy is to let the torque ripple be proportional to the speed, starting with smooth torque operation at low speed and gradually increase the allowed torque ripple. The consequence of such a strategy is that the rotor angular speed variation due to torque ripple can be held constant independent of the speed.

Iron Lamination Machine Torque Characteristic

The procedure used for calculating the current reference tables for the iron lamination switched reluctance machine is identical to the one used for

calculating tables for the iron powder switched reluctance machine. The difference lies in the input data - the torque and flux linkage as a function of rotor angular position and current. This torque function is calculated using the same finite element program that was used in the calculation of the torque for the iron powder machine. The result is seen in Fig. 4.25 and this should be compared with Fig. 4.5. The entire speed compensated current reference table for the iron lamination switched reluctance machine is seen in Fig. 4.26. This matrix is for the highest speed interval and is compensated for a speed of 4600 rpm.

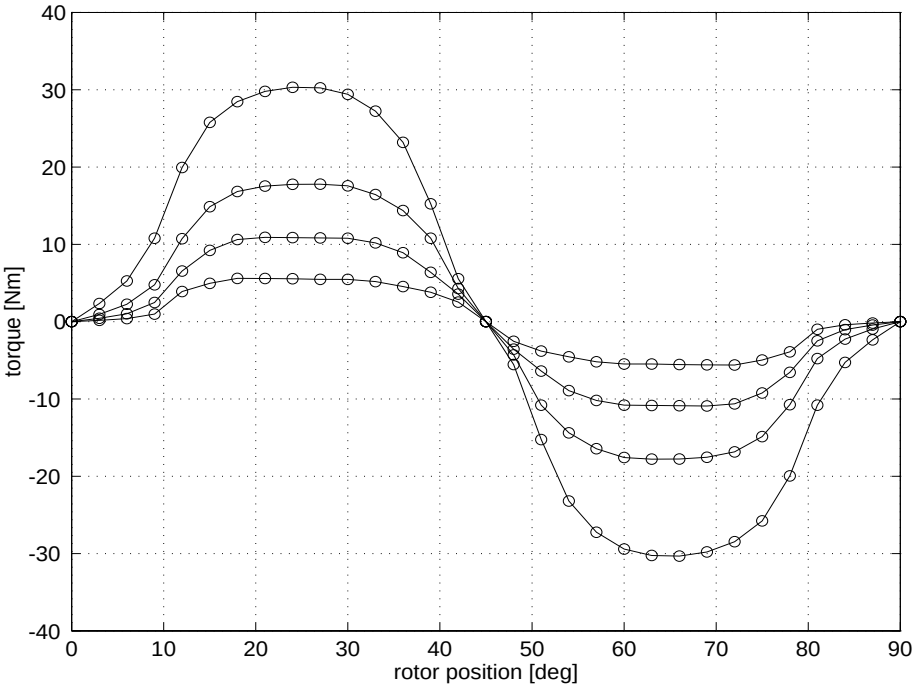

Fig. 4.25 *Torque as a function of current for four different current levels (60, 36, 24, and 15 A). The operating points in the figure are calculated using a finite element program.*

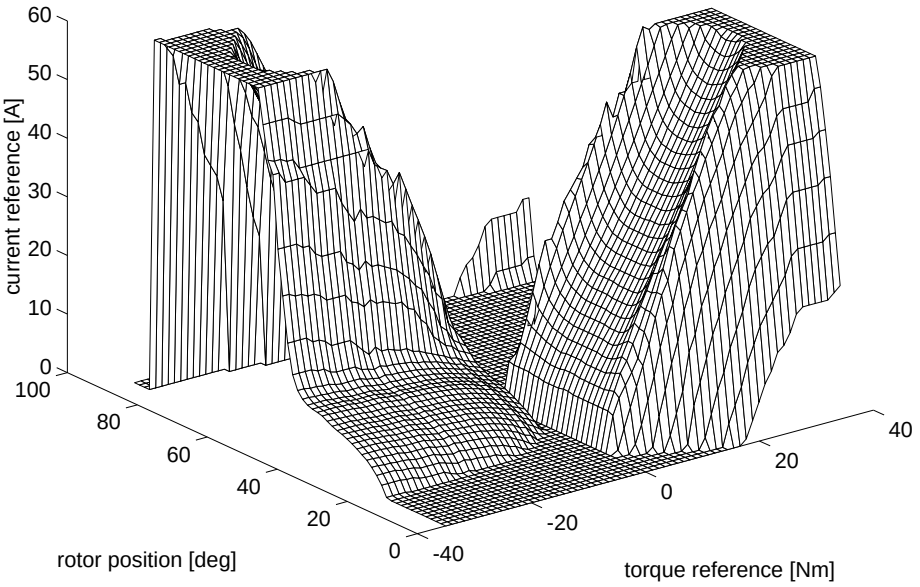

Fig. 4.26 *The entire speed compensated current reference matrix for the iron lamination machine for a speed of 4600 rpm.*

Summary

A table based torque control scheme for switched reluctance machines is presented. The control method, referred to as *indirect torque control*, is based on extensive à priori numerical calculations and allows the control designer to specify the acceptable torque ripple level. The only input to the control design program are two characteristic functions for the switched reluctance machine, namely the torque and the flux linkage both as a funcion of rotor angular position and current. The torque and flux linkage functions are calculated using a finite element program and the controller is based solely on these calculated functions.

Phase current reference values are calculated in order to produce the desired torque. In rotor angular position intervals where two phases can contribute to the overall torque, the combination of phase currents that gives the lowest copper losses is chosen. The currents are forced to follow their reference values by hysteresis controllers, which are implemented in a *current regulator* card.

The à priori calculated look-up tables governing the proper phase current reference values are programmed in two EPROMs. The size of the EPROMs is a compromise between cost and resolution. The *current*

reference generator card is updated for all phases with a frequency in excess of 100 kHz. Calculating the proper phase current reference values in real time with a DSP could not by far reach those updating frequencies. In fact, it is very difficult to find an explicit model for the non-linear behaviour of the switched reluctance machine and some form of look-up table will probably be required to solve the torque control problem even with a DSP. The high updating frequency of the table based controller is therefore attractive in high speed applications.

5

Simulations and Measurements

Simulation Scheme

The simulation scheme for one phase is shown in Fig. 5.1. The two other phases are modelled in the same way, and the only difference is the rotor angular position addressing look-up table I and II. For the second phase 120 degrees is added modulo 90 and for the third phase 240 degrees is added modulo 90 before look-up table I and II are addressed. The mutual effects between the phases are assumed to be zero. Furthermore, the static torque curve as a function of rotor angular position and current is used to model the torque production capability, which means that the iron losses are neglected in the model.

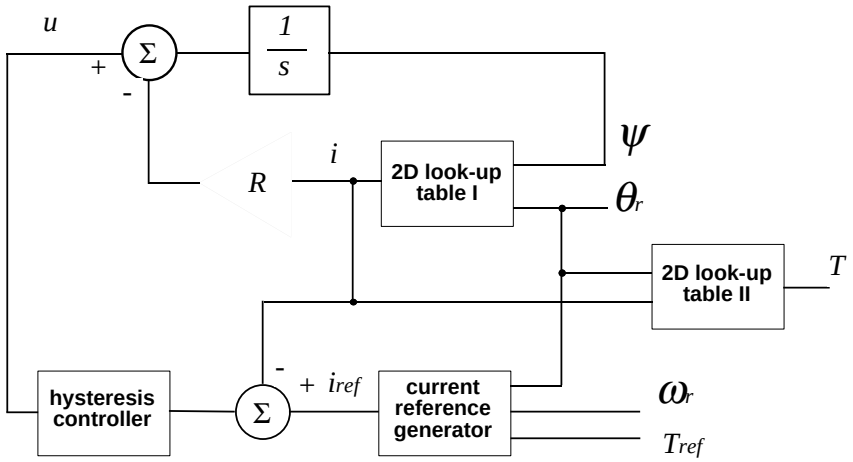

Fig. 5.1 *Simulation scheme for the electromagnetic part of the drive system.*

The machine nonlinearities are modelled in two look-up tables. The first one, look-up table I, is representing the non-linear relationship between the

flux linkage, rotor position and current and is depicted in Fig. 5.2. This matrix of data is formed by rotating the matrix describing the flux linkage as a function of current and rotor angular position. A plateau level is introduced at 60 A in Fig. 5.2. In the simulations this plateau level does not exist.

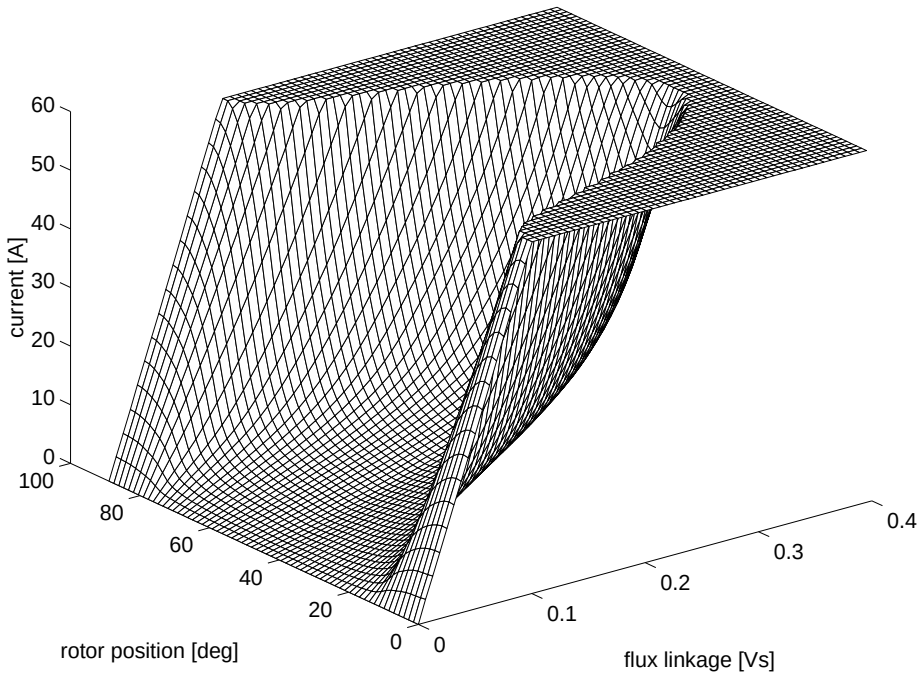

Fig. 5.2 *Phase current as a function of the rotor angular position and flux linkage, as implemented in the look-up table I.*

The voltage applied to the phase winding is subtracted by the resistive voltage drop and the result is the back emf, which is integrated to give the flux linkage. The flux linkage and the rotor angular position are addressing the look-up table I and the corresponding phase current is the result. These three states form at all times a unique magnetic state of the machine.

The second nonlinearity is the torque as a function of the current and the rotor angular position. This is modelled in look-up table II, and an example of this characteristic is seen in Fig. 5.3, which is an example for the switched reluctance machine with the iron laminated core.

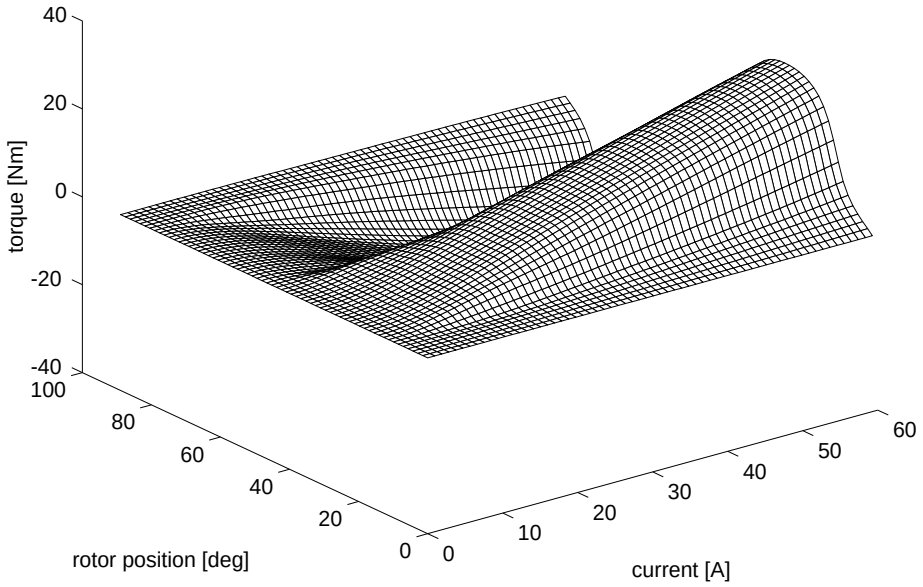

Fig. 5.3 *Torque as a function of rotor angular position and current as implemented in the look-up table II.*

The matrixes in look-up table I and II are intermediate results in the derivation of the torque controller for the machine.

The net torque acting on the shaft is formed by summing the torque from the three phases and subtracting the load torque. Integrating the net torque with the inverse of the equivalent rotor inertia as a scaling constant yields the rotor angular speed. The rotor angular speed is integrated to form the rotor angular position.

The torque controller, consisting of the current reference generator and the current hysteresis regulator, is the one described in Chapter 4.

Experimental Set Up

In order to test the dynamic performance of the switched reluctance machine it is mounted shaft-to-shaft via a rotating torque transducer to a DC machine. The DC machine is speed controlled and the switched reluctance machine is torque controlled. The switched reluctance machine and the DC machine electrical energy converters are coupled in parallel on the same DC link. Thus, the only power the DC source has to supply corresponds to the losses in the machines and the electrical rating of the DC

source is thereby reduced significantly. A schematic description of the measurement set up is seen in Fig. 5.4.

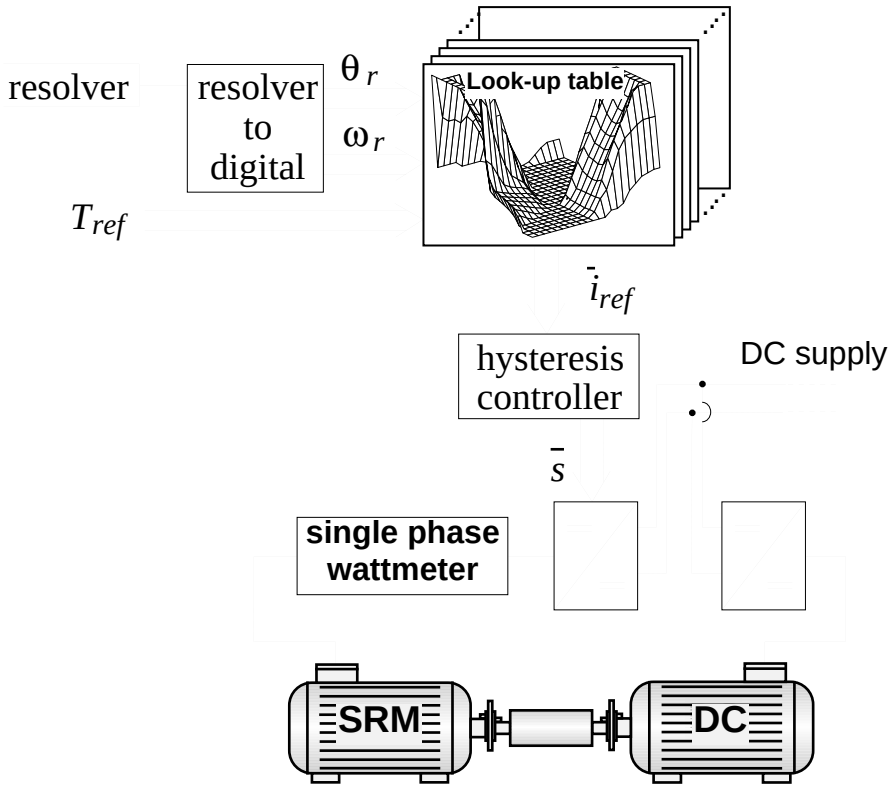

Fig. 5.4 *Schematic description of the measurement set up.*

The operational DC link voltage of the test system is 300 Volt and the DC supply is capable of power flow in both directions. This allows the switched reluctance machines to be tested in both motoring and generating mode, since the electrical energy converter for the DC machine operates in all four quadrants.

The loss measurements are based on the separation of losses. After determining the friction losses for the switched reluctance machines, the input power is measured using a high bandwidth power meter while the shaft power is measured using a rotating torque transducer and a hand held tachometer. The rms value of the current is measured by the power meter and the copper losses are calculated with compensation for the winding temperature.

Magnetic Characteristics

The most important characteristic of a switched reluctance machine is the flux linkage as a function of current and rotor angular position. This

characteristic is both calculated using a finite element program and measured using the integrator method, further described in the next section.

Measurements

The static magnetic characteristic of the switched reluctance machines is measured using the integrator method, argued in (Lovatt, 1992) to be the most accurate. The measurement set up for these measurements is not the same as the one described in Fig. 5.4. Here, a sinusoidal voltage is via a transformer applied to one phase coil when the rotor is in a locked position. The corresponding voltage and current waveforms are sampled. From the voltage equation

$$u = \frac{d\psi}{dt} + Ri \tag{5.1}$$

the flux linkage is formed by subtracting the resistive voltage drop from the terminal voltage and integrating the result.

The measurement system consists of a Macintosh computer equipped with an I/O card. The LabVIEW™ program is used for the data aquisition and the data files are stored in a format readable from MATLAB®, where the numerical integration is performed.

From a transformer a sinusoidal 50 Hz voltage is applied to the voltage terminal of the machine. The amplitude of the voltage is adjusted so that the peak current is held constant regardless of the position in which the rotor is locked. Three periods of the voltage and current waveforms are sampled with a sample time of 0.1 ms, which means that in all 600 samples of the voltage and current are registered for every rotor angular position. This procedure is repeated for rotor angular increments of three degrees between the unaligned and the aligned position. An example of the result of the numerical integration for the iron lamination machine and the iron powder machine is shown in Fig. 5.5. The result is for the aligned position.

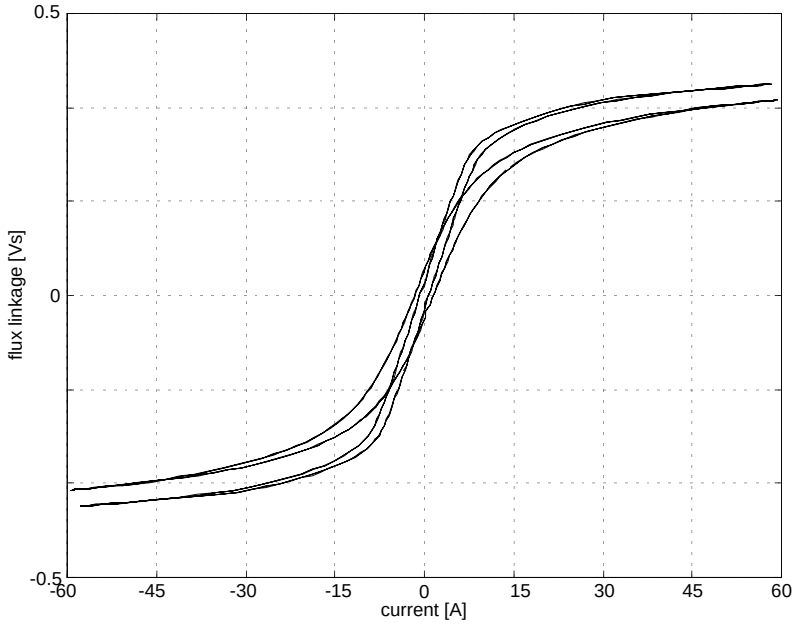

Fig. 5.5 *Flux linkage-current trajectory for both the switched reluctance machine with iron laminations (curve with highest amplitude) and for the one with the iron powder core (curve with greatest hysteresis) at the aligned position.*

Fig. 5.5 reveals that the machine built with the iron powder core shows a wider hysteresis. The hysteresis is not included in the simulations. Dehysterised curves are formed from the measurements above. If, for negative values of the flux linkage, the curve is mirrored in the *i*-axis and then mirrored in the ψ-axis, a set of curves for positive currents and flux linkages are formed. For every current value the mean value of the corresponding flux linkage values is calculated. An example of these average dehysterised curves is shown in Fig. 5.6, in which a number of conclusions can be drawn about what to expect from a switched reluctance machine built with a core of iron powder composite material:

- at the unaligned position, the magnetic characteristics are approximately the same;

- for low currents, the inclination of the curve for the machine with an iron powder core is not so high due to the lower relative permeability of the composite material;

- for higher currents when the core is saturated, the curve for the iron powder core has a lower flux linkage for the same current due to the lower saturation flux density of the iron powder composite material.

These characteristics imply that in order to convert the same amount of energy to mechanical work, a switched reluctance machine built with an iron powder core has to work with a somewhat higher current to compensate for the lower relative permeability and lower saturation flux density. For the same peak current the torque production capability is approximately 10 % lower.

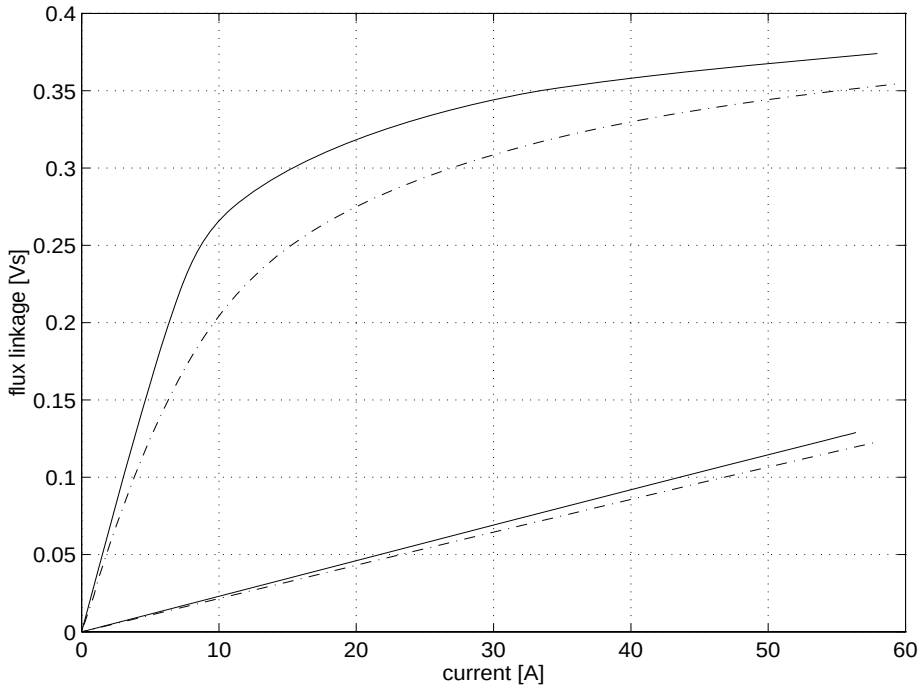

Fig. 5.6 *Dehysterised flux linkage curves for both the machines at the aligned and unaligned rotor position. The solid lines represent the iron lamination machine and the dash dotted lines represent the iron powder core machine.*

In Fig. 5.5 it is seen that a switched reluctance machine built with iron powder composite material has higher hysteresis than a machine built with conventional iron laminations, indicating that higher hysteresis losses in the core are expected. However, the benefits of using the iron powder core is the fact that the eddy current losses are negligable for the frequencies at which these machines operate.

Calculations

An example of equipotential lines for the magnetic vector potential for the switched reluctance machine with iron powder core is shown in Fig. 5.7.

Fig. 5.7 *Magnetic field lines for the switched reluctance machine with the iron powder core.*

The flux linkage as a function of current and rotor angular position is calculated for rotor positions between the unaligned and aligned position. The rotor is rotated with an increment of three degrees and for every rotor angular position the current interval ranges from 0 to 60 ampere. In Fig. 5.8 a comparison is made for the machine built with iron laminations. The points in the figure on the solid lines are the values calculated with a finite element program and they are connected with linear line segments. The dash dotted lines are the measured curves. The calculations match the measurements very well around the aligned position except at heavy saturation. The machine is not operating at such a high saturation, which means that the result from the finite element calculations is valid for controller design purposes. However, in the unaligned position, there is a clear discrepancy between the calculated and measured curves. This is probably because the finite element program calculates in only two dimensions and end leakage effects are not modelled. The finite element program used is ACE (2.41 and 2.5).

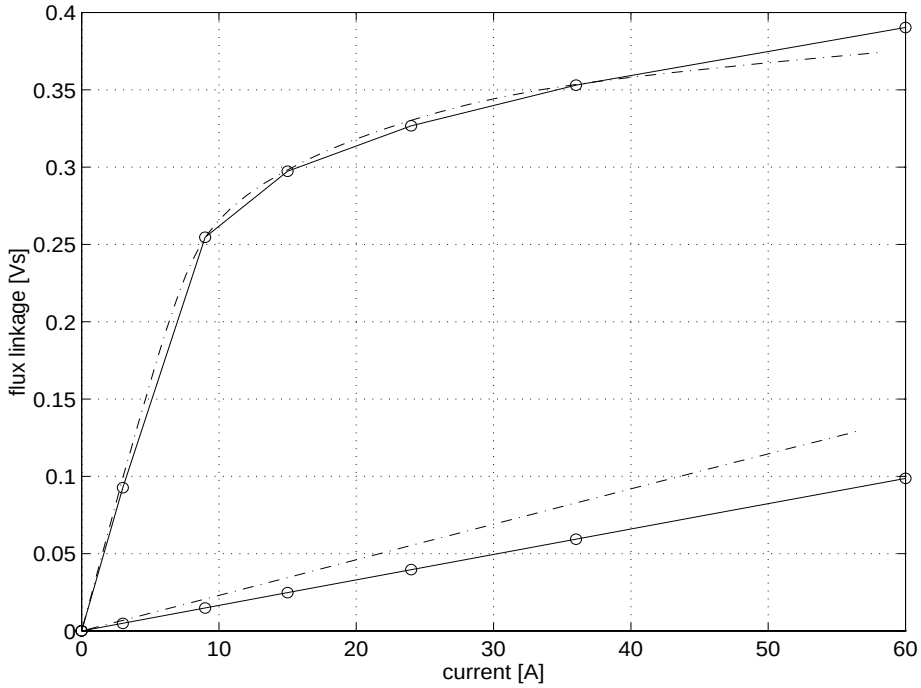

Fig. 5.8 *Flux linkage as a function of current for the switched reluctance machine with iron laminations at the aligned and unaligned position. The solid lines represent the calculated values and the dash dotted lines are measured values.*

The same measurements and calculations as described above are repeated for the machine built with an iron powder core, and the result is seen in Fig. 5.9. The same discrepancy around the unaligned position is observed. In addition, there is a difference around the aligned position as well. This can more easily be explained. During the manufacturing process of the iron powder core there was a misunderstanding, so the actual airgap in this machine is 0.25 mm instead of the intended 0.35 mm which was the airgap used for calculations. In consequence the inclination of the flux linkage curve, for low currents (before saturation), in the calculations is lower than the measured one.

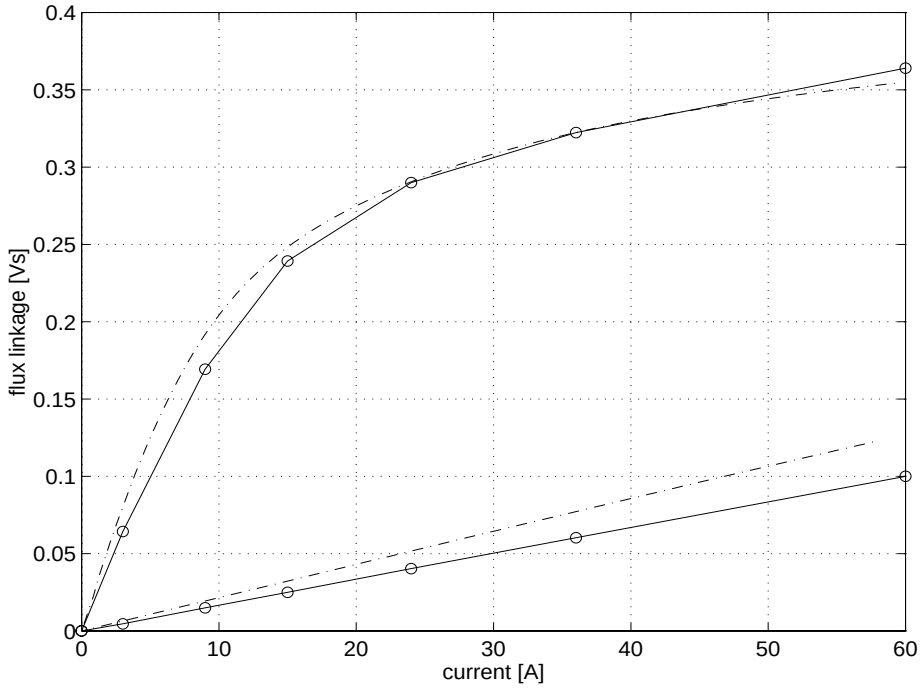

Fig. 5.9 *Flux linkage as a function of current for the switched reluctance machine with iron powder core at the aligned and unaligned position. The solid lines represent the calculated values and the dash dotted lines are measured values.*

For both machines, a flux linkage matrix is formed from the crude calculated data using interpolation and the result for the iron lamination machine is seen in Fig. 5.10. The flux linkage matrixes and the torque matrixes are the basis in the derivation of the torque controllers for the machines. The torque as a function of the current and the rotor angular position is calculated using the same finite element program. There is in principle no difference in how the electromagnetic data is acquired. The flux linkage and torque matrixes can of course be measured instead of calculated. The torque controller derivation algorithm explained in Chapter 4 performs in the same way.

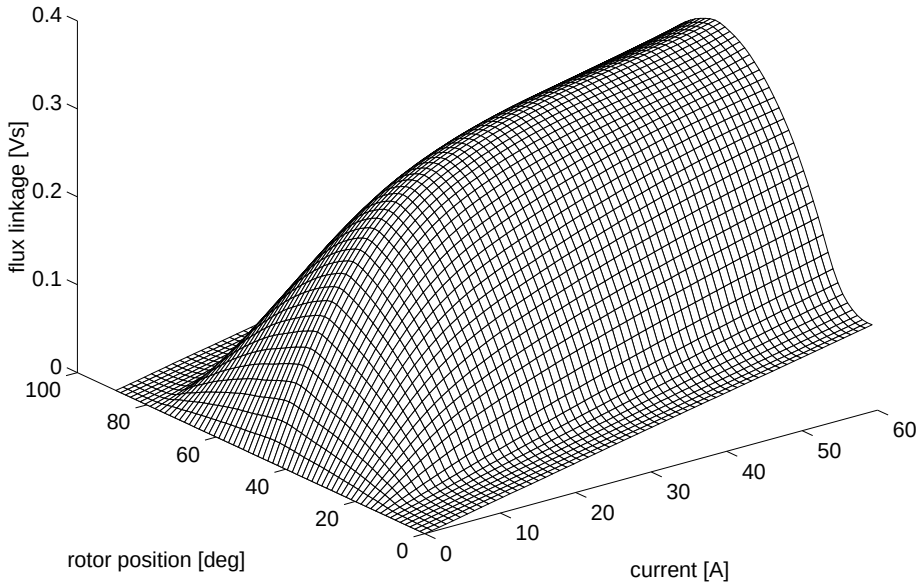

Fig. 5.10 *Flux linkage matrix formed from the crude calculated data for the switched reluctance machine with iron laminations.*

Losses

In this section, the losses are calculated at the nominal operating point. Measurements of the losses are performed throughout the entire operating area resulting in machine efficiency charts. The control algorithm producing current reference values for smooth torque operation is used for both machines.

Iron Losses in the Iron Powder Machine

Calculation of iron losses assumes that the time variation of the magnetic flux densities in every part of the machine are known. To derive this fully, a large computational power is needed as well as a much more complex model than the one presented here. A simplified approach leads to a qualitatively correct model that can be used in for instance switched reluctance machine design optimisation, a task for which the more complicated model would be of little use.

The starting point for deriving the time variation is discussed in Chapter 3, where the principle waveforms of the magnetic flux density are reviewed. It is possible to conclude how the flux linkage varies with time from simulations. The average magnetic flux density in the stator poles is found

by simply dividing the flux linkage by the number of turns and the cross sectional area of a stator pole,

$$B_{sp} = \frac{\psi_{sp}}{NA_{sp}} = \frac{\psi_{sp}}{Nl_{stk}\, t_s} \tag{5.2}$$

At the nominal operating point the applied voltage to the terminals is positive during the on-time and negative during the off-time, and the flux linkage is rising and falling linearly. Applying equation (5.2) to the waveform extracted from simulations yields the stator pole flux density variations seen in Fig. 5.11. The peak flux density in the stator poles is calculated to 1.93 T. The waveforms listed below are from the switched reluctance machine built with the iron powder core.

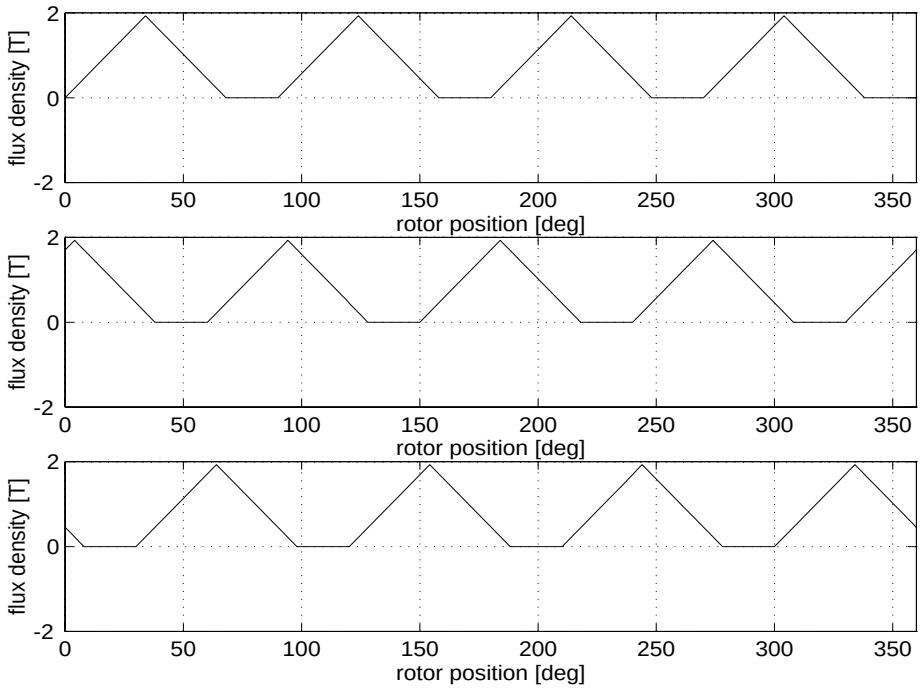

Fig. 5.11 *Stator pole flux density corresponding to phase 1 (top), phase 2 (middle) and phase 3 (bottom).*

The time variation of the flux density in the stator yoke is found by superimposing the stator pole flux density variations as described in Chapter 3. To find the correct amplitude for the waveform the stator yoke thickness vs the stator pole width has to be regarded. The scaling constant is

$$S_{sy} = \frac{t_s}{2y_s} = \frac{0.0187}{2 \cdot 0.0139} = 0.673 \tag{5.3}$$

Scaling the waveform for the stator yoke flux density variation results in the time variation in Fig. 5.12.

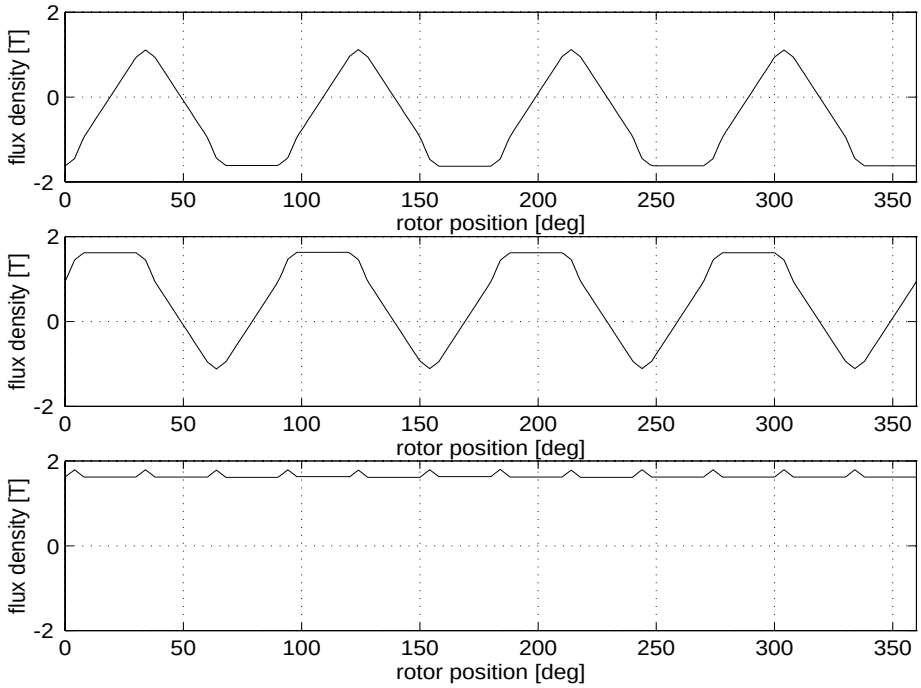

Fig. 5.12 *Stator yoke flux density variation in three of the six stator yoke sections.*

The rotor pole flux density variation, seen in Fig. 5.13, is given by the superposition described in Chapter 3 and scaled with unity since the stator and rotor poles are approximately equally wide.

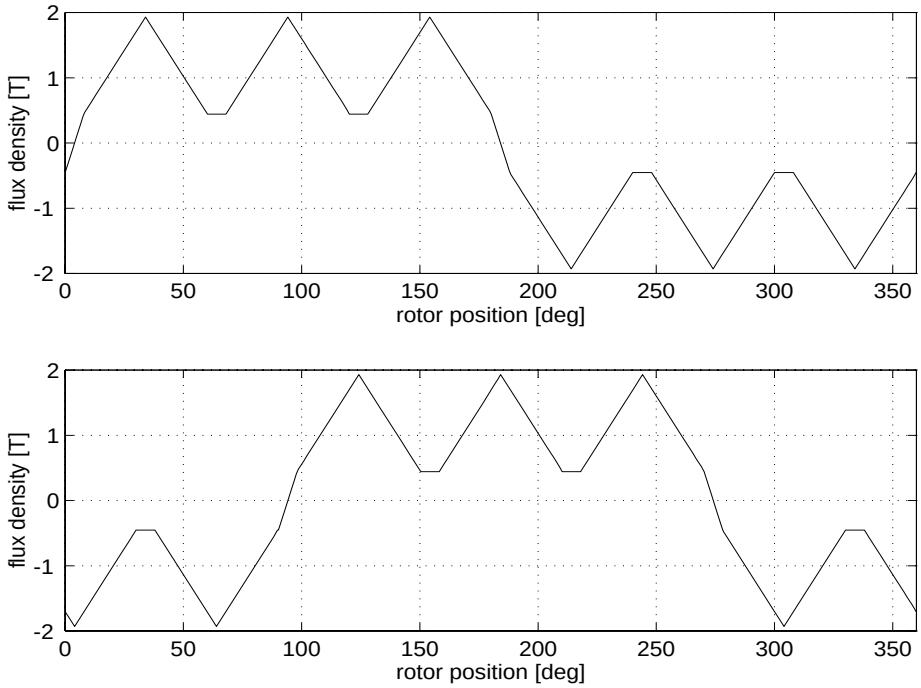

Fig. 5.13 *Rotor pole flux density variation.*

The rotor yoke flux density variation, seen in Fig. 5.14, is given by the waveform described in Chapter 3 scaled with

$$S_{ry} = \frac{t_r}{2y_r} = \frac{0.0209}{2 \cdot 0.0113} = 0.925 \tag{5.4}$$

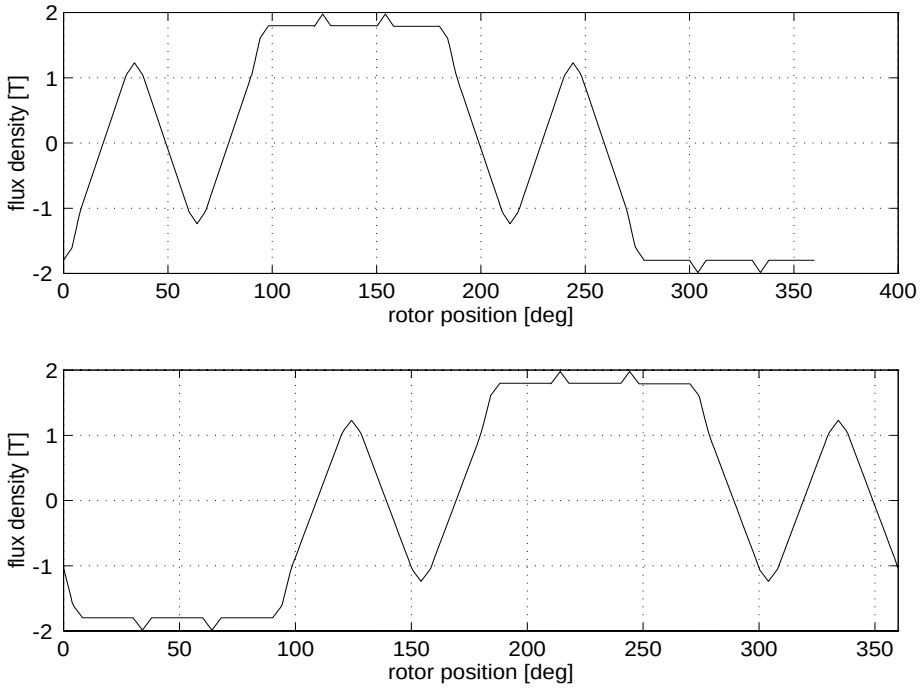

Fig. 5.14 *Rotor yoke flux density variation in two of the four rotor yoke sections.*

In the iron powder core based switched reluctance machine, the eddy current losses are assumed to be zero for the frequencies at which the machine operates. The iron losses consist only of hysteresis losses. The coercivity is

$$H_{c,\max} = 350 A/m \tag{5.5}$$

and the constant used for calculations of hysteresis losses when bias flux densities are involved (see equation 3.34) is set to

$$k_{dc} = 0.60 \tag{5.6}$$

which is the same value as the one found in (Köfler, 1990) for iron laminations with the same loss density as the iron powder composite.

The results from the calculations of the iron losses based on the expressions from Chapter 3 and the time variation of the magnetic flux density in Fig. 5.11 - 5.14 are summarised in TABLE I.

TABLE I. *Comparison between calculated and measured iron losses in the iron powder switched reluctance machine*

	stator poles	stator yoke	rotor poles	rotor yoke	total iron losses
calculated	160 W	230 W	112 W	59 W	561 W
measured	-	-	-	-	540 W

It is observed from TABLE I that 70 % of the iron losses are located in the stator. The deviation between the calculated and the measured value of the total iron losses is about 5 %, which is a good prediction considering the crude model. Since all the iron losses are hysteresis losses, the incentive to reduce these are of vital interest.

Iron Losses in the Laminated Machine

In the iron of the conventionally built switched reluctance machine there are both hysteresis and eddy current losses. From simulations it is deduced that the peak magnetic stator pole flux density according to equation (5.2) is 1.97 T. The results of the hysteresis loss and the eddy current loss calculations are listed in TABLE II and TABLE III.

TABLE II. *Calculated hysteresis losses in the iron lamination switched reluctance machine*

	stator poles	stator yoke	rotor poles	rotor yoke	total hyst. losses
calculated	48 W	68 W	22 W	18 W	156 W

TABLE III. *Calculated eddy current losses in the iron lamination switched reluctance machine*

	stator poles	stator yoke	rotor poles	rotor yoke	total eddy current losses
calculated	66 W	234 W	25 W	69 W	394 W

The total iron losses for the iron lamination machine are listed in TABLE IV.

TABLE IV. *Comparison between calculated and measured iron losses in the iron lamination switched reluctance machine*

	stator poles	stator yoke	rotor poles	rotor yoke	total iron losses
calculated	114 W	302 W	47 W	87 W	550 W
measured	-	-	-	-	511 W

It can be concluded that out of the total iron losses, 76 % of the losses are located in the stator. This matches roughly the percentage of the mass of the iron located in the stator compared to the total mass of the iron. This result is in close agreement with the conclusions drawn in (Boivie, 1995) regarding iron losses in switched reluctance machines.

Comments to the Iron Losses

From comparing TABLE I and TABLE IV it can be concluded that the iron losses in the machines are equal in magnitude. However, there is a difference in the nature of the losses. In the iron powder switched reluctance machine all the iron losses are hysteresis losses. The hysteresis losses are proportional to the frequency. The lamination machine has significantly lower hysteresis losses but the eddy current losses are higher. Since the eddy current losses are proportional to the square of the frequency, rewinding the machines for a higher speed will probably result in lower overall iron losses in the iron powder machine. In this observation lies the great potential for machine design using iron composite material.

Copper Losses in the Iron Powder Machine

Both machines are equipped with the same windings. The resistance at 20° C is obtained using 4-wire measurement. A comparison between the calculated and measured resistance is seen in TABLE V, which shows excellent agreement. The resistance is calculated using equation (3.54).

TABLE V. *Calculated and measured resistance @ 20° C*

calculated	measured
0.147 Ω	0.144 Ω

The temperature of all the phase windings were measured during the test process using thermoelements. The rms value of the current was calculated based on the current waveform extracted from simulations. Assuming that one period T of the simulated current contains K samples, the integral can be replaced by a sum which leads to

$$i_{rms} \approx \sqrt{\frac{1}{K}\sum_{n=1}^{K} i_n^2} \tag{5.7}$$

A comparison between calculated and measured rms value of the current at the nominal operating point is given in TABLE VI.

TABLE VI. *Calculated and measured rms value of the current*

calculated	measured
21.6 A	23.8 A

The actual rms value of the current is slightly higher than the one calculated. The reason is that the actual current has a higher amplitude than the one obtained from simulations, since the iron losses are not accounted for in the derivation of the current waveform that has to be applied to produce the nominal torque.

At the nominal operating point in the test, the temperature T of the windings is approximately 90° C. This means that the actual resistance is

$$R = 0.187\Omega \tag{5.8}$$

and the copper losses based on measured current are

$$P_{Cu} = 3 \cdot R \cdot i_{rms}^2 = 318W \tag{5.9}$$

Copper Losses in the Laminated Machine

The copper losses at the nominal operating point for the iron lamination switched reluctance machine are calculated and measured, and the results are shown in TABLE VII.

TABLE VII. *Calculated and measured rms value of the current*

calculated	measured
15.8 A	18.6 A

At the nominal operating point in the test, the temperature T of the windings is approximately 90° C. This means that the actual resistance is

$$R = 0.187\Omega \tag{5.10}$$

and total copper losses based on measured current are

$$P_{Cu} = 3 \cdot R \cdot i_{rms}^2 = 195W \tag{5.11}$$

Machine Efficiency Charts

Although the losses are only calculated at the nominal operating point, the losses and the efficiency are measured throughout the entire operating area. The efficiency charts are given in Figs. 5.15 and 5.16. The maximum efficiency for the iron lamination machine is 86 % and 84 % for the iron powder machine, and it occurs slightly below the nominal operating point. At the nominal operating point the efficiency for the iron lamination machine is 84 % and for the iron powder machine the efficiency is 82 %. The 2 % lower efficiency is mostly due to the smooth torque constraint leading to a higher rms value of the current for the iron powder machine. If torque ripple is allowed for the iron powder machine, simulations show that the copper losses are expected to drop approximately 100 W and thereby raising the efficiency to almost the same value as for the iron lamination machine. Allowing torque ripple for the lamination machine leads only to marginal reduction in the copper losses. At low speed and low load the efficiency is actually higher for the iron powder machine. It can not be eliminated that this might be due to measurement errors. Another possible explanation is that the eddy current losses due to the switching are high at these operating points.

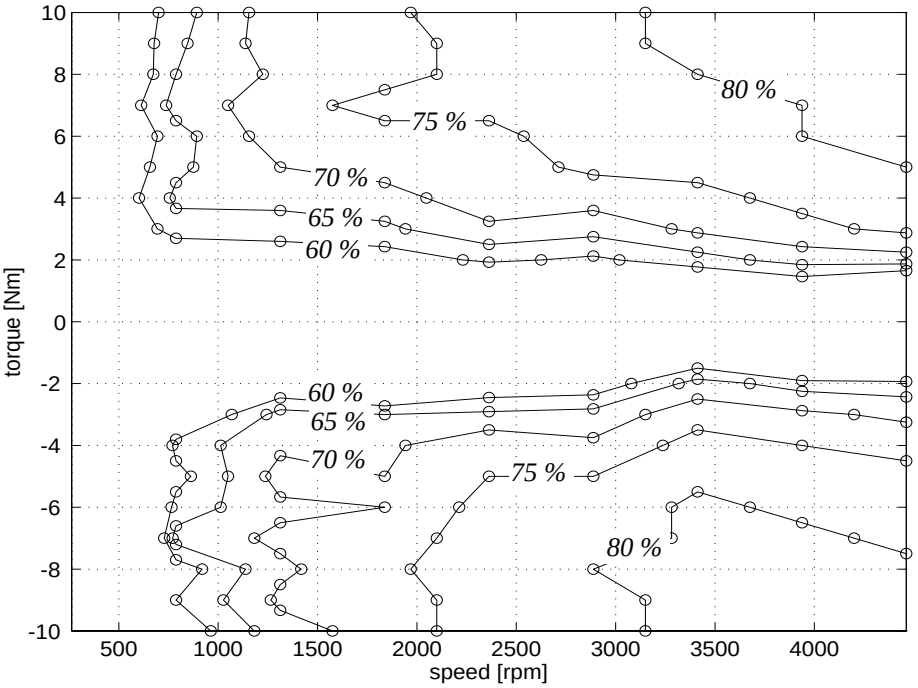

Fig. 5.15 *Efficiency contour plot showing lines of equal efficiency in both motoring and generating mode for the iron powder machine.*

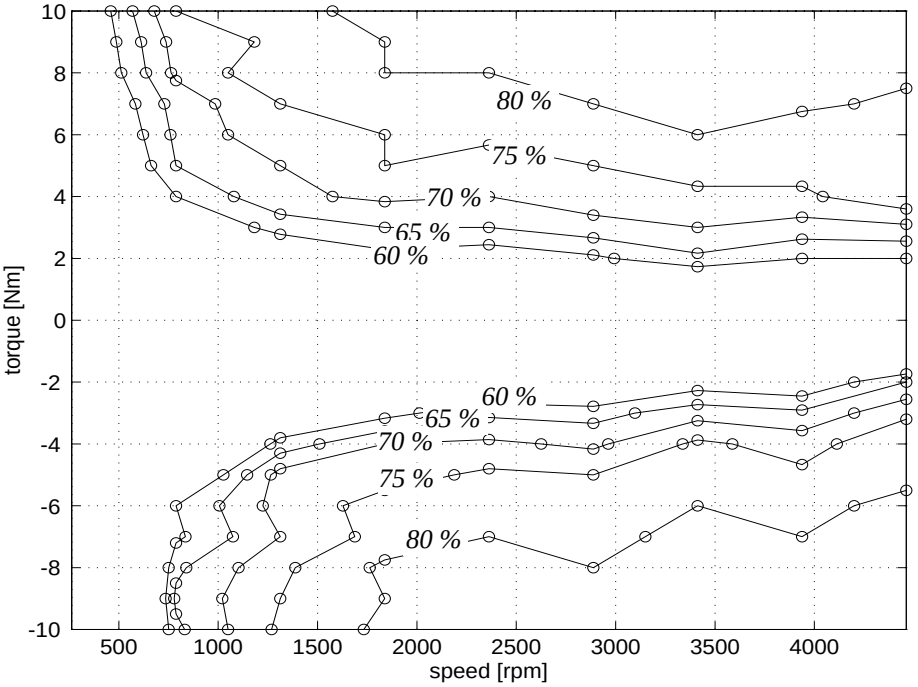

Fig. 5.16 *Efficiency contour plot showing lines of equal efficiency in both motoring and generating mode for the iron lamination machine.*

Dynamic Operation

A large number of simulations and measurements are performed, of which only a few are presented in this thesis. The simulations and measurements are grouped in pairs, showing the simulations first and then the measurements. Simulations and measurements are shown at low speed and at high speed, both for motoring mode and generating mode. In all the simulations and measurements, the actual current and the current reference are shown. For the iron powder switched reluctance machine, simulations are performed with the torque ripple limit control mode as well.

Iron Powder Machine Current Dynamics

Fig. 5.17 to Fig. 5.24 are comparisons between simulations and measurements of the phase current. Nominal load torque is applied. When deriving these current reference values smooth torque operation is assumed. The large peaks in the current are due to the poor torque production capability of the iron powder switched reluctance machine near the aligned and the unaligned position. This makes it costly to apply the smooth torque constraint. Generally, in motoring mode the actual current is somewhat higher than the simulated one and in generating mode the actual current is lower than the simulated one. This is due to the fact that the iron losses were neglected when deriving current reference values for smooth torque operation. The static torque characteristic was used.

The hysteresis band in the current regulator is set to 6 A and this matches simulations as well as measurements. The varying amplitude of the measured current ripple, especially at low speed, is due to limited resolution in the oscilloscope used for capturing the actual current. The measurements show that the average switching frequency when the current pulse occur is 7 kHz, a figure which is quite ordinary for IGBTs. No special attention is paid to adjust the current reference values at the trailing edge of the current pulses in both motoring and generating mode. The only sensible task for the controller is to switch off both transistors until the current reaches zero. That is the reason for the sudden fall of the current reference values at higher speeds as in Fig. 5.22 - 5.24.

The derivation of the current reference values for smooth torque is based on finite element calculations of the static torque characteristic. Any deviation from smooth torque is due to calculation errors in the finite element program.

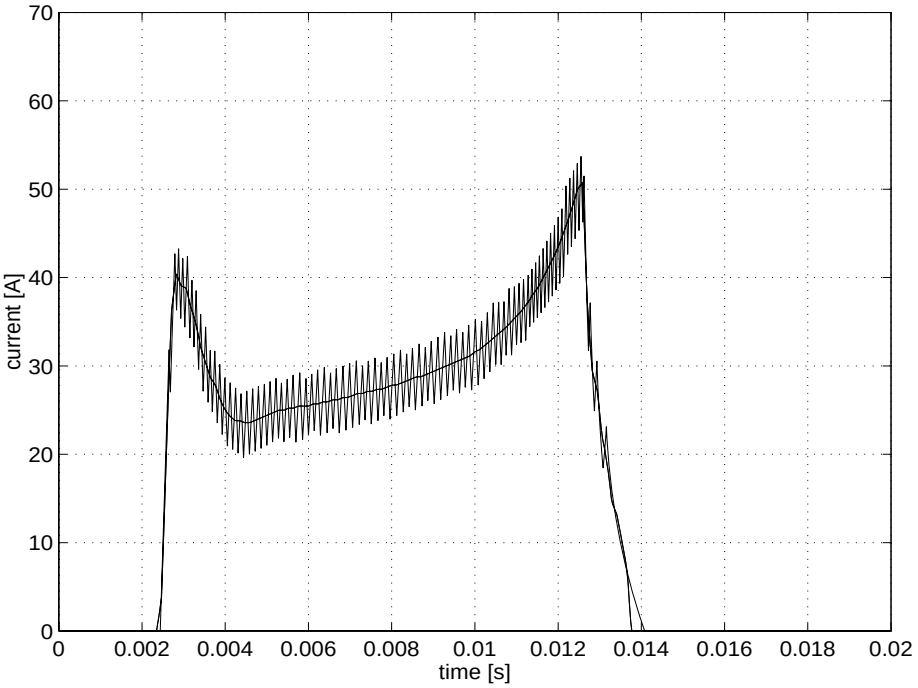

Fig. 5.17 *Simulated current waveform at 500 rpm and 9.5 Nm for the iron composite switched reluctance machine.*

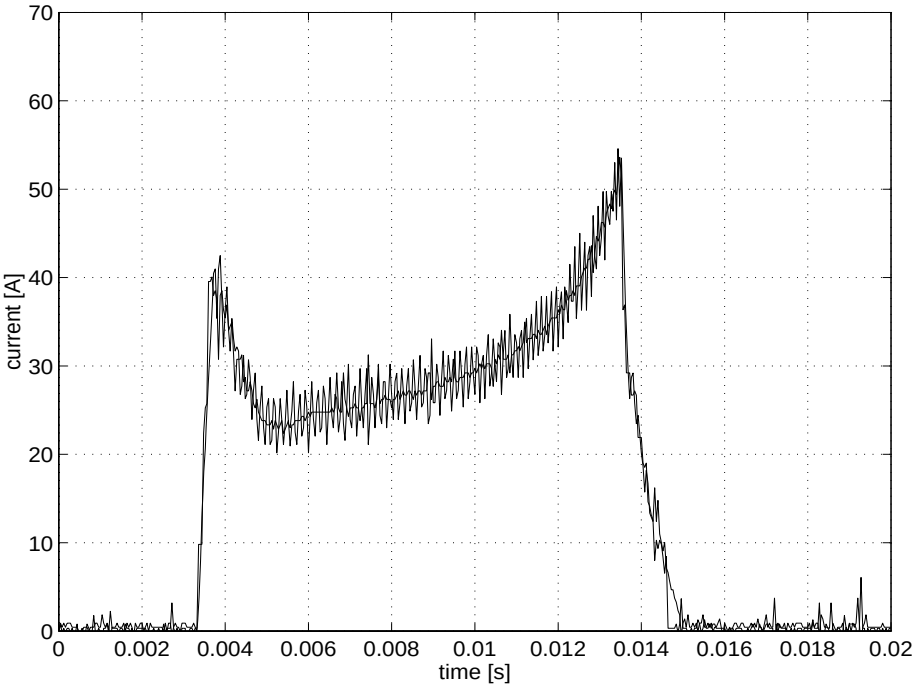

Fig. 5.18 *Measured current waveform at 500 rpm and 9.5 Nm for the iron composite switched reluctance machine.*

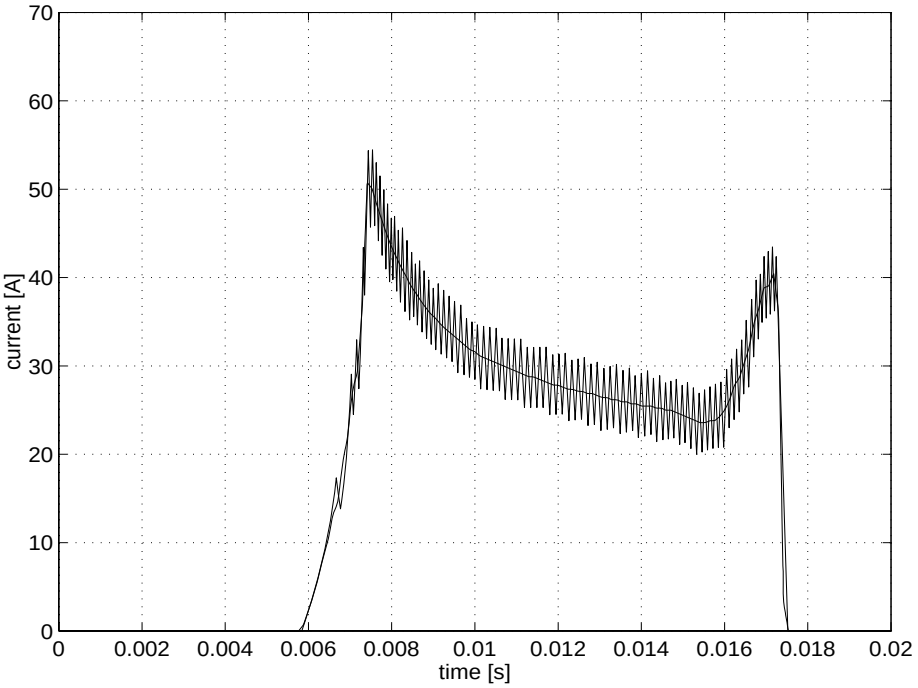

Fig. 5.19 *Simulated current waveform at 500 rpm and -9.5 Nm for the iron composite switched reluctance machine.*

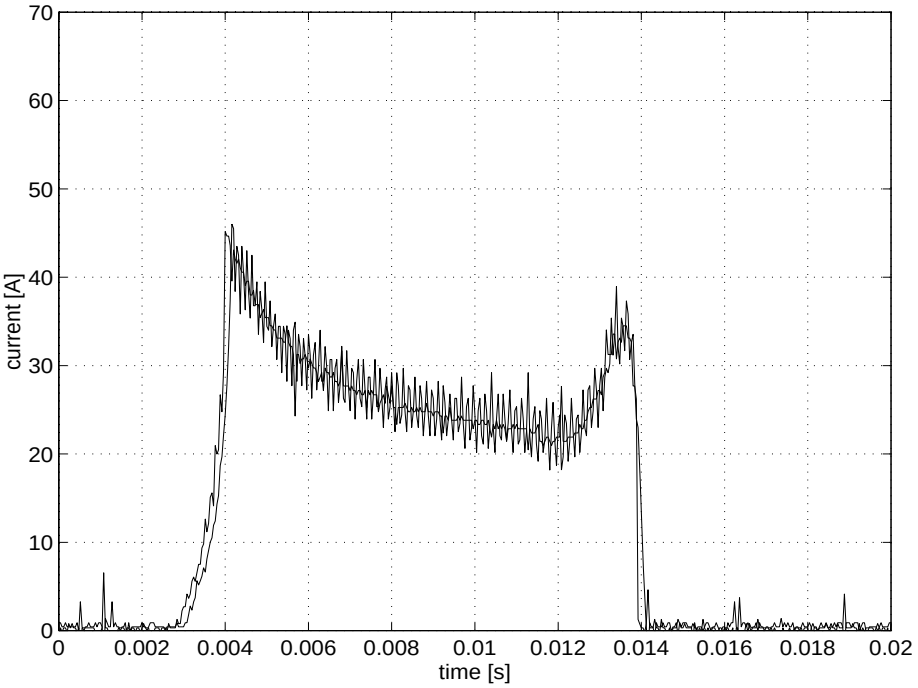

Fig. 5.20 *Measured current waveform at 500 rpm and -9.5 Nm for the iron composite switched reluctance machine.*

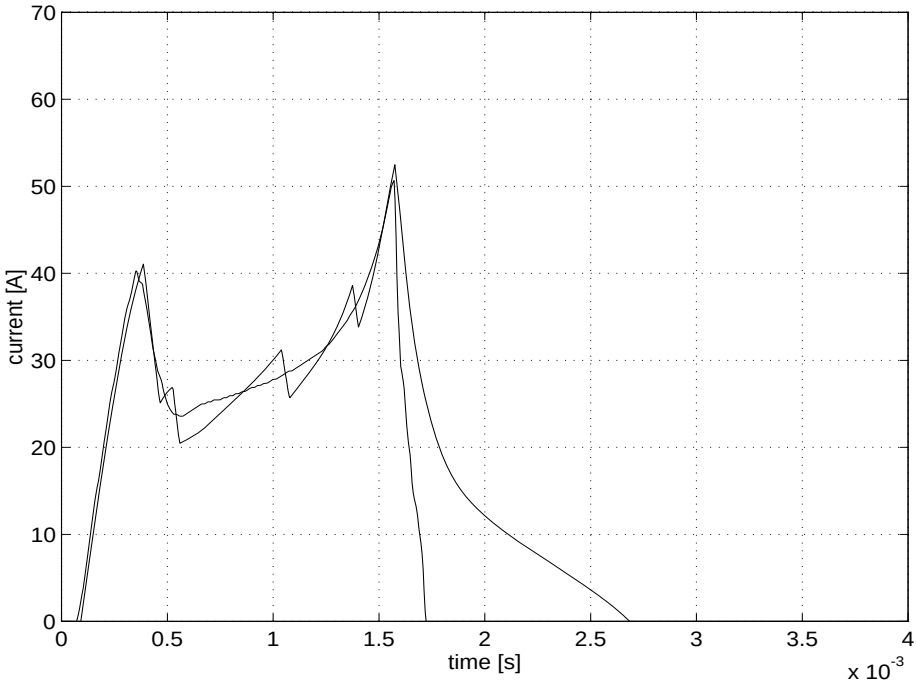

Fig. 5.21 *Simulated current waveform at 4000 rpm and 9.5 Nm for the iron composite switched reluctance machine.*

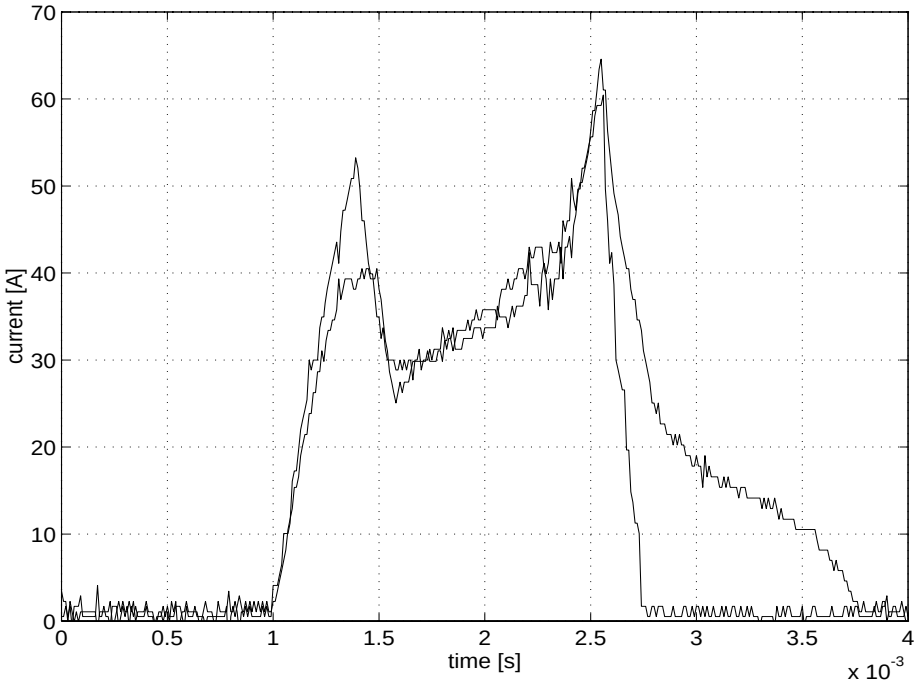

Fig. 5.22 *Measured current waveform at 4000 rpm and 9.5 Nm for the iron composite switched reluctance machine.*

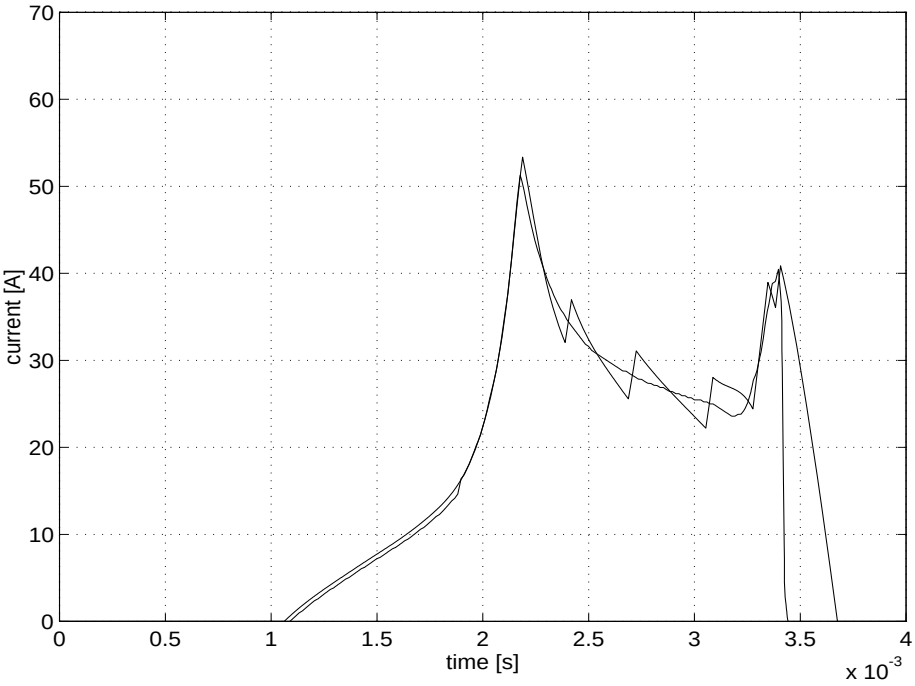

Fig. 5.23 *Simulated current waveform at 4000 rpm and -9.5 Nm for the iron composite switched reluctance machine.*

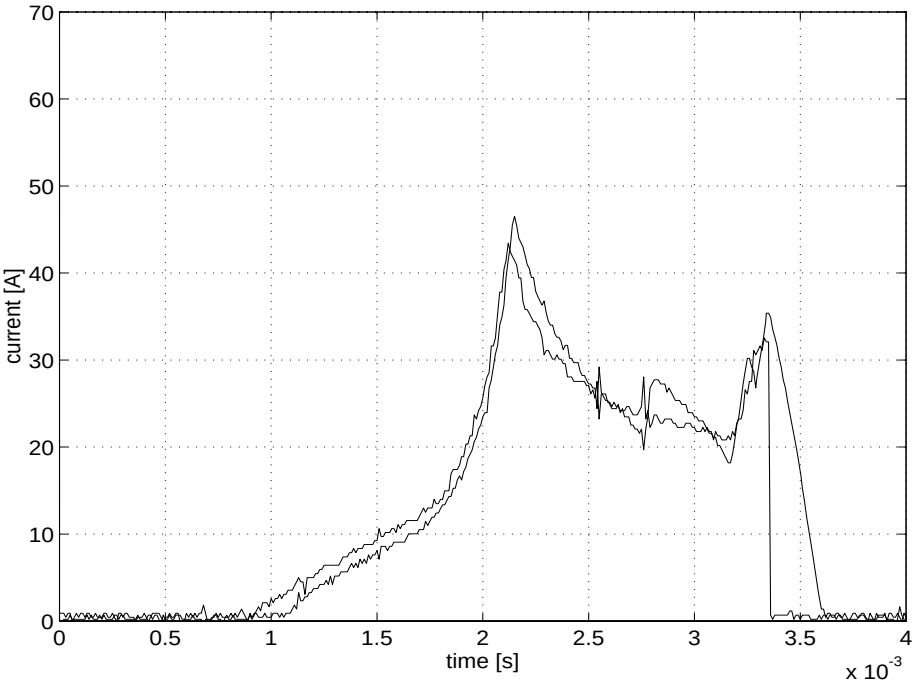

Fig. 5.24 *Measured current waveform at 4000 rpm and -9.5 Nm for the iron composite switched reluctance machine.*

Iron Lamination Machine Current Dynamics

The iron lamination switched reluctance machine is tested under the same conditions as the iron powder one. The same simulations and measurements are performed. A comparison between simulated and measured phase currents are shown in Fig. 5.25 to Fig. 5.32. The general statement regarding the amplitude of the actual current is valid for the iron lamination switched reluctance machine as well. In motoring mode, the actual current has to be slightly higher than the simulated one to overcome the iron losses in the machine. In generating mode, the iron losses help absorbing energy and the actual current is lower than the simulated one.

When comparing the torque production capability for the machines in Fig. 4.5 and Fig. 4.25, the iron lamination machine is slightly better at rotor angular positions near the aligned and unaligned position. Therefore, the penalty for producing smooth torque is not as great. The high current peaks at the leading and trailing edge of the current pulses are reduced, as well as the rms value of the current. This is consistent with the measurements regarding copper losses.

The average switching frequency during the current pulse is 7 kHz, the same as for the iron powder machine. The current regulator hysteresis band is 6 A.

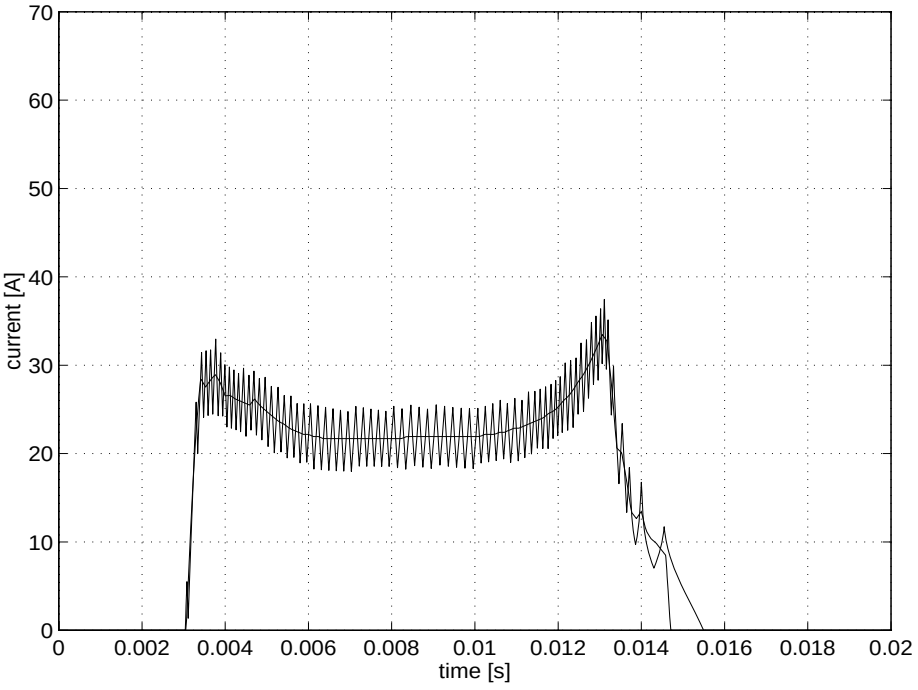

Fig. 5.25 *Simulated current waveform at 500 rpm and 9.5 Nm for the iron lamination switched reluctance machine.*

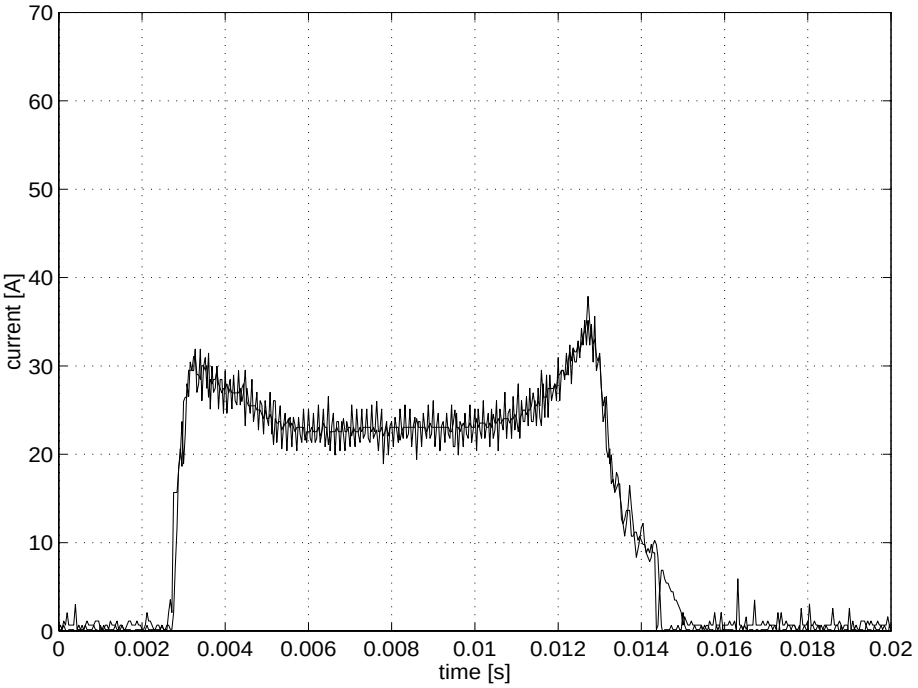

Fig. 5.26 *Measured current waveform at 500 rpm and 9.5 Nm for the iron lamination switched reluctance machine.*

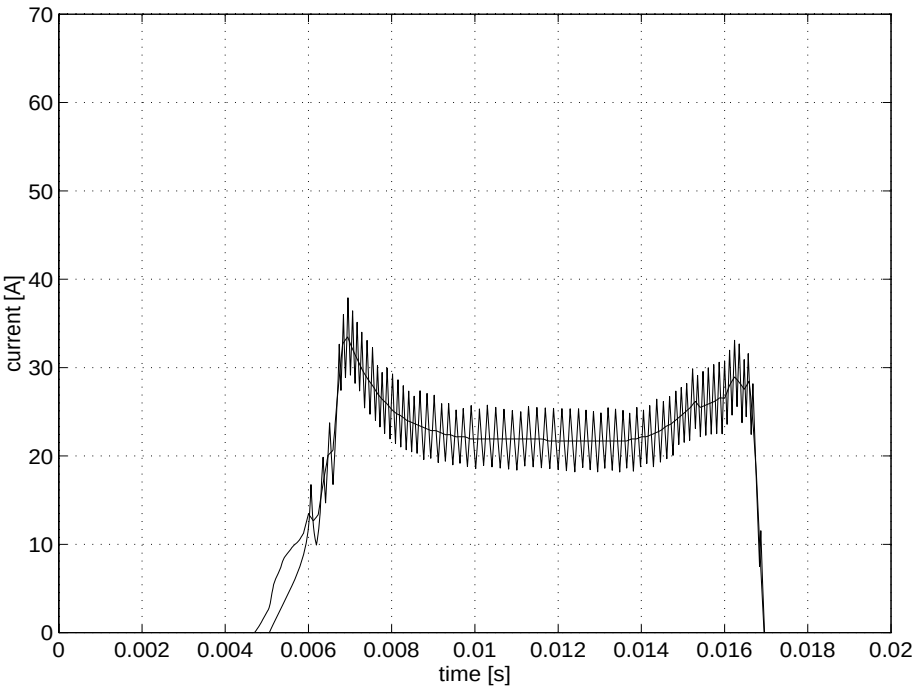

Fig. 5.27 *Simulated current waveform at 500 rpm and -9.5 Nm for the iron lamination switched reluctance machine.*

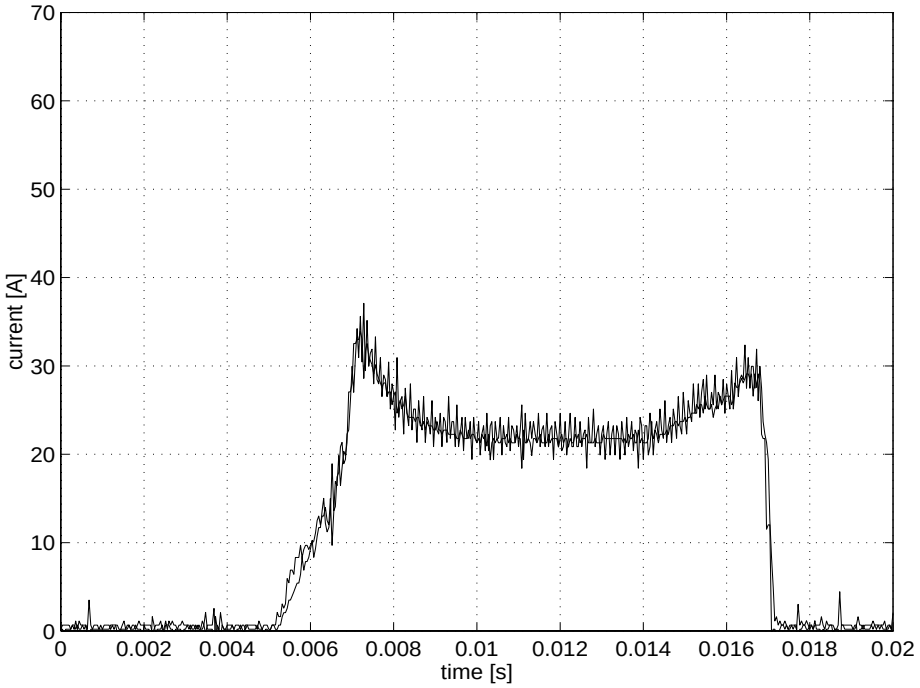

Fig. 5.28 *Measured current waveform at 500 rpm and -9.5 Nm for the iron lamination switched reluctance machine.*

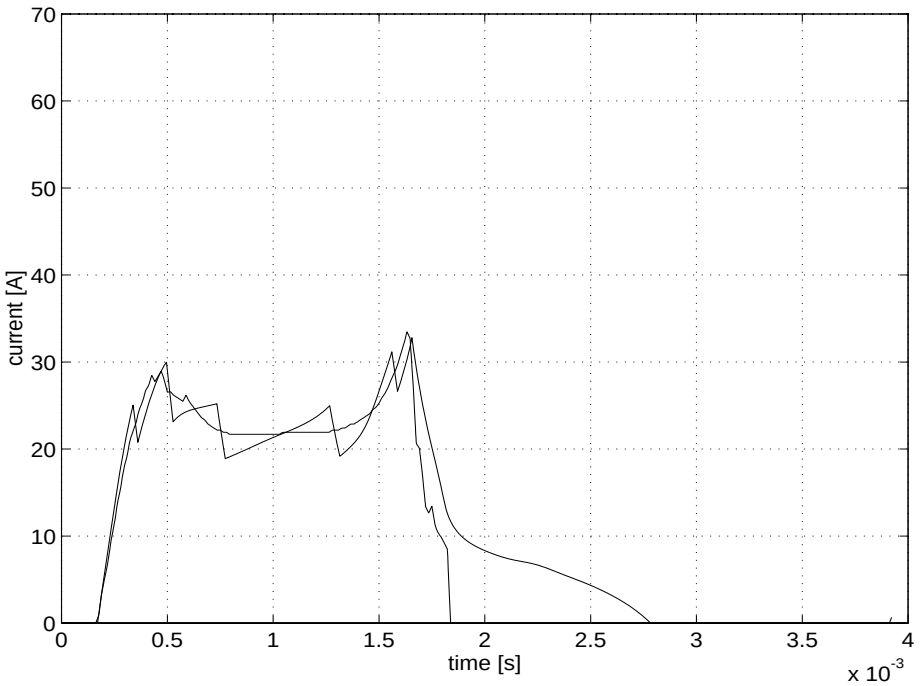

Fig. 5.29 *Simulated current waveform at 4000 rpm and 9.5 Nm for the iron lamination switched reluctance machine.*

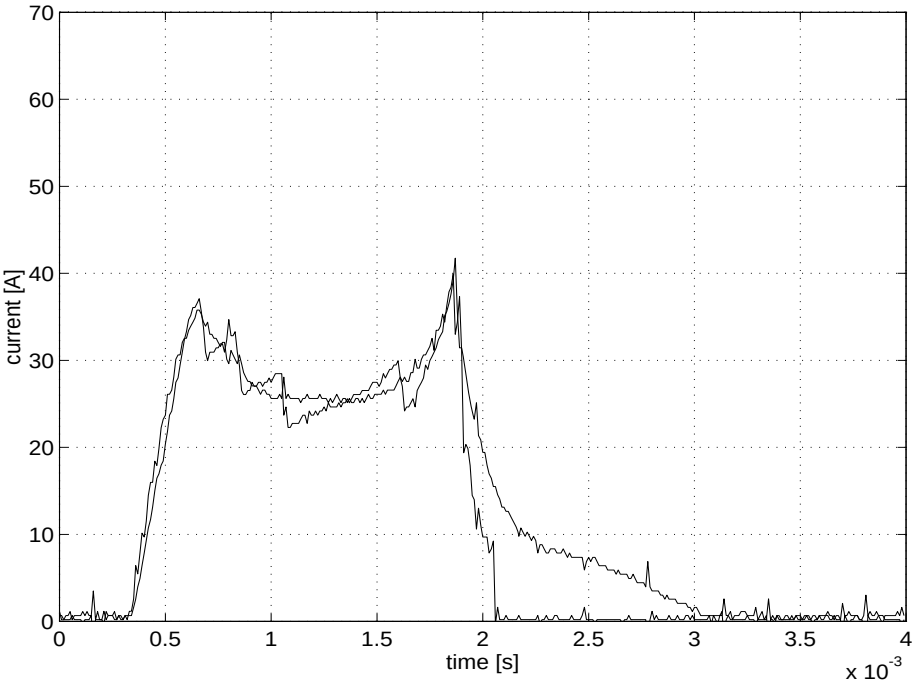

Fig. 5.30 *Measured current waveform at 4000 rpm and 9.5 Nm for the iron lamination switched reluctance machine.*

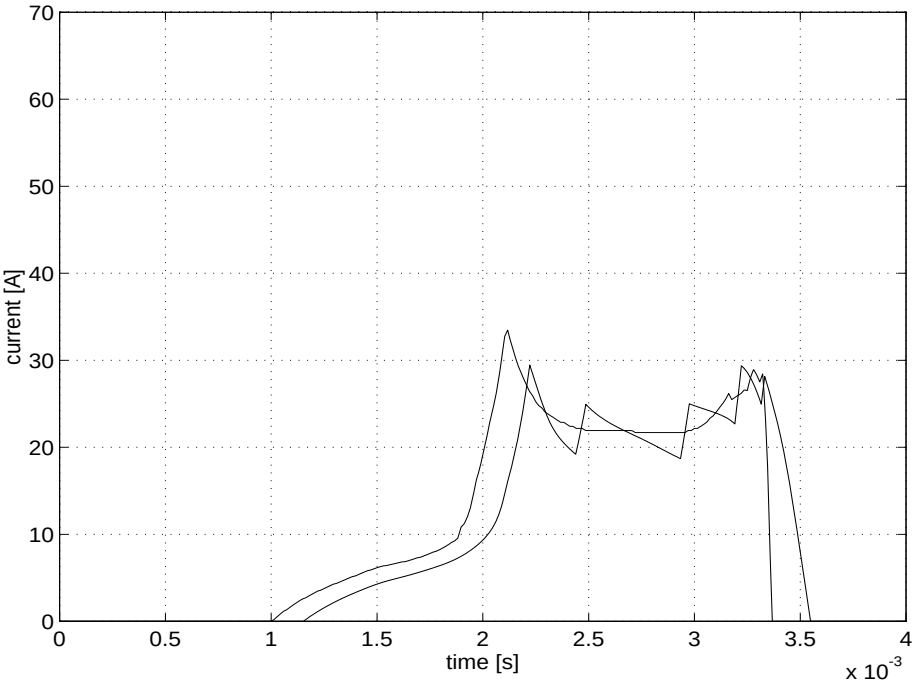

Fig. 5.31 *Simulated current waveform at 4000 rpm and -9.5 Nm for the iron lamination switched reluctance machine.*

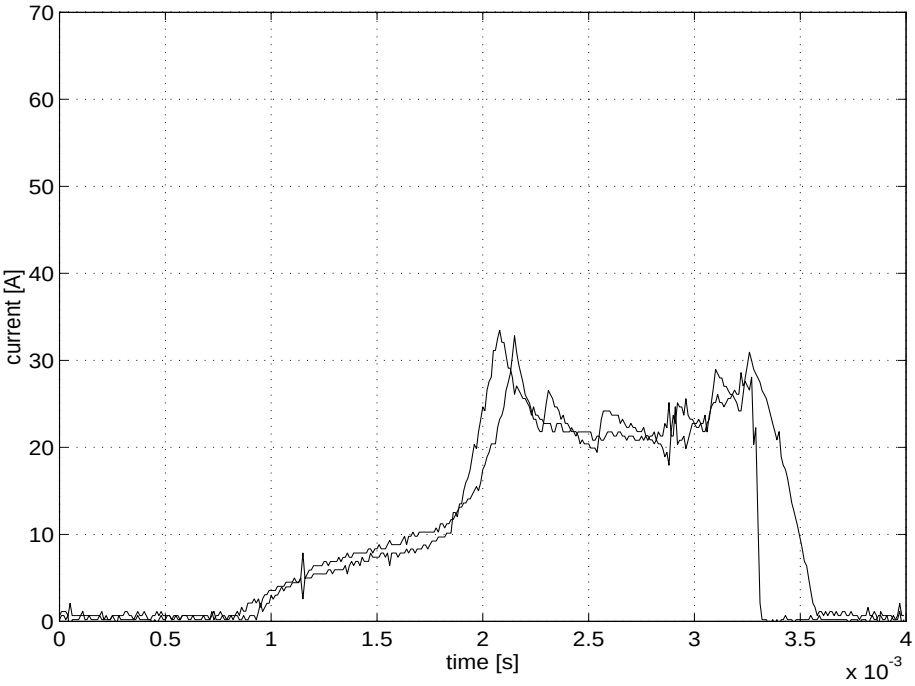

Fig. 5.32 *Measured current waveform at 4000 rpm and -9.5 Nm for the iron lamination switched reluctance machine.*

Dynamic Torque

Simulations of the dynamic torque show that it is possible to shape the current waveform to accomplish smooth torque in a three phase switched reluctance machine with six stator poles and four rotor poles. The high frequency torque ripple, seen in Fig. 5.33, is caused by the switching of the electrical energy converter. This is effectively dampened by the inertia of the machine rotor.

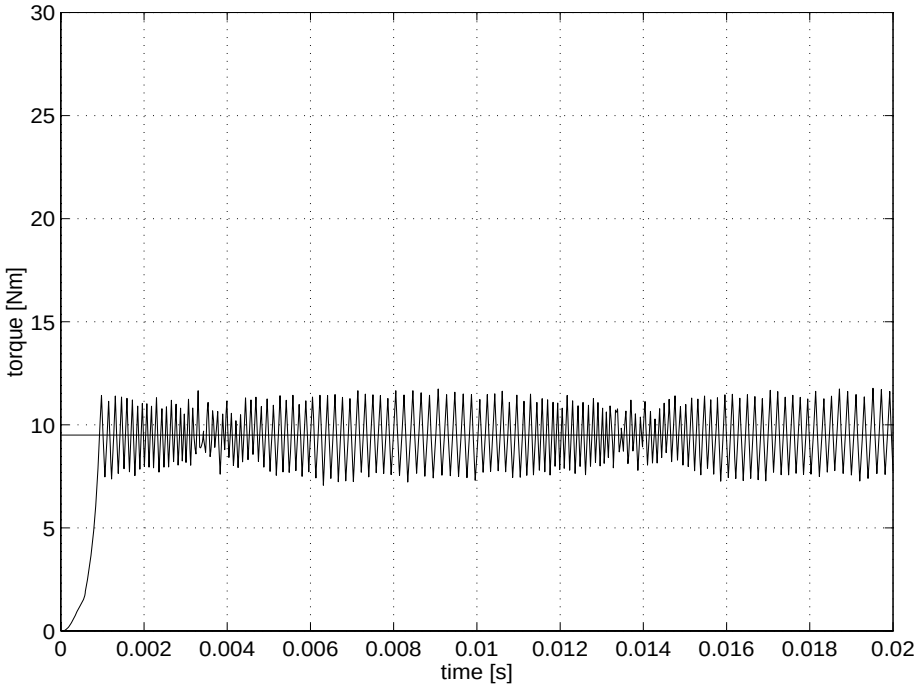

Fig. 5.33 *Simulated torque waveform at 500 rpm and 9.5 Nm for the iron lamination switched reluctance machine.*

At high speed, the ripple due to changing from one active phase to the next, is increasing. The current can not follow the desired reference current due to limited DC link voltage, and this affects the current waveform at the leading and the trailing edge of the current pulses. However, this increase in the torque ripple is marginal as can be seen in Fig. 5.34.

There exists no dynamic torque measurements. The VIBROMETER™ used for measuring the torque has limited bandwidth and is used only for average torque measurement. Bandwidth and dynamic resolution problems as well as problems with torsional oscillations in the experimental set-up makes it extremely difficult to measure the small superimposed torque ripple on a large average DC torque.

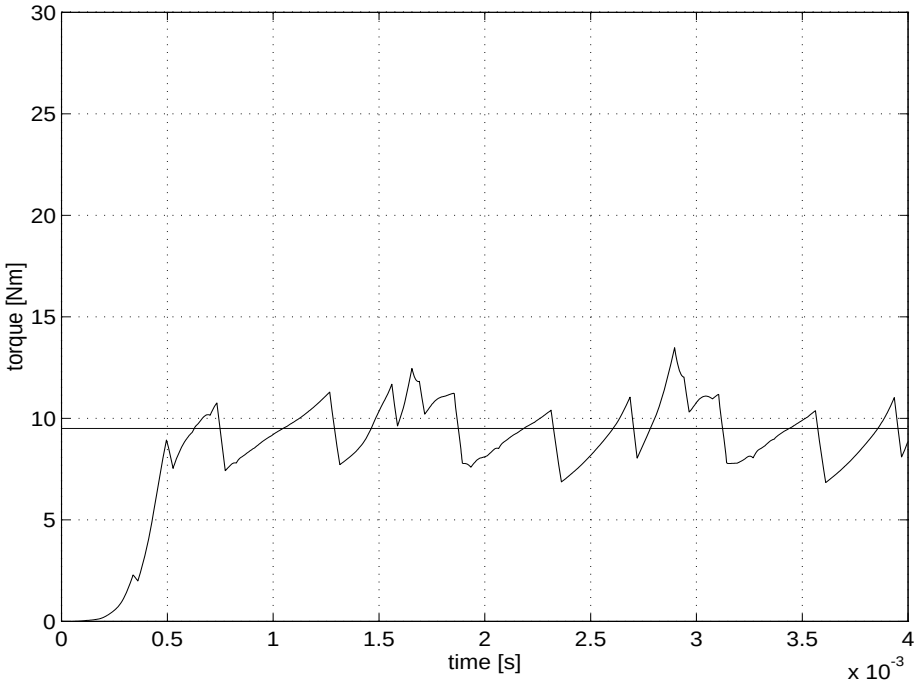

Fig. 5.34 *Simulated torque waveform at 4000 rpm and 9.5 Nm for the iron lamination switched reluctance machine.*

To demonstrate the torque ripple limit mode of operation, the torque ripple limit scaling constant is set to one and operation at 500 rpm and a torque reference of 9.5 Nm is simulated for the iron powder machine. This is seen in Fig. 5.35.

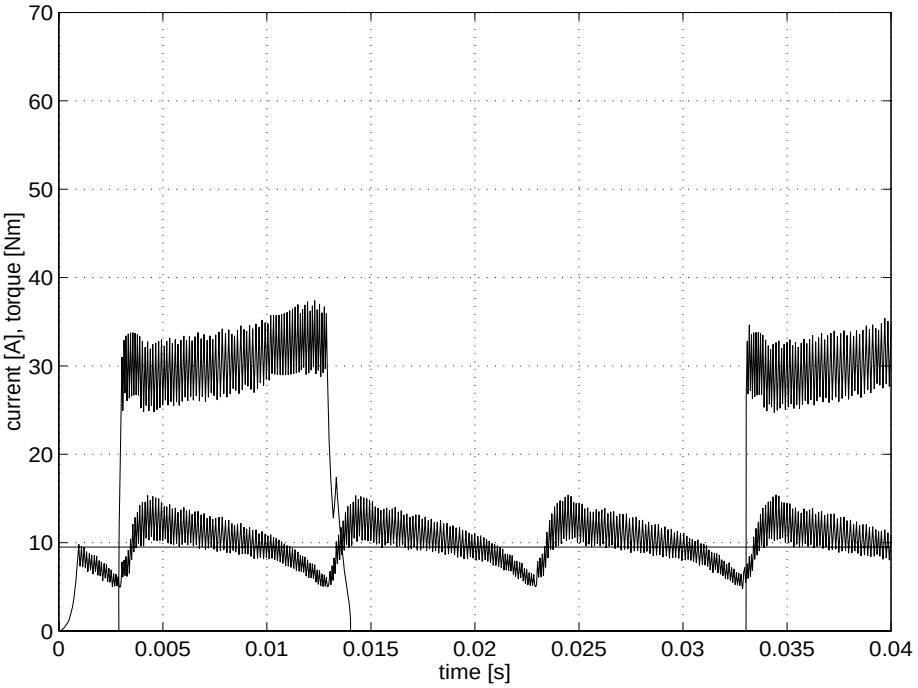

Fig. 5.35 *Torque and current for one phase in torque ripple limit control mode of operation for a speed of 500 rpm and 9.5 Nm.*

Calculations of the current in torque ripple limit control mode at rated speed and torque yield an rms value of 18.2 A. This value is to be compared with 21.6 A which is the current value simulated to give smooth torque operation. The reduction of the copper losses is approximately 30 % (or 100 W) compared to smooth torque operation.

The dynamical torque response is seen in Fig. 5.36. Depending on the rotor angular position, the time for a complete torque reversal varies between 0.25 ms and 1 ms. This variation might influence the choice of parameters in a speed controller, but that is beyond the scope of this thesis. In this simulation the speed and the DC link voltage is considered constant during the reversal.

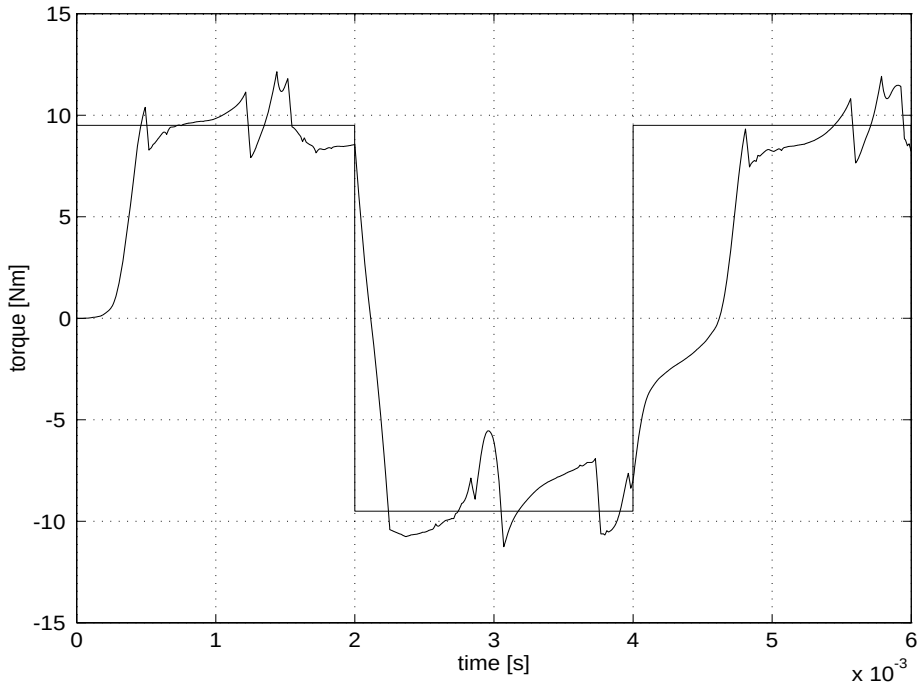

Fig. 5.36 *Simulated step change in the torque reference from full positive torque to full negative torque at the average speed of 4600 rpm.*

Nominal Operating Point Flux Linkage - Current Trajectory

At the nominal operating point, the simulated flux linkage - current trajectories in Fig. 5.37 are followed. In this figure some distinct differencies between the machines are seen. The iron powder composite material has lower saturation flux density, lower relative permeability. The flux linkage - current trajectory for the iron powder machine is extended to higher currents since smooth torque is required. Near the aligned and unaligned rotor angular position, excessive peaks in the current is needed for smooth torque operation.

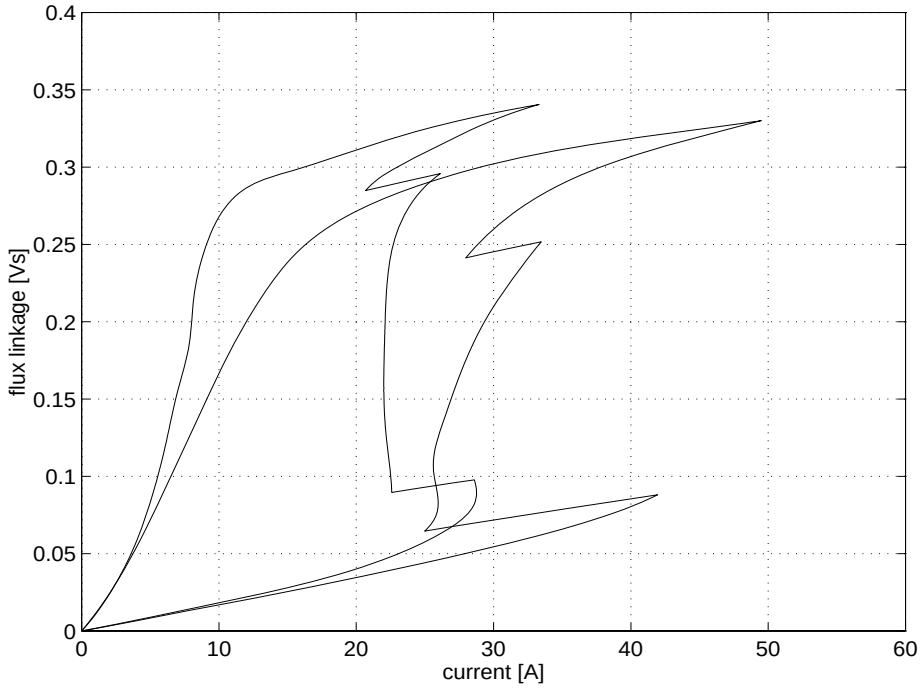

Fig. 5.37 *Simulated flux linkage current loops at 4600 rpm and 9.5 Nm. The trajectory which is extended to higher currents is associated with the iron powder composite switched reluctance machine.*

Summary

Two different switched reluctance machines are tested. One is a conventionally built machine, and the other is built with a novel iron composite material as a flux conductor. This composite material has a unique combination of electrical, magnetic and mechanical characteristics, making it a competitor in machine applications where a high electrical frequency is expected.

At the nominal operating point (rated load and speed), calculations and measurements show that the iron losses are approximately the same for the two machines. It can also be concluded that 70 - 75 % of the iron losses are confined to the stator, a figure that equals the weight of the stator iron compared to the overall iron weight. At the nominal operating point, the iron losses are approximately 500 W, whereas the copper losses for the iron lamination machine are 200 W and the copper losses for the iron powder machine are 300 W.

The difference in the copper losses is mainly due to the constraint imposed on the torque. Smooth torque operation leads to pronounced current peaks in the current waveforms for the iron powder machine, since the torque

production capability is lower than for the iron lamination machine at rotor angular positions near the aligned and unaligned position. In other words, smooth torque operation leads to a higher efficiency penalty for the iron powder machine. Simulations show that if a torque ripple is allowed in the iron powder machine, the copper losses are reduced almost to the level found for the iron lamination machine. Allowing torque ripple for the lamination machine reduces the copper losses marginally. The same efficiency is therefore expected at the nominal operating point, the difference being the quality of the torque.

Although smooth torque operation is achieved, the noise level from the switched reluctance machines is higher than the noise level from an induction machine of the same size. This is an observation based on the subjective perception of the author, rather than measurements on the actual sound power level.

6

Conclusions

A torque controlled switched reluctance machine drive system has been developed. The unique aspects of this work are

- a switched reluctance machine in a soft magnetic composite material is built and tested,
- a new torque control system for switched reluctance machines is presented,
- an improved empirical iron loss model that does not require extensive iron loss measurements on the iron core.

A table based torque controller for switched reluctance machines is presented. The switched reluctance machine is a non-linear system and the torque as a function of current is difficult to describe in algebraic equations. Therefore, the proposed torque control system is based on extensive à priori calculations of current reference values for all the phases. These current reference values are stored in two EPROMs on a *current reference generator* card that has an updating frequency in excess of 100 kHz. The phase currents are controlled with hysteresis controllers, one for each phase, with selectable hystersis band.

The main advantages with this approach are

- smooth torque operation is possible,
- high controller updating frequency, attractive for high speed applications,

- great flexibility in the sense that for every individual switched reluctance machine type, individual current reference tables can be calculated and stored in EPROMs.

Knowing the torque and the flux linkage as a function of rotor angular position and current, the control designer is able to choose the mode of operation. Torque is controlled by *indirect torque control*, which means that for every rotor angular position and angular velocity the most suitable current reference values are calculated to accomplish this torque. In *smooth torque control* mode, current reference values are calculated for smooth torque, and in *torque ripple limit control* mode the control designer is able to specify a certain amount of torque ripple. Depending on the machine geometry, this may lead to a higher efficiency.

A model for the iron losses at the nominal operating point in switched reluctance machines is described. The model separates the eddy current and the hysteresis losses and give an approximate description of the loss distribution. The calculated iron losses match the measurements at the nominal operating point.

It is shown that for the switched reluctance machines used in this thesis, which are wound for a speed of 4600 rpm, the iron losses in the iron powder machine equal the iron losses in the lamination machine at the nominal operating point. If the machines were to be rewound for even higher speeds, the iron losses in the iron powder machine are expected to be lower than those of the iron laminatied one. Thus, the iron powder composite material can be used as a flux conductor in switched reluctance machines. Since almost all the losses in the composite material consist of hysteresis losses, future research will be focused on reduction of the coercivity.

As to the magnitude and distribution of the losses it is shown that the iron losses exceed the copper losses. At the nominal operating point the iron losses are approximately 500 W whereas the copper losses are only 200 W for the iron lamination machine and 300 W for the iron powder machine. Higher copper losses in the iron powder machine are mostly due to the smooth torque constraint. The iron powder machine has lower torque production capability at rotor angular positions near the aligned and unaligned position. This causes high current peaks in the current reference values at the leading and trailing edge of the current pulses. However, if torque ripple is allowed it is shown that the current reference peaks are

reduced significantly for the iron powder machine. This leads to less stress on the power semiconductors as well as a lower rms value of the current and the copper losses are reduced by almost 100 W. The conclusion is that the excessive copper losses are mainly machine geometry dependent rather than material dependent, and smooth torque constraint imposes a higher efficiency penalty for the iron powder machine. At the nominal operating point, the expected efficiency (based on simulations) for the iron powder switched reluctance machine in torque ripple limit control mode is 84 % which equals the iron lamination machine.

However, calulations show that if the switched reluctance machine used in this thesis is equipped with the best available standard iron laminations an efficiency of 90 % is expected at the nominal operating point. This is due to the iron losses, that reduces from 500 W to approximately 200 W. It is important to note that investigations on machine design is beyond the scope of this thesis and the comparisons of the efficiencies are based on a given machine geometry.

Topics for Future Research

In order for the switched reluctance machine to compete favourably with other electrical machines, the advantages (as well as drawbacks) of using a switched reluctance machine have to be clarified. The theoretical as well as practical limits for the torque production capability must be examined. Therefore, it is important to find the optimal machine geometries in terms of torque per volume or torque per weight or other figures of merit, and to compare these with other machine types. The parametrisation of the copper and iron losses as well as the torque production capability as functions of the machine geometry provide an opportunity to apply optimisation algorithms. Thus, it will be possible to find the optimal machine geometry under a given number of constraints.

In order to theoretically predict optimal performance, a thermal model of switched reluctance machines must be examined, and compared with thermal models of other electrical machines. The impact of the lower thermal conductivity for the iron composite material should be investigated. If the iron composite material is to be used in high speed applications, an investigation of the mechanical properties is of vital interest.

Models of iron losses due to high frequency switching must be developed in order to accurately predict iron losses at operating points other than the nominal operating point. Since losses in the iron composite material are mainly hysteresis losses, at least at the frequencies involved in most electrical machines, research on how to reduce the coercive force in the composite is important. In addition to that, a more theoretical model (based on physical principles) of the iron losses in the iron composite material should be developed.

Finally, the iron composite material could be applied to other machine types than the switched reluctance machine. Construction of a permanent magnet synchronous machine based on iron composite material would provide interesting information on machine design using iron composites.

References

[1] Alaküla, M., Cedell, T., Persson, M., Sjöberg, L. (1995), *"An Iron Composite Based Switched Reluctance Machine"*, Conf. Proceedings Stockholm Power Tech, June 1995, pp. 251 - 255.

[2] Boivie, J. (1995), *"Losses in a Small Switched Reluctance Machine"*, Tech. Lic. thesis, Department of Electric Power Engineering, Royal Institute of Technology, Stockholm, Sweden.

[3] Bojrup, M., Karlsson, P. (1995), *"Torque Control of a Switched Reluctance Machine"*, M. Sc. thesis, Department of Industrial Electrical Engineering and Automation, Lund Institute of Technology, Lund, Sweden.

[4] Brogren, J., Staf, O. (1995), *"TAGE - tabellhanterare*, (in Swedish)

[5] Cedell, T. (1995), *"Magnetostrictive Materials and Selected Applications"*, Ph. D. dissertation, KFS, Lund, Sweden.

[6] De Doncker, R.W., Lyons, J.P. (1991), *"An Auxiliary Quasi-Resonant DC Link Inverter for Switched Reluctance Machines"*, EPE Conference Proceedings, Pt. 4, 1991, pp. 18 - 23.

[7] Ehsani, M., Husain, I., Mahajan, S., Ramani, K.R. (1994), *"New Modulation Encoding Techniques for Indirect RotorPosition Sensing in Switched Reluctance Motors"* , IEEE Transactions on Industry Applications, Vol. 30, No. 1, January/February 1994, pp. 85 - 91.

[8] Fitzgerald, A.E., Kingsley, C., Umans, S.D. (1988), *"Electric Machinery"*, 4th Edition, McGraw-Hill Book Co.

[9] Harris, M.R., Miller, T.J.E. (1988), *"Comparison of Design and Performance Parameters in Switched Reluctance and Induction Motors"*, 1988.

[10] Hayashi, Y., Miller, T.J.E. (1994), *"A New Approach to Calculating Core Losses in the SRM"*, IAS Conference Proceedings, October 1994, Vol. 1, pp. 322 - 328.

[11] Krishnan, R., Bharadwaj, A.S. (1991), *"A Comparative Study of Various Motor Drive Systems for Aircraft Applications"*, 1991.

[12] Köfler, H. (1990), *"Losses in Electrical Machines"*, Post graduate course lecture notes, TKK OFFSET, Helsinki University of Technology, Helsinki, Finland.

[13] Lawrenson, P.J., Stephenson, J.M., Blenkinsop, P.T., Corda, J., Fulton, N.N. (1980), *"Variable-Speed Switched Reluctance Motors"*, IEE Proc., Vol. 127, pt. B, No. 4, July 1980, pp. 253 - 265.

[14] Lawrenson, P.J. (1992), *"Switched Reluctance Drives: A Perspective"*, Int. Conference on Electrical Machines, pp. 12 - 21, 1992.

[15] Lovatt, H.C., Stephenson, J.M. (1992), *"Measurement of Magnetic Characteristics of Switched Reluctance Motors"*, Int. Conference on Electrical Machines, Vol. 2, pp. 465 - 469, 1992.

[16] MacMinn, S.R. (1989), *"Control of a Switched-Reluctance Aircraft Engine Starter-Generator Over a Very Wide Speed Range"* .

[17] Materu, P., Krishnan, R. (1992), *"Estimation of Switched Reluctance Motor Losses"*, IEEE Transactions on Industry Applications, Vol. 28, No. 3, May/June 1992, pp. 668 - 679.

[18] Miller, T.J.E. (1985), *"Converter Volt-Ampere Requirements of the Switched Reluctance Motor Drive"*, IEEE Transactions on Industry Applications, Vol. 1A-21, No. 5, September/October 1985, pp. 1136 - 1144.

[19] Miller, T.J.E., Cossar, C., Hutton, A.J. (1989), *"Design of a Synchronous Reluctance Motor Drive"* .

[20] Miller, T.J.E. (1993), *"Switched Reluctance Motors and Their Control"*, Oxford University Press, Oxford, England.

[21] Moreira, J.C. (1992), *"Torque Ripple Minimization in Switched Reluctance Motors via Bi-Cubic Spline Interpolation"* .

[22] *Motor- och Generatorplåt (icke orienterad elektroplåt)* (in Swedish), Surahammars Bruks AB, Surahammar, Sweden.

[23] Park, S.S., Lipo, T.A., *"New Series Resonant Converter for Variable Reluctance Motor Drive"*.

[24] Radun, A.V. (1994), *"Design Considerations for the Switched Reluctance Motor"*, IAS Conference Proceedings, October 1994, Vol. 1, pp. 290 - 297.

[25] Radun, A.V. (1992), *"High-Power Density Switched Reluctance Motor Drive for Aerospace Applications"*, IEEE Transactions on Industry Applications, Vol. 28, No. 1, January/February 1992, pp. 113 - 119.

[26] Ray, W.F., Al-Bahadly, I.H. (1993), *"Sensorless Methods for Determing the Rotor Position of Switched Reluctance Motors"*, EPE Conference Proceeding, 1993, pp. 7 - 13.

[27] Reay, D.S., Green, T.C., Williams, B.W. (1993), *"Neural Networks used for Torque Ripple Minimisation from a Switched Reluctance Motor"*, EPE Conference Poceedings, 1993, pp. 1 - 6.

[28] Rochford, C., Kavanagh, R.C., Egan, M.G., Murphy, J.M.D. (1993), *"Development of Smooth Torque in Switched Reluctance Motors using Self-Learning Techniques"*, EPE Conference Proceeding, 1993, pp. 14 - 19.

[29] Schramm, D.S., Williams, B.W., Green, T.C. (1992), *"Torque Ripple Reduction of Switced Reluctance Motors by Phase Current Optimal Profiling"* .

[30] Slemon, G. (1966), *"Magnetoelectric Devices"*, John Wiley & Sons, Inc., New York, United States of America.

[31] Stephenson, J.M., Corda, J. (1979), *"Computation of Torque and Current in Doubly Salient Reluctance Motors From Nonlinear*

Magnetization Data", Proceedings IEE, Vol. 126, No. 5, May 1979, pp. 393 - 396.

[32] Wallace, A.K., Spee, R., Martin, L.G. (1987), *"Current Harmonics and Acoustic Noise in AC Adjustable-Speed Drives"*, IEEE Transactions on Industry Applications, Vol. 26, No. 2, March/April 1990, pp. 267 - 273.

[33] Vucosavic, S., Stefanovic, V.R. (1991), *"SRM Inverter Topologies: A Comparative Evaluation"*, IEEE Transactions on Industry Applications, Vol. 27, No. 6, November/December 1991, pp. 1034 - 1047.

References

[ ] Alaküla, M., Cedell, T., Persson, M., Sjöberg, L. (1995), *"An Iron Composite Based Switched Reluctance Machine"*, Conf. Proceedings Stockholm Power Tech, June 1995, pp. 251 - 255.

[1] Amin, B. (1992), *"Electromagnetic Performance Comparison in Electrical Machines"*, ETEP, Vol. 2, No. 2, March/April 1992, pp. 83 - 90.

[2] Blaabjerg, F., Pedersen, J.K. (1993), *"Digital Implemented Random Modulation Strategies for AC and Switched Reluctance Drives"*, 1993.

[3] Blake, R.J., Davis, R.M., Ray, W.F., Fulton, N.N., Lawrenson, P.J., Stephenson, J.M. (1980), *"The Control of Switched Reluctance Motors for Battery Electric Road Vehicles"* .

[4] Boivie, J. (1993), *"Iron Loss Model and Measurements of the Losses in a Switched Reluctance Motor"* , IEE Proceedings, EMD September 1993, pp. 219 - 222.

[ ] Boivie, J. (1995), *"Losses in a Small Switched Reluctance Machine"*, Tech. Lic. thesis, Department of Electric Power Engineering, Royal Institute of Technology, Stockholm, Sweden.

[ ] Bojrup, M., Karlsson, P. (1995), *"Torque Control of a Switched Reluctance Machine"*, M. Sc. thesis, Department of Industrial Electrical Engineering and Automation, Lund Institute of Technology, Lund, Sweden.

[5] Bose, B.K., Miller, T.J.E., Szczesny, P.M., Bicknell, W.H. (1985), *"Microcomputer Control of Switched Reluctance Motor"* .

[ ] Brogren, J., Staf, O. (1995), *"TAGE - tabellhanterare*, (in Swedish)

[6] Byrne, J.V. (1972), *"Tangential Forces in Overlapped Pole Geometries Incorporating Ideally Saturable Material"*, IEEE Transactions on Magnetics, Vol. Mag-8, No. 1, March 1972, pp. 2 - 9.

[7] Cameron, D.E., Lang, J.H., Umans, S.D. (1992), *"The Origin and Reduction of Acoustic Noise in Doubly Salient Varieble-Reluctance Motors"*, IEEE Transactions on Industry Applications, Vol. 28, No. 6, November/December 1992, pp. 1250 - 1255.

[8] Cedell, T. (1995), *"Magnetostrictive Materials and Selected Applications"*, Ph. D. dissertation, KFS, Lund, Sweden.

[8] Chappell, P.H. (1988), *"Current Pulses in Switced Reluctance Motors"*, IEE Proceedings, Vol. 135, Pt. B, No. 5, September 1988, pp. 224 - 230.

[9] Corda, J., Olaca, M. (1993), *"Analysis of Losses in Power Electronic Converter of SR Drive"*, EPE Conference Proceedings, 1993, pp. 49 - 53.

[10] Craggs, J.L. (1993), *"Specifying and Measuring the Noise Level of Electric Motors in Operation"*, IEEE Transactions on Industry Applications, Vol. 29, No. 3, May/June 1993, pp. 611 - 615.

[11] Davis, R.M., *"The Switched Reluctance Drive"*.

[12] De Doncker, R.W., Lyons, J.P. (1991), *"An Auxiliary Quasi-Resonant DC Link Inverter for Switched Reluctance Machines"*, EPE Conference Proceedings, Pt. 4, 1991, pp. 18 - 23.

[13] Egan, M.G., Harrington, M.B., Murphy, J.M.D. (1991), *"PWM-Based Position Sensorless Control of Variable Reluctance Motor Drives"*, EPE Conference Proceedings, Pt. 4, 1991, pp. 24 - 29.

[14] Ehsani, M., Husain, I., Mahajan, S., Ramani, K.R. (1994), *"New Modulation Encoding Techniques for Indirect RotorPosition Sensing in Switched Reluctance Motors"* , IEEE Transactions on

Industry Applications, Vol. 30, No. 1, January/February 1994, pp. 85 - 91.

[15] El-Antably, A.M. (1980), *"Energy Efficient Motors of the Reluctance Type"*, Conference Proceedings on the 11th Energy Technology Conference, 1980.

[16] Elmas, C., Zelaya de la Parra, H. (1992), *"A DSP Controlled Switched Reluctance Drive System for Wide Range of Operating Speeds"*, 1992.

[17] Faiz, J., Finch, J.W. (1993), *"Aspects of Optimisation for Switched Reluctance Motors"*, IEEE Transactions on Energy Conversion, Vol. 8, No. 4, December 1993, pp. 704 - 713.

[ ] Fitzgerald, A.E., Kingsley, C., Umans, S.D. (1988), *"Electric Machinery"*, 4th Edition, McGraw-Hill Book Co.

[ ] Fukui, K.,Watanabe, I, Morita, M. (1972), *"Compressed Iron Powder Core for Electrical Machines"*, IEEE Transactions on Magnetics, September 1972, pp. 682 - 684.

[18] Fulton, N.N. (1992), *"SR Drives for Battery Electric Traction - A Comparative Assessment"*, 1992.

[19] Harris, M.R., Miller, T.J.E. (1988), *"Comparison of Design and Performance Parameters in Switched Reluctance and Induction Motors"*, 1988.

[20] Hayashi, Y., Miller, T.J.E. (1994), *"A New Approach to Calculating Core Losses in the SRM"*, IAS Conference Proceedings, October 1994, Vol. 1, pp. 322 - 328.

[ ] Huang, H., Debruzzi, M., Riso, T. (1993), *"A Novel Stator Construction for High Power Density and High Efficiency Permanent Magnet Brushless DC Motors"*, SAE International Congress and Exposition, March 1993.

[21] Jones, D. (1989), *"Current Status of Switched Reluctance Motors"*, Intelligent Motion.

[22] Krishnan, R., Bharadwaj, A.S. (1991), *"A Comparative Study of Various Motor Drive Systems for Aircraft Applications"*, 1991.

[23] Krishnan, R. (1986), *"Selection Criteria for Servo Motor Drives"*.

[ ] Köfler, H. (1990), *"Losses in Electrical Machines"*, Post graduate course lecture notes, TKK OFFSET, Helsinki University of Technology, Helsinki, Finland.

[24] Lai, J.C.S., Milthorpe, J.F., Pulle, D.W.J., Huynh, N. (1993), *"Acoustic Studies of Switched Reluctance Motors"*, Internoise Conference Proceedings, 1993, pp. 1175 - 1178.

[25] Lawrenson, P.J., Stephenson, J.M., Blenkinsop, P.T., Corda, J., Fulton, N.N. (1980), *"Variable-Speed Switched Reluctance Motors"*, IEE Proc., Vol. 127, pt. B, No. 4, July 1980, pp. 253 - 265.

[26] Lawrenson, P.J. (1983), *"Switched-Reluctance Motor Drives"*, Electronics and Power, February 1983.

[27] Lawrenson, P.J. (1992), *"Switched Reluctance Drives: A Perspective"*, Int. Conference on Electrical Machines, pp. 12 - 21, 1992.

[28] Lovatt, H.C., Stephenson, J.M. (1992), *"Measurement of Magnetic Characteristics of Switched Reluctance Motors"*, Int. Conference on Electrical Machines, Vol. 2, pp. 465 - 469, 1992.

[29] MacMinn, S.R. (1989), *"Control of a Switched-Reluctance Aircraft Engine Starter-Generator Over a Very Wide Speed Range"* .

[30] Materu, P., Krishnan, R. (1992), *"Estimation of Switched Reluctance Motor Losses"*, IEEE Transactions on Industry Applications, Vol. 28, No. 3, May/June 1992, pp. 668 - 679.

[31] Miller, T.J.E., Cossar, C., Hutton, A.J. (1989), *"Design of a Synchronous Reluctance Motor Drive"* .

[32] Miller, T.J.E. (1985), *"Converter Volt-Ampere Requirements of the Switched Reluctance Motor Drive"*, IEEE Transactions on Industry Applications, Vol. 1A-21, No. 5, September/October 1985, pp. 1136 - 1144.

[33] Miller, T.J.E., Bower, P.G., Becerra, R., Ehsani, M., *"Four-Quadrant Brushless Reluctance Motor Drive"*.

[34] Miller, T.J.E. (1993), *"Switched Reluctance Motors and Their Control"* .

[ ] Miller, T.J.E. (1993), *"Switched Reluctance Motors and Their Control"*, Oxford University Press, Oxford, England.

[35] Moghbelli, H., Adams, G.E., Hoft, R.G. (1991), *"Performance of a 10-Hp Switched Reluctance Motor and Comparison with Induction Motors"*, IEEE Transactions on Industry Applications, Vol. 27, No. 3, May/June 1991, pp. 531 - 538.

[36] Moghbelli, H.H., Rashid, M.H. (1990), *"Performance Review of AC Adjustable Drives"* .

[37] Moreira, J.C. (1992), *"Torque Ripple Minimization in Switched Reluctance Motors via Bi-Cubic Spline Interpolation"* .

[ ] *Motor- och Generatorplåt (icke orienterad elektroplåt)* (in Swedish), Surahammars Bruks AB, Surahammar, Sweden.

[38] Ortmann, R., Schöner, H.P. (1993), *"Turn-Off Angle Control of Switched Reluctance Motors for Optimum Torque Output"*, EPE Conference Proceedings, 1993, pp. 20 - 25.

[39] Park, S.S., Lipo, T.A., *"New Series Resonant Converter for Variable Reluctance Motor Drive"*.

[40] Patterson, D., Spée, R. (1994), *"The Design and Developement of an Axial Flux Permanent Magnet Brushless DC Motor for Wheel Drive in a Solar Powered Vehicle"*, IAS Conference Proceedings, October 1994, Vol. 1, pp. 188 - 195.

[41] Pillay, P., Samudio, R., Ahmed, M., Patel, R. (1994), *"A Chopper Controlled SRM Drive for Reduced Noise and Improved Ride-Through Capability Using Super Capacitors"*, IAS Conference Proceedings, October 1994, Vol. 1, pp. 313 - 321.

[42] Pulle, D.W.J., Lai, J.C.S., Milthorpe, J.F., Huynh, N. (1993), *"Quantification and analysis of Acoustic Noise in Switched Reluctance Drives"*, EPE Conference Proceedings, 1993, pp. 65 - 70.

[43] Pulle, D.W.J., Eijkel, C.J.M., Fluitman, J.H.J., Leeuwis, H., van Mierlo, D.J.M., *"A New Magnetoresistive Based Sensor for Switched Reluctance Drives"*.

[44] Radun, A.V. (1994), *"Design Considerations for the Switched Reluctance Motor"*, IAS Conference Proceedings, October 1994, Vol. 1, pp. 290 - 297.

[45] Radun, A.V. (1992), *"High-Power Density Switched Reluctance Motor Drive for Aerospace Applications"*, IEEE Transactions on Industry Applications, Vol. 28, No. 1, January/February 1992, pp. 113 - 119.

[46] Ray, W.F., Al-Bahadly, I.H. (1993), *"Sensorless Methods for Determing the Rotor Position of Switched Reluctance Motors"*, EPE Conference Proceeding, 1993, pp. 7 - 13.

[47] Ray, W.F., Lawrenson, P.J., Davis, R.M., Stephenson, J.M., Fulton, N.N., Blake, R.J. (1986), *"High-Performance Switched Reluctance Brushless Drives"*, IEEE Transactions on Industry Applications, Vol. 1A-22, No. 4, Juli/August 1986, pp. 722 - 729.

[48] Reay, D.S., Green, T.C., Williams, B.W. (1993), *"Neural Networks used for Torque Ripple Minimisation from a Switched Reluctance Motor"*, EPE Conference Poceedings, 1993, pp. 1 - 6.

[49] Richter, E., Miller, T.J.E. (1992), *"Technology of High-Efficiency Motors"*, Int. Conf. on Electrical Machines Proceedings, 1992, pp. 190 - 194.

[50] Rochford, C., Kavanagh, R.C., Egan, M.G., Murphy, J.M.D. (1993), *"Development of Smooth Torque in Switched Reluctance Motors using Self-Learning Techniques"*, EPE Conference Proceeding, 1993, pp. 14 - 19.

[51] Schramm, D.S., Williams, B.W., Green, T.C. (1992), *"Torque Ripple Reduction of Switced Reluctance Motors by Phase Current Optimal Profiling"* .

[ ] Slemon, G. (1966), *"Magnetoelectric Devices"*, John Wiley & Sons, Inc., New York, United States of America.

[52] Staton, D.A., Soong, W.L., Deodhar, R.P., Miller, T.J.E. (1994), *"Unified Theory of Torque Production in AC, DC and Reluctance Motors"*, IAS Conference Proceedings, October 1994, Vol. 1, pp. 149 - 156.

[53] Stephenson, J.M., Corda, J. (1979), *"Computation of Torque and Current in Doubly Salient Reluctance Motors From Nonlinear Magnetization Data"*, Proceedings IEE, Vol. 126, No. 5, May 1979, pp. 393 - 396.

[54] Stephenson, J.M., Lawrenson, P.J., Fulton, N.N., *"High Power Switched Reluctance Drives"*.

[55] Sugden, D.M., Randall, S.P., Webster, P.D. (1986), *"Low-Power Controlled-Speed Drives using SR Motors"* .

[56] Török, V., Loreth, K. (1993), *"The World's Simplest Motor for Variable Speed Control? The Cyrano Motor, a PM-Biased SR-Motor of High Torque Density"* .

[57] Vallese, F.J. (1985), *"Design and Operation of High-Power Variable Reluctance Motor based Drive Systems"*, Massachusetts Institute of Technology.

[58] van der Broeck, H., Gerling, D., Bolte, E. (1993), *"Switched Reluctance Drive and PWM Induction motor Drive Compared for Low Cost Applications"*, EPE Conference Proceedings, 1993, pp. 71 - 76.

[59] Verma, S.P., Balan, A., *"Measurement Techniques for Vibration and Acoustic Noise of Electrical machines"*.

[60] Vucosavic, S., Stefanovic, V.R. (1991), *"SRM Inverter Topologies: A Comparative Evaluation"*, IEEE Transactions on Industry Applications, Vol. 27, No. 6, November/December 1991, pp. 1034 - 1047.

[61] Wallace, A.K., Spee, R. (1987), *"Performance Evaluation of AC Adjustable Speed Drives"* .

[62] Weibull, H., Carlsson, A., Sjöberg, L., Ekdahl, I. (1994), *"Data Acquisition and Data Prossesing for Resonance Characteristic"* .

[63] Weller, A., Trawinski, P. (1991), *"Design and Control of Low Power Switched Reluctance Motors (< 1 kW)"*, EPE Conference Proceedings, Pt. 4, 1991, pp. 1 - 6.

[64] West, J.G.W. (1993), *"DC, Induction, Reluctance and PM Motors for Electric Vehicles"*, IEE Colloqium on "Motors and drive systems for battery-powered propulsion" - 15th april 1993.

[65] Wu, C.Y., Pollock, C. (1993), *"Time Domain Analysis of Vibration and Acoustic Noise in the Switched Reluctance Drive"* .

A

Instrumentation

- current sensor, LEM MODULE LA50 - P
- torque transducer, VIBROMETER TG-5/BP
- power meter, NORMA AC/DC POWER ANALYZER D 5135
- resolver, THOMSON - CSF 12T11BC252gSSK197

B

Machine Core Materials

Iron Powder Composite Material

The prototype composite material was developed at the Department of Production and Material Engineering (Lund Institute of Technology) and Höganäs AB. The Department of Industrial Electrical Engineering and Automation was consulted regarding the demands on the material making it a suitable competitor for a magnetic flux conductor in electrical machines.

The composites used in the switched reluctance machine are made by mixing fluid, epoxy resin and iron flakes, coated with a thin electrically insulating layer. The mixture is compacted in a uniaxial pressing tool at approximately 800 MPa.

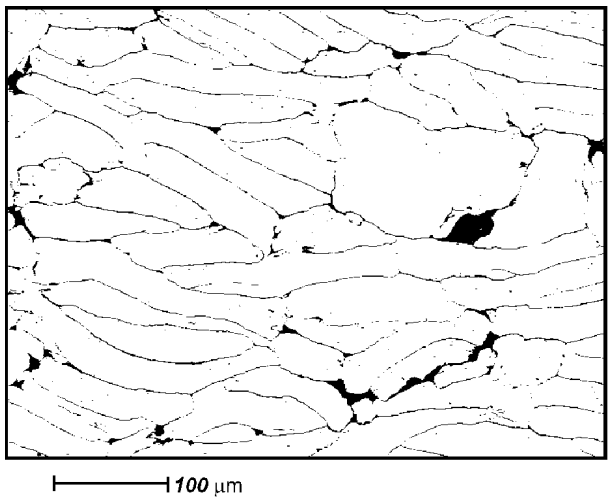

Fig. B.1 *A cut away view of the iron powder core at 200 times enlargement (picture is taken from (Cedell, 1995)).*

Another important characterisic is the fact that the iron particles are flakes rather than spherical particles. This is seen in Fig. B.1, where the flakes are oriented in the direction of the magnetic flux. This increases the relative permeability in the direction of the flux at the expense of the permeability in the perpendicular direction.

The most important characteristics are summarised in TABLE B-I, and more information on the composite material is found in (Cedell, 1995 and Alaküla et al, 1995).

TABLE B-I

Iron Composite Material Data		
saturation flux density	B_{sat}	*1.8 T*
maximum relative permeability	$\mu_{r,\max}$	*400*
coercive force	H_c	*350 A/m*
elastic modulus	E	*90 GPa*
rupture stress	σ_B	*150 MPa*
thermal conductivity	λ	*30 W/mK*

A model for the iron losses is described in Chapter 3 and a comparison between calculated and measured iron losses for a sinusoidal flux density is given in Fig. B.2, for 0.5 T and 1.0 T. The iron loss curve for 1.5 T is only calculated. The measurements are done by Höganäs AB.

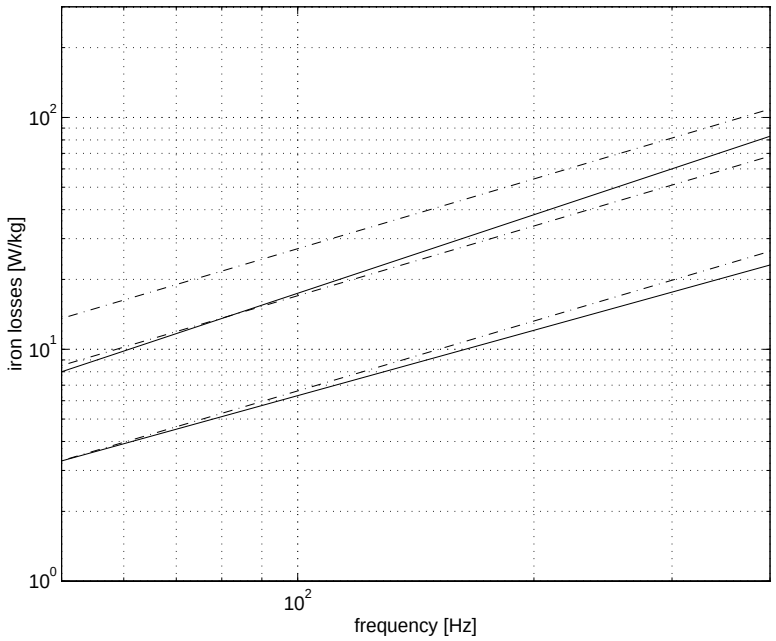

Fig. B.2 *A comparison between the calculated (dash dotted line) and the measured (solid line) loss characteristics for the iron powder composite.*

Iron Lamination

The iron laminations are made of non-oriented FeSi alloy, consisting of 1 % Si. The laminate thickness is 0.65 mm, and the laminate is sold by Surahammar AB under the product name DK70. The most important characteristics for DK70 are listed in TABLE B-II.

TABLE B-II

DK70 Material Data		
saturation flux density	B_{sat}	*2.0 T*
maximum relative permeability	$\mu_{r,\max}$	*3000*
coercive force	H_c	*100 A/m*
elastic modulus	E	*210 GPa*
rupture stress	σ_B	*410 MPa*
thermal conductivity	λ	*40 W/mK*

No data on iron losses as a function of peak flux density and frequency are available other than at 50 Hz and 1.0 T and 1.5 T. The curves in Fig. B.3

are thus a comparison of the modelled iron losses for the iron laminate and the iron powder composite.

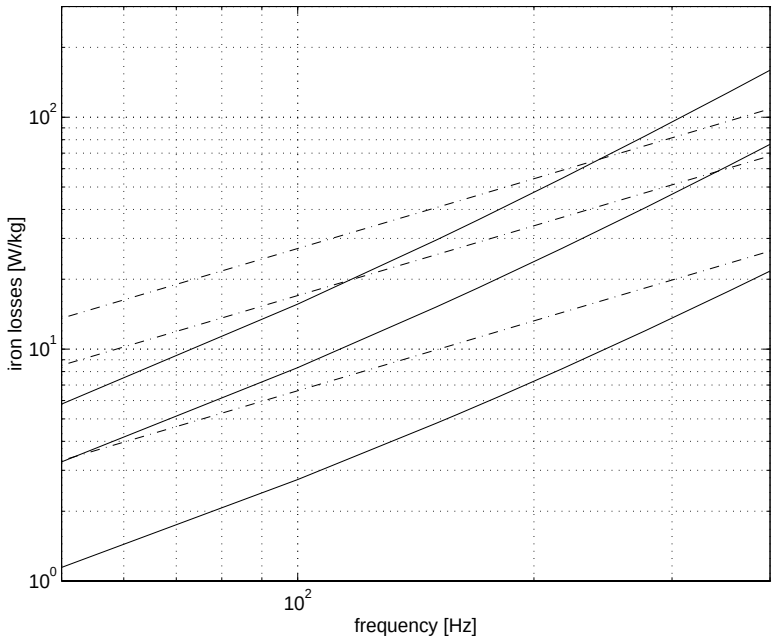

Fig. B.3 *Calculated losses for the iron powder composite material (dash dotted line) and the iron lamination DK 70 (solid line) for a flux density of 0.5 T, 1.0 T and 1.5 T.*

As expected, the iron powder composite has much higher losses at low frequencies. The loss curves intersect at various frequencies for different flux density levels. The curves in Fig. B.3 can be interpreted in such a way that it is possible to rewind a switched reluctance machine for another base speed so that the total iron losses are smaller in the machine with the iron powder composite than in the machine with iron laminations. However, the difficulties in calculating the iron losses in a switched reluctance machine with non-sinusoidal flux waveforms, dc bias flux density and heavy magnetic saturation makes it difficult to predict such a frequency of intersection from the data in Fig. B.3.

C

Machine Data

TABLE C-I

Switched Reluctance Machine Data		
number of stator poles	N_s	*6*
number of rotor poles	N_r	*4*
stack length	l_{stk}	*110.0 mm*
stator pole height	d_s	*18.6 mm*
stator pole width	t_s	*18.7 mm*
stator yoke width	y_s	*13.9 mm*
rotor pole height	d_r	*10.9 mm*
rotor pole width	t_r	*20.9 mm*
rotor yoke width	y_r	*11.3 mm*
stator outer diameter	D_s	*138.0 mm*
rotor outer diameter	D_r	*72.4 mm*
shaft diameter	D_{sh}	*28.0 mm*
copper wire diameter	D_w	*0.80 mm*
# of turns per coil	N	*84*
fillfactor	$fill$	*0.47*
airgap length	δ	*0.30 mm*
stator slot area	A_{slot}	*5.39 cm^2*
coil copper area	A_{Cu}	*1.27 cm^2*
iron mass	M_{Fe}	*8.4 kg*
copper mass	M_{Cu}	*2.1 kg*
stator outer volume	V_s	*1.65 dm^3*

One phase winding consists of two coils wound on diametrically opposite stator poles. The two coils are coupled in parallel. Each one of the coils consists of three copper wires with the diameter given in TABLE C-I, wound in parallel.

The data on machine stator outer volume and mass are included only so that the reader may form an opinion of the machine torque and power density. An explanation of the measures are seen in Fig. C.1.

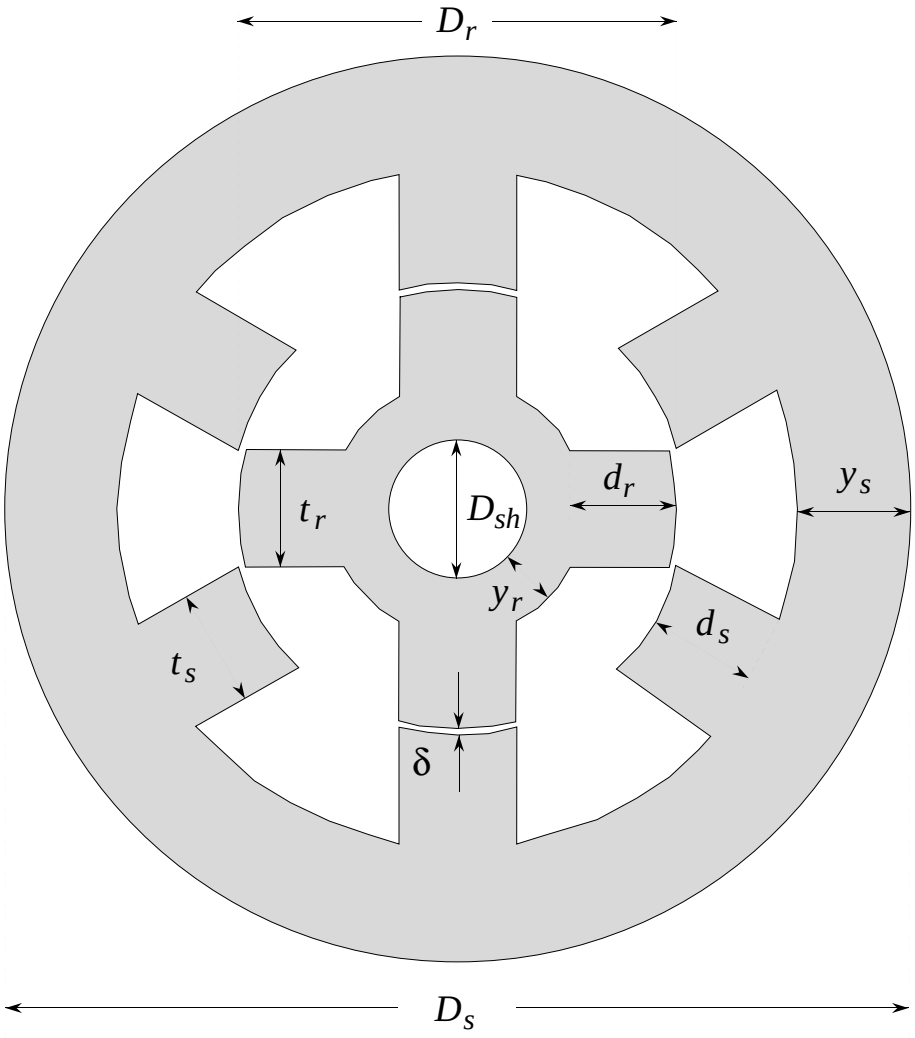

Fig. C.1 *A cross sectional view of the switched reluctance machine magnetic circuit showing the defined measures.*

D

List of Symbols

A	area	m^2
B	magnetic flux density	T
C	capacitance	F
d	pole depth	m
d	lamination thickness	m
D	diameter	m
e	electromotive force	V
f	frequency	Hz
H	magnetic field strength	A/m
i	current	A
J	inertia	kg m^2
k_{dc}	iron loss calculation constant	
k_{ripple}	torque ripple constant	
l	length	m
L	inductance	H
m	number of phases	
M	mass	kg
n	number of revolutions per minute	min^{-1}
N	number of turns	
N	number of poles	
P	power	W
P	power density	W/kg

R	resistance	Ω
R	reluctance	A/Vs
t	pole width	m
T	temperature	°K
T	torque	Nm
u	voltage	V
V	volume	m^3
W	energy	J
x	winding overhang radius	m
y	yoke width	m

Greek letters

α	copper resistivity temperature coefficient	/K
δ	airgap length	m
θ_r	rotor angular position	rad
λ	slot pitch	m
ρ	resistivity	Ωm
ρ	density	kg/m^3
σ	winding length correction factor	
σ	conductivity	$(\Omega m)^{-1}$
ϕ	magnetic flux	Wb
ψ, Ψ	flux linkage	Vs
ω_r	rotor angular speed	rad/s

subscripts

Cu	copper
eq	equivalent
e	eddy current
Fe	iron
h	hysteresis
oh	winding overhang
r	rotor

ref	reference value
rms	root mean square
rp	rotor pole
ry	rotor yoke
s	stator
sh	shaft
sp	stator pole
stk	stack
sy	stator yoke
w	winding